

Update of one-loop corrections for $e^+e^- \rightarrow f\bar{f}$, first run of SANC system

A. Andonov, D. Bardin, S. Bondarenko*,
 P. Christova, L. Kalinovskaya, and G. Nanava

Laboratory for Nuclear Problems, JINR,

** Bogoluobov Laboratory of Theoretical Physics, JINR,*

ul. Joliot-Curie 6, RU-141980 Dubna, Russia

Abstract

We present a description of calculations of the amplitude for $e^+e^- \rightarrow f\bar{f}$ process with account of electroweak and QED one-loop corrections. This study is performed within the framework of the project SANC. The calculations are done within the OMS (on-mass-shell) renormalization scheme in two gauges: in R_ξ , which allows an explicit control of gauge invariance by examining cancellation of gauge parameters and search for gauge-invariant subsets of diagrams, and in the unitary gauge as a cross-check. The formulae we derived are realized in two independent FORTRAN codes, `eeffLib`, which was written in an old fashioned way, i.e. manually, and another one, created automatically with an aid of `s2n.f` (symbols to numbers) software — a part of SANC system. We present a comprehensive comparison with the results of the well-known program ZFITTER for all the light fermion production channels, as well as with the results existing in the world literature for the process $e^+e^- \rightarrow t\bar{t}$.

Submitted to *Particles and Nuclei*

Work supported by INTAS N° 00-00313.

E-mails: andonov@nusun.jinr.ru, bardin@nusun.jinr.ru, bondarenko@jinr.ru
 penchris@nusun.jinr.ru, kalinov@nusun.jinr.ru, nanava@nusun.jinr.ru

Contents

Introduction	4
1 Amplitudes	7
1.1 Born amplitudes	7
1.2 One-loop amplitude for $e^+e^- \rightarrow f\bar{f}$	7
2 Building Blocks in the OMS Approach	9
2.1 Bosonic self-energies	9
2.1.1 Z, γ bosonic self-energies and $Z-\gamma$ transition	9
2.1.2 W boson self-energy	14
2.1.3 Bosonic self-energies and counterterms	16
2.2 Fermionic self-energies	17
2.2.1 Fermionic self-energy diagrams	17
2.3 The $Zf\bar{f}$ and $\gamma f\bar{f}$ vertices	19
2.3.1 Scalar form factors	20
2.4 Library of form factors for Bff clusters	20
2.4.1 Library of QED form factors for Att clusters	21
2.4.2 Form factors of the Z cluster	22
2.4.3 Form factors of the H cluster	25
2.4.4 Form factors of the W cluster	28
2.5 Library of scalar form factors in the limit $m_f = 0$	34
2.6 Library of scalar form factors for electron vertex	36
2.7 Amplitudes of boxes	37
2.7.1 AA box contribution	37
2.7.2 ZA box contribution	39
2.7.3 The WW box	43
2.7.4 The ZZ box	45
2.7.5 Transition to the L, Q, D basis	48
2.7.6 Box–Born interferences	49
3 Scalar form factors for electroweak amplitude	49
3.1 Vertices scalar form factors	49
3.2 Bosonic self-energies and bosonic counterterms	50
3.3 Total scalar form factors of the one-loop amplitude	52
4 Improved Born Approximation cross-section	52
4.1 Improved Born Approximation cross-section	52
4.2 The $e^+e^- \rightarrow f\bar{f}$ process in the helicity amplitudes	54
5 Annex	55
5.1 QED vertices and soft-photon contributions	55
5.1.1 Initial-state radiation (ISR)	56
5.1.2 Initial–final state interference (IFI)	56

5.1.3	Final-state radiation (FSR)	57
5.1.4	Non-factorized final-state vertex 'anomalous' contributions	57
5.2	An alternative form of the cross-section for QED boxes	57
6	Numerical results and discussion	61
6.1	Flags of <code>eeffLib</code>	61
6.2	<code>eeffLib</code> -ZFITTER comparison of scalar form factors	63
6.3	<code>eeffLib</code> -ZFITTER comparison of IBA cross-section	64
6.4	Comparison with a code generated by <code>s2n.f</code>	69
6.5	About a comparison with the other codes	70
	Acknowledgments	71
	References	74

List of Figures

1	The six-fermion $e^+e^- \rightarrow t\bar{t}$ process.	4
2	$Z(\gamma)$ boson self-energy; $Z\text{-}\gamma$ transition.	10
3	W boson self-energy.	15
4	Fermionic self-energy diagrams.	17
5	$Zf\bar{f}$ and $\gamma f\bar{f}$ vertices with counterterms.	19
6	A cluster.	21
7	Z cluster.	22
8	H cluster.	26
9	W cluster.	29
10	Direct and crossed AA boxes.	37
11	Direct and crossed ZA boxes.	40
12	Crossed and direct WW boxes.	43
13	Crossed and direct ZZ boxes.	46
14	Electron and final fermion vertices in $e\bar{e} \rightarrow (\gamma, Z) \rightarrow f\bar{f}$	49
15	Bosonic self-energies and counterterms for $e\bar{e} \rightarrow (Z, \gamma) \rightarrow f\bar{f}$	51
16	Relative EWRC to the $e^+e^- \rightarrow t\bar{t}$ differential cross-section.	72
17	Relative EWRC to $e^+e^- \rightarrow t\bar{t}$ total cross-section.	73

List of Tables

1	EWFF for the process $e^+e^- \rightarrow f\bar{f}$. <code>eeffLib-ZFITTER</code> comparison.	65
2	<code>eeffLib-ZFITTER</code> comparison of the differential cross-section, leptonic channels.	66
3	<code>eeffLib-ZFITTER</code> comparison of the differential cross-section, quarkonic channels.	67
4	<code>eeffLib-ZFITTER</code> comparison of the total EW cross-sections.	68
5	EWFF for the process $e^+e^- \rightarrow t\bar{t}$. Comparison of <code>eeffLib-s2n.f.</code>	69
6	$\frac{d\sigma^{(1)}}{d\cos\vartheta}$ for the process $e^+e^- \rightarrow t\bar{t}$. Comparison of <code>eeffLib-s2n.f.</code>	70
7	$\frac{d\sigma^{(1)}}{d\cos\vartheta}$ for the process $e^+e^- \rightarrow t\bar{t}$ with soft photons, $E_\gamma^{\max} = \sqrt{s}/10$	70

Introduction

The process $e^+e^- \rightarrow f\bar{f}$ with taking into account of the higher-order Standard Model (SM) corrections has been studied already several decades, yet in pre-LEP times. We mention papers from late seventies, [1], [2], [3] and [4], which eventually lead to producing of precision theoretical predictions realized in the well-known computer codes of LEP-era: ZFITTER [5], BHM [6] ALIBABA [7] and TOPAZO [8]. These codes played a very important role throughout the full life-time of LEP providing experimental community with precision tools for fitting of experimental data to the SM predictions, see, for instance [9]–[10]. A comprehensive review of underlying theory and methods which has been used for creation of these codes may be found in the monograph [11].

At LEP, the higher-order corrections for process $e^+e^- \rightarrow f\bar{f}$ might be studied ignoring external fermion masses, since the cms energy was far below $t\bar{t}$ threshold. However, studies of finite mass effects has been started more than ten years ago [12], [13] and [14] in connection with experiments at future linear colliders (see, for instance, the reviews [15] and [16]).

New wave of papers on finite mass effect was triggered by studies of the electroweak radiative corrections (EWRC) in the MSSM which may involve additional heavy fermions and sfermions, [17]–[18].

The process $e^+e^- \rightarrow t\bar{t}$ in reality is a six-fermion process (see [19]); one of the channels is shown in Fig. 1.

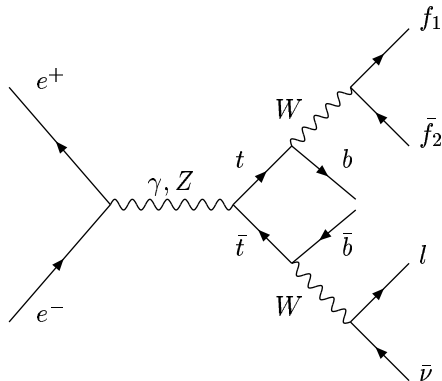


Figure 1: The six-fermion $e^+e^- \rightarrow t\bar{t}$ process.

However, the cross-section of a hard subprocess, $\sigma(e^+e^- \rightarrow t\bar{t})$, with tops on the mass shell is an ingredient within various approaches, such as DPA [20] or the so-called Modified Perturbation Theory (MPT), see [21].

One should emphasise that the treatment of even one-loop corrections with taking into account of finite-state fermion masses is extremely cumbersome and practically undouble ‘manually’. Nowadays, all the calculations of such a kind are being performed with the aid of automatic computer systems, among

which one should mention first of all `FeynArts` package, which exists already more than ten years [22] and which is able to compute the cross-section of the process $\sigma(e^+e^- \rightarrow t\bar{t})$ at the one-loop level.

In this article, we present a review of a new calculation (based on preprints [23]–[25]) of the $e^+e^- \rightarrow f\bar{f}$ process at the one-loop level made with an aid of the computer system `SANC` where all the calculations from the Lagrangians up to numbers are going to be eventually automatized. This system is being created at the site `brg.jinr.ru`. It roots back to dozens of supporting `form` [26] codes written by authors of the book [11] while working on it. Later on, the idea came up to collect, order, unify and upgrade these codes up to the level of a ‘computer system’. Its first phase is described in [25].

One of main goals of this new calculation was to create a platform for the treatment of any $2f \rightarrow 2f$ process within the `SANC` and to cross-check its results against the results obtained with the other existing codes for a rather complicated $2f \rightarrow 2f$ process at one-loop level taking into account final state masses.

At present, `SANC`, like `FeynArts`, uses the OMS renormalization scheme, a complete presentation of which was made in [11]. However, for the first time the calculations are performed in two gauges simultaneously: R_ξ and the unitary gauge.

Note, that there was wide experience of calculations in the R_ξ gauge for processes such as $H \rightarrow f\bar{f}, WW, ZZ, \gamma Z, \gamma\gamma$, or $e^+e^- \rightarrow ZH, WW$. So, in [27] and [28] a complete set of one-loop counterterms for the SM is given. Electromagnetic form factors for arbitrary ξ are discussed in [29] and [30]. Explicit expressions can be found in the CERN library program `EEWW` [31].

However, we are not aware of the existence of calculations in the R_ξ gauge for the $e^+e^- \rightarrow t\bar{t}$ process, although there are many studies in the $\xi = 1$ gauge [12]–[14] and [17]–[18].

Additional purposes of this review are:

- to explicitly demonstrate gauge invariance in R_ξ by examining cancellation of gauge parameters for gauge-invariant subsets of diagrams;
- to offer a possibility to compare the results with those in the unitary gauge, as a cross-check;
- to present a self-contained list of results for one-loop amplitude in terms of Passarino–Veltman functions A_0, B_0, C_0 and D_0 (as well as *special* functions a_0, b_0, c_0 and d_0 which originate because of a particular form of the photonic propagator in the R_ξ gauge) and their combinations in the spirit of the book [11], where the process $e^+e^- \rightarrow t\bar{t}$ was not covered; this review may thus be considered as an Annex to the book, which completes its pedagogical aims for $2f \rightarrow 2f$ processes at one loop;

- to provide a FORTRAN code, `eeffLib` [32] for the calculation of the cross-section of this process for a complementary use within the MPT framework;
- to compare the results derived with the aid of `eeffLib` with the results of another code, which was created automatically using the `s2n.f` software — a part of SANC system, thereby benchmarking `s2n.f` software.

This review consists of seven sections.

In Section 1, we present the Born amplitude of the process, basically to introduce our notation and then define *the basis* in which the one-loop amplitude was calculated. We explain *the splitting* between QED and EW corrections and between ‘dressed’ γ and Z exchanges.

Section 2 contains explicit expressions for all *the building blocks*: self-energies, vertices and boxes, both QED and EW. Note that no diagram was computed by hand. They all were supplied by the SANC system.

In Section 3, we describe the procedure of construction of *the scalar form factors* of the one-loop amplitudes out of the building blocks. One of the aims of this section was to create a frame for a subsequent realization of the renormalization procedure within the SANC project.

Section 4 contains explicit expressions for the improved Born approximation (IBA) cross-section and the explicit expressions for helicity amplitudes made of the scalar form factors at the one-loop level.

Section 5 contains some additional expressions for different QED contributions that might be derived analytically. They are not in the main stream of our approach: Lagrangian \rightarrow scalar form factors \rightarrow helicity amplitudes \rightarrow one-loop differential cross-section. However, they are useful for the pedagogical reasons, and their coding in complementary FORTRAN branches of `eeffLib` provided us with the powerful internal cross-checks of our codes for numerical calculations. In reality, the `eeffLib` version of February 2002 has three QED branches.

Finally, in Section 6 we present results of a comprehensive numerical comparison between `eeffLib` and ZFITTER. Here we also present a comparison with another of our codes, which was created automatically using the `s2n.f` software. We also present a comprehensive comparison between the results derived with our two codes and the results existing in the world literature. In particular, we found a high-precision agreement with `FeynArts` results up to 11 digits for the differential cross-sections with virtual corrections, and with recent results of [33] within 8 digits, even when the soft photon radiation is included, see [34]–[35].

1 Amplitudes

1.1 Born amplitudes

We begin with the Born amplitudes for the process $e^+(p_+)e^-(p_-) \rightarrow f(q_-)\bar{f}(q_+)$, which is described by the two Feynman diagrams with γ and Z exchange. The Born amplitudes are:

$$A_\gamma^B = eQ_e eQ_f \gamma_\mu \otimes \gamma_\mu \frac{-i}{Q^2} = -i 4\pi\alpha(0) \frac{Q_e Q_f}{Q^2} \gamma_\mu \otimes \gamma_\mu, \quad (1.1)$$

$$\begin{aligned} A_Z^B &= \left(\frac{e}{2s_W c_W} \right)^2 \gamma_\mu \left[I_e^{(3)} \gamma_+ - 2Q_e s_W^2 \right] \otimes \gamma_\mu \left[I_f^{(3)} \gamma_+ - 2Q_f s_W^2 \right] \frac{-i}{Q^2 + M_Z^2} \\ &= -ie^2 \frac{1}{4s_W^2 c_W^2 (Q^2 + M_Z^2)} \left[I_e^{(3)} I_f^{(3)} \gamma_\mu \gamma_+ \otimes \gamma_\mu \gamma_+ + \delta_e I_f^{(3)} \gamma_\mu \otimes \gamma_\mu \gamma_+ \right. \\ &\quad \left. + I_e^{(3)} \delta_f \gamma_\mu \gamma_+ \otimes \gamma_\mu + \delta_e \delta_f \gamma_\mu \otimes \gamma_\mu \right], \end{aligned} \quad (1.2)$$

where $\gamma_\pm = 1 \pm \gamma_5$ and the symbol \otimes is used in the following short-hand notation:

$$\begin{aligned} &\gamma_\mu (L_1 \gamma_+ + Q_1) \otimes \gamma_\nu (L_2 \gamma_+ + Q_2) \\ &= \bar{v}(p_+) \gamma_\mu (L_1 \gamma_+ + Q_1) u(p_-) \bar{u}(q_-) \gamma_\nu (L_2 \gamma_+ + Q_2) v(q_+); \end{aligned} \quad (1.3)$$

furthermore

$$\delta_f = v_f - a_f = -2Q_f s_W^2. \quad (1.4)$$

Introducing the LL , QL , LQ , and QQ structures, correspondingly (see last Eq. (1.2)), we have four structures to which the complete Born amplitude may be reduced: one for the γ exchange amplitude and four for the Z exchange amplitude ($\gamma_\mu \otimes \gamma_\mu$ structure presents in both amplitudes).

1.2 One-loop amplitude for $e^+e^- \rightarrow f\bar{f}$

For the $e^+e^- \rightarrow f\bar{f}$ process at one loop, it is possible to consider a gauge-invariant subset of *electromagnetic corrections* separately: QED vertices, AA and ZA boxes. Together with QED bremsstrahlung diagrams, it is free of infrared divergences. The total electroweak amplitude is a sum of ‘dressed’ γ and Z exchange amplitudes, plus the contribution from the weak box diagrams (WW and ZZ boxes).

Contrary to the Born amplitude, the one-loop amplitude may be parametrized by 6 form factors, a number equal to the number of independent helicity amplitudes for this process if the electron mass is ignored and the unpolarized case is studied¹.

¹If the initial-state masses were not ignored too, we would have ten independent helicity amplitudes, ten structures and ten scalar form factors.

We work in the so-called LQD basis, in which the amplitude may be schematically represented as:

$$[i\gamma_\mu\gamma_+F_L^e(s) + i\gamma_\mu F_Q^e(s)] \otimes [i\gamma_\mu\gamma_+F_L^f(s) + i\gamma_\mu F_Q^f(s) + m_f ID_\mu F_D^f(s)], \quad (1.5)$$

with

$$D_\mu = (q_+ - q_-)_\mu. \quad (1.6)$$

Every form factor in the R_ξ gauge could be represented as a sum of two terms:

$$F_{L,Q,D}^\xi(s) = F_{L,Q,D}^{(1)}(s) + F_{L,Q,D}^{\text{add}}(s). \quad (1.7)$$

The first term corresponds to the $\xi = 1$ gauge and the second contains all ξ dependences and vanishes for $\xi = 1$ by construction.

The LQD basis was found to be particularly convenient to explicitly demonstrate the cancellation of all ξ -dependent terms. We checked the cancellation of these terms in several groups of diagrams separately: the so-called A , Z , and H clusters, defined below; the W cluster together with the self-energies and the WW box; and the AA , ZA and ZZ boxes. Therefore, for our process we found seven separately gauge-invariant subgroups of diagrams: three in the QED sector, and four in the EW sector.

The ‘dressed’ γ exchange amplitude is

$$A_\gamma^{\text{IBA}} = i \frac{4\pi Q_e Q_f}{s} \alpha(s) \gamma_\mu \otimes \gamma_\mu, \quad (1.8)$$

which is identical to the Born amplitude of Eq. (1.2) modulo the replacement of $\alpha(0)$ by the running electromagnetic coupling $\alpha(s)$:

$$\alpha(s) = \frac{\alpha}{1 - \frac{\alpha}{4\pi} [\Pi_{\gamma\gamma}^{\text{fer}}(s) - \Pi_{\gamma\gamma}^{\text{fer}}(0)]}. \quad (1.9)$$

In the LQD basis the Z exchange amplitude has the following Born-like structure in terms of six (LL , QL , LQ , QQ , LD and QD) form factors:

$$\begin{aligned} \mathcal{A}_Z^{\text{IBA}} = & i e^2 \frac{\chi_Z(s)}{s} \left\{ \gamma_\mu\gamma_+ \otimes \gamma_\mu\gamma_+ \tilde{F}_{LL}(s,t) + \gamma_\mu \otimes \gamma_\mu\gamma_+ \tilde{F}_{QL}(s,t) \right. \\ & + \gamma_\mu\gamma_+ \otimes \gamma_\mu \tilde{F}_{LQ}(s,t) + \gamma_\mu \otimes \gamma_\mu \tilde{F}_{QQ}(s,t) \\ & \left. + \gamma_\mu\gamma_+ \otimes (-im_f D_\mu) \tilde{F}_{LD}(s,t) + \gamma_\mu \otimes (-im_f D_\mu) \tilde{F}_{QD}(s,t) \right\}, \end{aligned} \quad (1.10)$$

where we introduce the notation for $\tilde{F}_{ij}(s, t)$:

$$\begin{aligned}
\tilde{F}_{LL}(s, t) &= I_e^{(3)} I_f^{(3)} F_{LL}(s, t), \\
\tilde{F}_{QL}(s, t) &= \delta_e I_f^{(3)} F_{QL}(s, t), \\
\tilde{F}_{LQ}(s, t) &= I_e^{(3)} \delta_f F_{LQ}(s, t), \\
\tilde{F}_{QQ}(s, t) &= \delta_e \delta_f F_{QQ}(s, t), \\
\tilde{F}_{LD}(s, t) &= I_e^{(3)} I_f^{(3)} F_{LD}(s, t), \\
\tilde{F}_{QD}(s, t) &= \delta_e I_f^{(3)} F_{QD}(s, t).
\end{aligned} \tag{1.11}$$

Note that *tilded* form factors absorb couplings, which leads to a compactification of formulae for the amplitude and IBA cross-section, while explicit expressions will be given for *untilded* quantities. The representation of Eq. (1.10) is very convenient for the subsequent discussion of one-loop amplitudes.

Furthermore, in Eq. (1.10) we use the Z/γ propagator ratio with an s -dependent (or constant) Z width:

$$\chi_Z(s) = \frac{1}{4s_w^2 c_w^2} \frac{s}{s - M_Z^2 + i \frac{\Gamma_Z}{M_Z} s}. \tag{1.12}$$

2 Building Blocks in the OMS Approach

We start our discussion by presenting various *building blocks*, used to construct the one-loop form factors of the processes $e^+e^- \rightarrow f\bar{f}$ in terms of the A_0 , B_0 , C_0 and D_0 functions. They are shown in order of increasing complexity: self-energies, vertices, and boxes.

2.1 Bosonic self-energies

2.1.1 Z, γ bosonic self-energies and $Z-\gamma$ transition

In the R_ξ gauge there are 14 diagrams that contribute to the *total* Z and γ bosonic self-energies and to the $Z-\gamma$ transition. They are shown in Fig. 2.

With S_{ZZ} , $S_{Z\gamma}$ and $S_{\gamma\gamma}$ standing for the sum of all diagrams, depicted by a grey circle in Fig. 2, we define the three corresponding self-energy functions Σ_{AB} :

$$S_{ZZ} = (2\pi)^4 i \frac{g^2}{16\pi^2 c_w^2} \Sigma_{ZZ}, \tag{2.1}$$

$$S_{Z\gamma} = (2\pi)^4 i \frac{g^2 s_w}{16\pi^2 c_w} \Sigma_{Z\gamma}, \tag{2.2}$$

$$S_{\gamma\gamma} = (2\pi)^4 i \frac{g^2 s_w^2}{16\pi^2} \Sigma_{\gamma\gamma}. \tag{2.3}$$

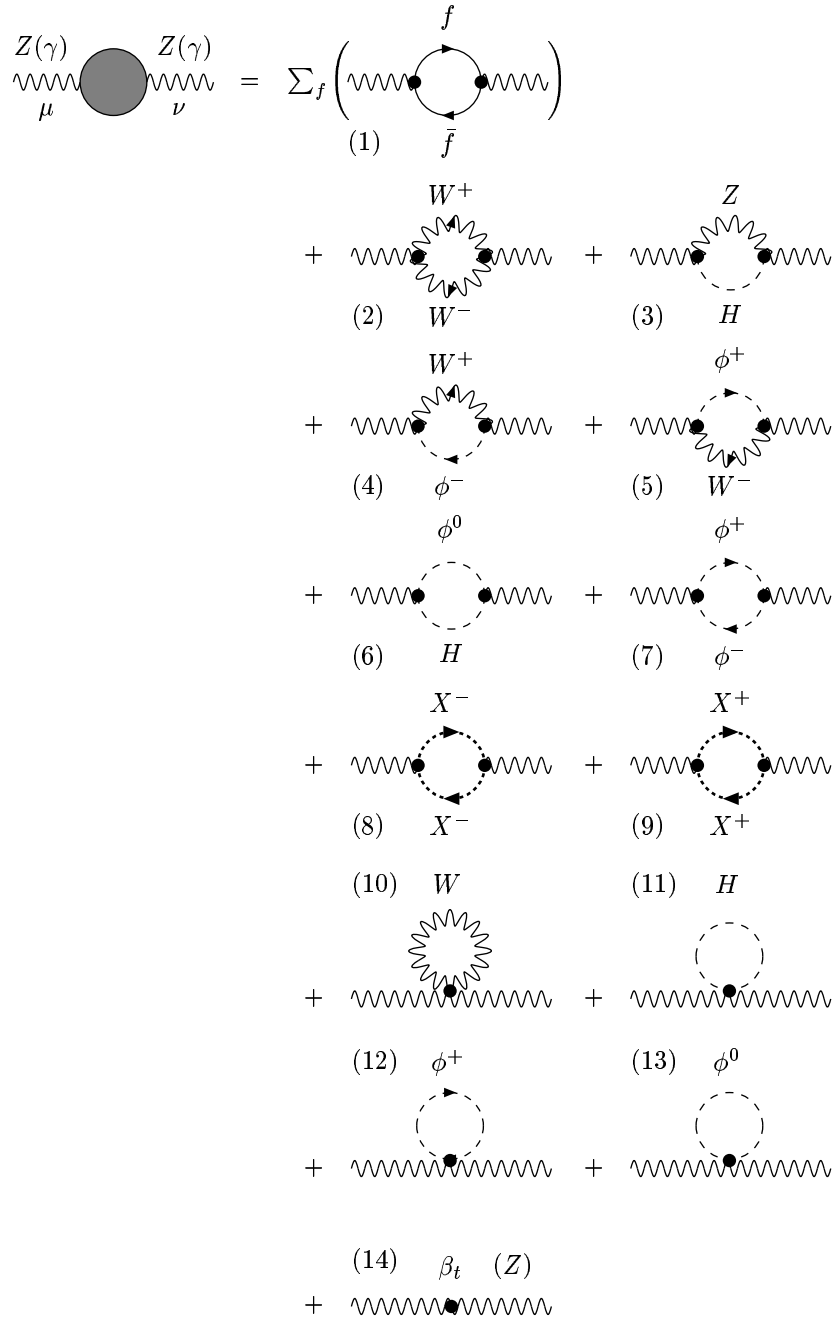


Figure 2: $Z(\gamma)$ boson self-energy; $Z-\gamma$ transition.

All **bosonic** self-energies and transitions may be naturally split into *bosonic* and *fermionic* components.

- Bosonic components of Z, γ self-energies and $Z-\gamma$ transitions (see diagrams Fig. 2)

$$\begin{aligned} \Sigma_{ZZ}^{\text{bos}}(s) &= M_Z^2 \left\{ \frac{1}{3} \frac{1}{R_Z} \left(\frac{1}{2} - c_W^2 - 9c_W^4 \right) \right. \\ &\quad \left. - \frac{3}{2} \left[(1 + 2c_W^4) \frac{1}{r_{HZ}} - \frac{1}{2} - c_W^2 + \frac{8}{3}c_W^4 + \frac{1}{2}r_{HZ} \right] \right\} \frac{1}{\varepsilon} + \Sigma_{ZZ}^{\text{bos},F}(s), \end{aligned} \quad (2.4)$$

$$\begin{aligned} \Sigma_{ZZ}^{\text{bos},F}(s) &= \frac{M_Z^2}{12} \left\{ \left[4c_W^2 (5 - 8c_W^2 - 12c_W^4) + (1 - 4c_W^2 - 36c_W^4) \frac{1}{R_Z} \right] \right. \\ &\quad \times B_0^F(-s; M_W, M_W) \\ &\quad + \left[\frac{1}{R_Z} + 10 - 2r_{HZ} + (r_{HZ} - 1)^2 R_Z \right] B_0^F(-s; M_H, M_Z) \\ &\quad + \left[\frac{18}{r_{HZ}} + 1 + (1 - r_{HZ}) R_Z \right] L_\mu(M_Z^2) \\ &\quad + r_{HZ} \left[7 - (1 - r_{HZ}) R_Z \right] L_\mu(M_H^2) \\ &\quad + 2c_W^2 \left(\frac{18}{r_{HW}} + 1 + 8c_W^2 - 24c_W^4 \right) L_\mu(M_W^2) \\ &\quad + \frac{4}{3} (1 - 2c_W^2) \frac{1}{R_Z} - 6 (1 + 2c_W^4) \frac{1}{r_{HZ}} \\ &\quad \left. - 3(1 + 2c_W^2) - 9r_{HZ} - (1 - r_{HZ})^2 R_Z \right\}. \end{aligned} \quad (2.5)$$

Here $L_\mu(M^2)$ denotes the log containing the 't Hooft scale μ :

$$L_\mu(M^2) = \ln \frac{M^2}{\mu^2}, \quad (2.6)$$

and it should be understood that, contrary to the one used in [11], we define here

$$B_0(-s; M_1, M_2) = \frac{1}{\varepsilon} + B_0^F(-s; M_1, M_2), \quad (2.7)$$

meaning that B_0^F also depends on the scale μ . We will not explicitly maintain μ in the arguments list of L_μ and B_0^F . Leaving μ unfixed, we retain an opportunity to control μ independence (and therefore UV finiteness) in numerical realization of one-loop form factors, providing thereby an additional cross-check.

Next, it is convenient to introduce the dimensionless quantities $\Pi_{z\gamma}^{\text{bos}}(s)$ and $\Pi_{\gamma\gamma}^{\text{bos}}(s)$ (vacuum polarizations):

$$\Sigma_{z\gamma}^{\text{bos}}(s) = -s\Pi_{z\gamma}^{\text{bos}}(s), \quad (2.8)$$

$$\Sigma_{\gamma\gamma}^{\text{bos}}(s) = -s\Pi_{\gamma\gamma}^{\text{bos}}(s). \quad (2.9)$$

In Eqs. (2.5) and (2.7) and below, the following abbreviations are used:

$$c_w^2 = \frac{M_w^2}{M_z^2}, \quad r_{ij} = \frac{m_i^2}{m_j^2}, \quad R_w = \frac{M_w^2}{s}, \quad R_z = \frac{M_z^2}{s}. \quad (2.10)$$

Since only finite parts will contribute to resulting expressions for physical amplitudes, which should be free from ultraviolet poles, it is convenient to split every divergent function into singular and finite parts:

$$\Pi_{\gamma\gamma}^{\text{bos}}(s) = 3\frac{1}{\varepsilon} + \Pi_{\gamma\gamma}^{\text{bos},F}(s), \quad (2.11)$$

$$\Pi_{\gamma\gamma}^{\text{bos},F}(s) = (3 + 4R_w)B_0^F(-s; M_w, M_w) + 4R_w L_\mu(M_w^2), \quad (2.12)$$

and

$$\Pi_{z\gamma}^{\text{bos}}(s) = \left(\frac{1}{6} + 3c_w^2 + 2R_w\right)\frac{1}{\varepsilon} + \Pi_{z\gamma}^{\text{bos},F}(s), \quad (2.13)$$

$$\begin{aligned} \Pi_{z\gamma}^{\text{bos},F}(s) &= \left[\frac{1}{6} + 3c_w^2 + 4\left(\frac{1}{3} + c_w^2\right)R_w\right]B_0^F(-s; M_w, M_w) \\ &\quad + \frac{1}{9} - \left(\frac{2}{3} - 4c_w^2\right)R_w L_\mu(M_w^2). \end{aligned} \quad (2.14)$$

With the Z boson self-energy, Σ_{zz} , we construct a useful ratio:

$$\mathcal{D}_z(s) = \frac{1}{c_w^2} \frac{\Sigma_{zz}(s) - \Sigma_{zz}(M_z^2)}{M_z^2 - s}, \quad (2.15)$$

which also has bosonic and fermionic parts. The bosonic component is:

$$\mathcal{D}_z^{\text{bos}}(s) = \frac{1}{c_w^2} \left(-\frac{1}{6} + \frac{1}{3}c_w^2 + 3c_w^4\right)\frac{1}{\varepsilon} + \mathcal{D}_z^{\text{bos},F}(s), \quad (2.16)$$

with the finite part:

$$\begin{aligned} \mathcal{D}_z^{\text{bos},F}(s) &= \frac{1}{c_w^2} \left\{ \left(\frac{1}{12} + \frac{4}{3}c_w^2 - \frac{17}{3}c_w^4 - 4c_w^6\right) \right. \\ &\quad \left. \times \frac{M_z^2}{M_z^2 - s} \left[B_0^F(-s; M_w, M_w) - B_0^F(-M_z^2; M_w, M_w) \right] \right\} \end{aligned} \quad (2.17)$$

$$\begin{aligned}
& - \left(\frac{1}{12} - \frac{1}{3}c_w^2 - 3c_w^4 \right) B_0^F(-s; M_w, M_w) \\
& + \left(1 - \frac{1}{3}r_{HZ} + \frac{1}{12}r_{HZ}^2 \right) \\
& \times \frac{M_Z^2}{M_Z^2 - s} \left[B_0^F(-s; M_H, M_Z) - B_0^F(-M_Z^2; M_H, M_Z) \right] \\
& - \frac{1}{12} \left[1 - (1 - r_{HZ})^2 R_Z \right] B_0^F(-s; M_H, M_Z) \\
& - \frac{1}{12} R_Z (1 - r_{HZ}) \left[r_{HZ} (L_\mu(M_H^2) - 1) - L_\mu(M_Z^2) + 1 \right] - \frac{1}{9} (1 - 2c_w^2) \Big\}.
\end{aligned}$$

- Fermionic components of the Z and γ bosonic self-energies and of the Z - γ transition

These are represented as sums over all fermions of the theory, \sum_f . They, of course, depend on vector and axial couplings of fermions to the Z boson, v_f and a_f , and to the photon, electric charge eQ_f , as well as on the colour factor c_f and fermion mass m_f . The couplings are defined as usual:

$$v_f = I_f^{(3)} - 2Q_f s_w^2, \quad a_f = I_f^{(3)}, \quad (2.18)$$

with weak isospin $I_f^{(3)}$, and

$$\begin{aligned}
Q_f &= -1 \text{ for leptons, } +\frac{2}{3} \text{ for up quarks, } -\frac{1}{3} \text{ for down quarks,} \\
c_f &= 1 \text{ for leptons, } 3 \text{ for quarks.}
\end{aligned} \quad (2.19)$$

The three main self-energy functions are:

$$\Sigma_{ZZ}^{\text{fer}}(s) = -\sum_f c_f \left[(v_f^2 + a_f^2) s B_f(-s; m_f, m_f) + 2a_f^2 m_f^2 B_0(-s; m_f, m_f) \right], \quad (2.20)$$

$$\Sigma_{\gamma\gamma}^{\text{fer}}(s) = -s \Pi_{\gamma\gamma}^{\text{fer}}(s), \quad (2.21)$$

$$\Sigma_{Z\gamma}^{\text{fer}}(s) = -s \Pi_{Z\gamma}^{\text{fer}}(s). \quad (2.22)$$

The quantities $\Pi_{\gamma\gamma}^{\text{fer}}$ and $\Pi_{Z\gamma}^{\text{fer}}$ are different according to different couplings, but proportional to one function B_f (see Eq. (5.252) of [11] for its definition):

$$\Pi_{\gamma\gamma}^{\text{fer}}(s) = 4 \sum_f c_f Q_f^2 B_f(-s; m_f, m_f), \quad (2.23)$$

$$\Pi_{Z\gamma}^{\text{fer}}(s) = 2 \sum_f c_f Q_f v_f B_f(-s; m_f, m_f). \quad (2.24)$$

As usual, we subdivided them into singular and finite parts:

$$\begin{aligned}\Pi_{Z\gamma}^{\text{fer}}(s) &= -\frac{1}{3}\left(\frac{1}{2}N_f - 4s_w^2 \sum_f c_f Q_f^2\right)\frac{1}{\bar{\epsilon}} + \Pi_{Z\gamma}^{\text{fer},F}(s), \\ \Sigma_{ZZ}^{\text{fer}}(s) &= \left\{-\frac{1}{2}\sum_f c_f m_f^2 + \frac{s}{3}\left[\left(\frac{1}{2} - s_w^2\right)N_f + 4s_w^4 \sum_f c_f Q_f^2\right]\right\}\frac{1}{\bar{\epsilon}} + \Sigma_{ZZ}^{\text{fer},F}(s).\end{aligned}\quad (2.25)$$

In Eq. (2.25), $N_f = 24$ is the total number of fermions in the SM. We do not show explicit expressions for finite parts, marked with superscript F , because these might be trivially derived from Eq. (2.20) and Eqs. (2.23)–(2.24) by replacing complete expressions for B_f and B_0 with their finite parts B_f^F and B_0^F , correspondingly.

2.1.2 W boson self-energy

Next we consider the W boson self-energy, which is described, in the R_ξ gauge, by 17 diagrams, shown in Fig. 3.

First, we present an explicit expression for its bosonic component:

$$\begin{aligned}\Sigma_{WW}^{\text{bos}}(s) &= M_W^2 \left\{ -\frac{19}{6} \frac{1}{R_W} - \frac{1}{4} \left[\frac{6}{r_{HW}} \left(\frac{1}{c_W^4} + 2 \right) - \frac{3}{c_W^2} + 10 + 3r_{HW} \right] \right\} \frac{1}{\bar{\epsilon}} \\ &\quad + \Sigma_{WW}^{\text{bos},F}(s),\end{aligned}\quad (2.26)$$

where

$$\begin{aligned}\Sigma_{WW}^{\text{bos},F}(s) &= \frac{M_W^2}{12} \left\{ \left[(1 - 40c_W^2) \frac{1}{R_W} + 2 \left(\frac{5}{c_W^2} - 27 - 8c_W^2 \right) \right. \right. \\ &\quad \left. \left. + \frac{s_W^4}{c_W^2} \left(\frac{1}{c_W^2} + 8 \right) R_W \right] B_0^F(-s; M_W, M_Z) \right. \\ &\quad \left. + \left[\frac{1}{R_W} + 2(5 - r_{HW}) + (1 - r_{HW})^2 R_W \right] B_0^F(-s; M_W, M_H) \right. \\ &\quad \left. - 8s_W^2 \left(\frac{5}{R_W} + 2 - R_W \right) B_0^F(-s; M_W, 0) \right. \\ &\quad \left. + r_{HW} \left[7 - (1 - r_{HW}) R_W \right] L_\mu(M_H^2) \right. \\ &\quad \left. + \frac{1}{c_W^2} \left[\frac{18}{r_{HW}} \frac{1}{c_W^2} + 1 - 16c_W^2 + s_W^2 \left(\frac{1}{c_W^2} + 8 \right) R_W \right] L_\mu(M_Z^2) \right. \\ &\quad \left. + \left[2 \left(\frac{18}{r_{HW}} - 7 \right) - \left(\frac{1}{c_W^2} - 2 + r_{HW} \right) R_W \right] L_\mu(M_W^2) \right. \\ &\quad \left. - \frac{4}{3} \frac{1}{R_W} - 12 \left(\frac{1}{2} \frac{1}{c_W^4} + 1 \right) \frac{1}{r_{HW}} - 3 \left(\frac{1}{c_W^2} + 2 \right) - 9r_{HW} \right. \\ &\quad \left. - \left[\left(\frac{1}{c_W^2} + 6s_W^2 \right) \frac{1}{c_W^2} - r_{HW} (2 - r_{HW}) \right] R_W \right\}.\end{aligned}\quad (2.27)$$

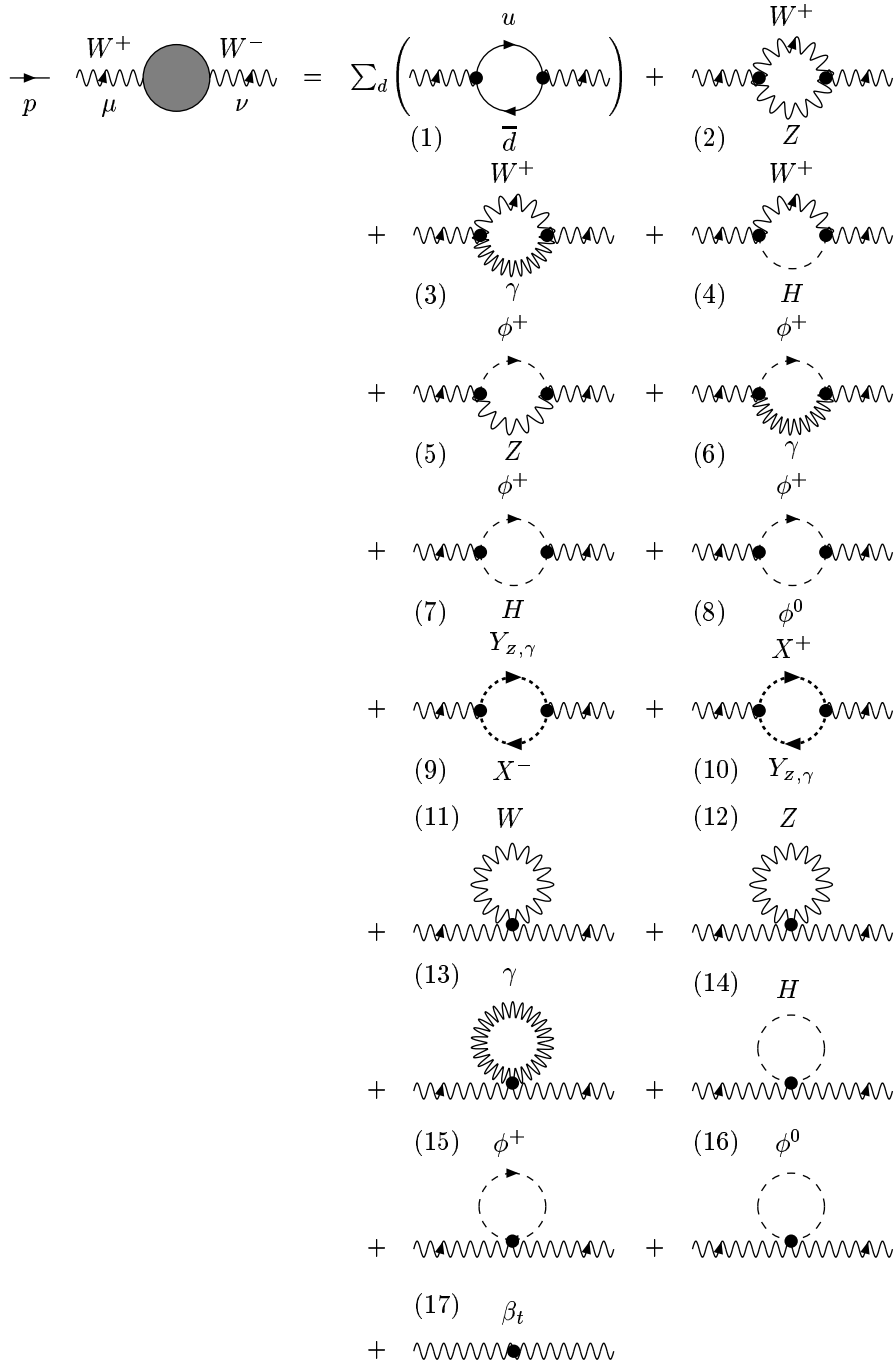


Figure 3: W boson self-energy.

Secondly, we give its fermionic component:

$$\Sigma_{ww}^{\text{fer}}(s) = -s \sum_{f=d} c_f B_f(-s; m_{f'}, m_f) + \sum_f c_f m_f^2 B_1(-s; m_{f'}, m_f), \quad (2.28)$$

where summation in the first term extends to all *doublets* of the SM.

2.1.3 Bosonic self-energies and counterterms

Bosonic self-energies and transitions enter one-loop amplitudes either directly through the functions $\mathcal{D}_z(s)$, $\Pi_{\gamma\gamma}(s)$ and $\Pi_{z\gamma}(s)$, or by means of bosonic counterterms, which are made of self-energy functions at zero argument, owing to *electric charge renormalization*, or at $p^2 = -M^2$, that is on a mass shell, owing to *on-mass-shell renormalization* (OMS scheme).

- Electric charge renormalization

The electric charge renormalization introduces the quantity $z_\gamma - 1$:

$$(z_\gamma - 1) = s_w^2 \left[\Pi_{\gamma\gamma}(0) - \frac{2}{M_W^2} \overline{\Sigma}_{3Q}(0) \right], \quad (2.29)$$

with bosonic (see Eq. (6.161) of [11]):

$$(z_\gamma - 1)^{\text{bos}} = s_w^2 \left[3 \left(\frac{1}{\bar{\epsilon}} - L_\mu(M_W^2) \right) + \frac{2}{3} \right], \quad (2.30)$$

and fermionic

$$(z_\gamma - 1)^{\text{fer}} = s_w^2 \left[\left(-\frac{4}{3} \sum_f c_f Q_f^2 \right) \frac{1}{\bar{\epsilon}} + \Pi_{\gamma\gamma}^{\text{fer},F}(0) \right] \quad (2.31)$$

components.

- ρ -parameter

Finally, two self-energy functions enter Veltman's parameter $\Delta\rho$, a gauge-invariant combination of self-energies, which naturally appears in the one-loop calculations:

$$\Delta\rho = \frac{1}{M_W^2} \left[\Sigma_{ww}(M_W^2) - \Sigma_{zz}(M_Z^2) \right], \quad (2.32)$$

with individual components where we explicitly show the pole parts:

$$\Delta\rho^{\text{bos}} = \left(-\frac{1}{6c_w^2} - \frac{41}{6} + 7c_w^2 \right) \frac{1}{\bar{\epsilon}} + \Delta\rho^{\text{bos},F}, \quad (2.33)$$

$$\Delta\rho^{\text{fer}} = \frac{1}{3} \frac{s_w^2}{c_w^2} \left(\frac{1}{2} N_f - 4s_w^2 \sum_f c_f Q_f^2 \right) \frac{1}{\bar{\epsilon}} + \Delta\rho^{\text{fer},F}. \quad (2.34)$$

The finite part of $\Delta\rho^{\text{bos}}$ is given explicitly by

$$\begin{aligned}
\Delta\rho^{\text{bos},F} &= \left(\frac{1}{12c_W^4} + \frac{4}{3c_W^2} - \frac{17}{3} - 4c_W^2 \right) \\
&\times \left[B_0^F(-M_W^2; M_W, M_Z) - c_W^2 B_0^F(-M_Z^2; M_W, M_W) \right] \\
&+ \left(1 - \frac{1}{3}r_{HW} + \frac{1}{12}r_{HW}^2 \right) B_0^F(-M_W^2; M_W, M_H) \\
&- \left(1 - \frac{1}{3}r_{HZ} + \frac{1}{12}r_{HZ}^2 \right) \frac{1}{c_W^2} B_0^F(-M_Z^2; M_Z, M_H) \\
&- 4s_W^2 B_0^F(-M_W^2; M_W, 0) \\
&+ \frac{1}{12} \left[\left(\frac{1}{c_W^4} + \frac{6}{c_W^2} - 24 + r_{HW} \right) L_\mu(M_Z^2) \right. \\
&- \left. \left(\frac{1}{c_W^2} + 14 + 16c_W^2 - 48c_W^4 + r_{HW} \right) L_\mu(M_W^2) \right. \\
&\left. + s_W^2 r_{HW}^2 \left[L_\mu(M_H^2) - 1 \right] - \frac{1}{c_W^4} - \frac{19}{3c_W^2} + \frac{22}{3} \right], \quad (2.35)
\end{aligned}$$

while the finite part of $\Delta\rho^{\text{fer}}$ is not shown, since it is trivially derived from the defining equation (2.32) by replacing the total self-energies with their finite parts.

2.2 Fermionic self-energies

2.2.1 Fermionic self-energy diagrams

The total self-energy function of a fermion in the R_ξ gauge is described by the six diagrams of Fig. 4.

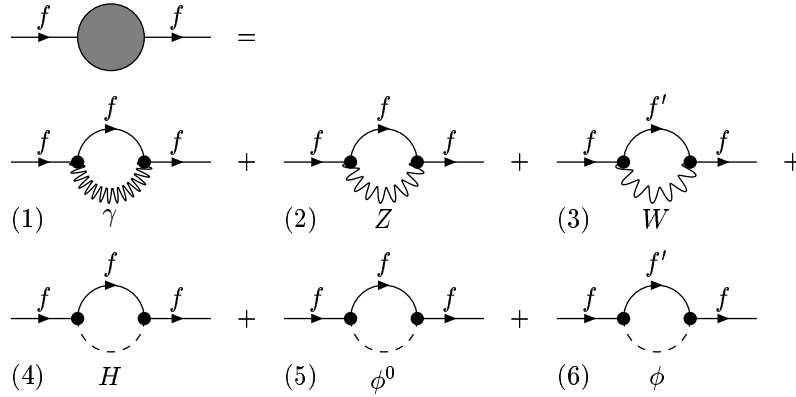


Figure 4: Fermionic self-energy diagrams.

A detailed calculation of the wave-function renormalization factors $\sqrt{z_{L,R}}$ associated with these diagrams may be found, for instance, in [5].

It is convenient to distinguish the electromagnetic components,

$$(\sqrt{z_L} - I)_f^{em} = (\sqrt{z_R} - I)_f^{em} = s_w^2 Q_f^2 \left(-\frac{1}{2\bar{\epsilon}} + \frac{1}{\bar{\epsilon}} + \frac{3}{2} \ln \frac{m_f^2}{\mu^2} - 2 \right), \quad (2.36)$$

and the weak components,

$$\left| \sqrt{z_{L,R}} \right| - I = (w_v \pm w_a), \quad (2.37)$$

where five non-zero contributions are:

$$\begin{aligned} w_v^z = & -\frac{1}{8} \frac{1}{c_w^2} \left\{ (v_f^2 + a_f^2 + 2a_f^2 r_{fz}) \frac{1}{\bar{\epsilon}} + (v_f^2 + a_f^2) \left(\frac{1}{r_{fz}} \left[B_0^F(-m_f^2; M_Z, m_f) \right. \right. \right. \\ & + L_\mu(M_Z^2) - 1 \left. \left. \left. + 2(1 + 2r_{fz}) M_Z^2 B_{0p}(-m_f^2; m_f, M_Z) - L_\mu(m_f^2) \right) \right. \right. \\ & + 2a_f^2 r_{fz} \left(\frac{1}{r_{fz}} \left[B_0^F(-m_f^2; M_Z, m_f) + L_\mu(M_Z^2) - 1 \right] \right. \\ & \left. \left. - 6M_Z^2 B_{0p}(-m_f^2; m_f, M_Z) - L_\mu(m_f^2) + 1 \right) \right\}, \quad (2.38) \end{aligned}$$

$$\begin{aligned} w_v^w = & -\frac{1}{16} \left\{ \frac{1}{\bar{\epsilon}} (2 + r^+) - r^+ + \frac{1}{r_{fw}} \left[(2 + r^+) \left[L_\mu(M_W^2) - r_{f'w} L_\mu(m_{f'}^2) \right] \right. \right. \\ & + (2 + 2r_{fw} + r^- + r^+ r^-) \left[B_0^F(-m_f^2; M_W, m_{f'}) - 1 \right] \left. \left. + 2M_W^2 \left[2 - r^+ - (r^-)^2 \right] B_{0p}(-m_f^2; M_W, m_{f'}) \right\}, \quad (2.39) \end{aligned}$$

$$\begin{aligned} w_v^H = & -\frac{1}{16} r_{fw} \left\{ \frac{1}{\bar{\epsilon}} + r_{Hf} \left[B_0^F(-m_f^2; M_H, m_f) + L_\mu(M_H^2) - 1 \right] \right. \\ & \left. - 2(4r_{fH} - 1) M_H^2 B_{0p}(-m_f^2; m_f, M_H) - L_\mu(m_f^2) + 1 \right\}, \quad (2.40) \end{aligned}$$

$$\begin{aligned} w_a^z = & -\frac{1}{4c_w^2} v_f a_f \left\{ \frac{1}{\bar{\epsilon}} - \frac{1}{r_{fz}} \left[B_0^F(-m_f^2; M_Z, m_f) + L_\mu(M_Z^2) - 1 \right] \right. \\ & \left. + 2B_0^F(-m_f^2; M_Z, m_f) + L_\mu(m_f^2) - 2 \right\}, \quad (2.41) \end{aligned}$$

$$\begin{aligned} w_a^w = & \frac{1}{16} \left\{ -\frac{1}{\bar{\epsilon}} (2 - r^-) + r^- + \frac{1}{r_{fw}} \left[(2 - r^-) \left[L_\mu(M_W^2) - r_{f'w} L_\mu(m_{f'}^2) \right] \right. \right. \\ & \left. \left. + (2 - 2r_{fw} - r^+ + r^+ r^-) \left[B_0^F(-m_f^2; M_W, m_{f'}) - 1 \right] \right\}, \quad (2.42) \end{aligned}$$

with $r^\pm = r_{fw} \pm r_{f'w}$ and f' being the weak isospin partner of fermion f .

2.3 The $Zf\bar{f}$ and $\gamma f\bar{f}$ vertices

Consider now the sum of all vertices and corresponding counterterms whose contribution originates from the fermionic self-energy diagrams of Fig. 4. This sum is shown in Fig. 5.

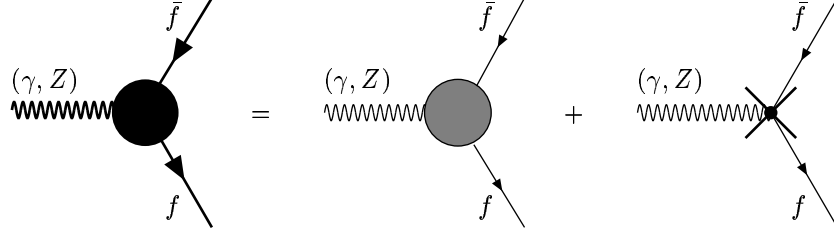


Figure 5: $Zf\bar{f}$ and $\gamma f\bar{f}$ vertices with fermionic counterterms.

The formulae which determine the counterterms are:

$$F_Q^{\gamma,ct} = 2(\sqrt{z_R} - I), \quad (2.43)$$

$$F_L^{\gamma,ct} = (\sqrt{z_L} - I) - (\sqrt{z_R} - I), \quad (2.44)$$

$$F_Q^{z,ct} = \delta_f^2 (\sqrt{z_R} - I), \quad (2.45)$$

$$F_L^{z,ct} = \sigma_f^2 (\sqrt{z_R} - I) - \delta_f^2 (\sqrt{z_R} - I), \quad (2.46)$$

where

$$\delta_f = v_f - a_f, \quad \sigma_f = v_f + a_f. \quad (2.47)$$

For the sum of all $\gamma \rightarrow f\bar{f}$ and $Z \rightarrow f\bar{f}$ vertices (the *total* $\gamma(Z)f\bar{f}$ vertex depicted by a grey circle in Fig. 5) we use the standard normalization

$$i\pi^2 = (2\pi)^4 i \frac{1}{16\pi^2}, \quad (2.48)$$

and define

$$V_\mu^\gamma(s) = (2\pi)^4 i \frac{1}{16\pi^2} G_\mu(s), \quad (2.49)$$

$$V_\mu^Z(s) = (2\pi)^4 i \frac{1}{16\pi^2} Z_\mu(s), \quad (2.50)$$

while we denote the individual vertices as follows:

$$G_\mu(s) = G_\mu^A(s) + G_\mu^Z(s) + G_\mu^W(s) + G_\mu^H(s), \quad (2.51)$$

$$Z_\mu(s) = Z_\mu^A(s) + Z_\mu^Z(s) + Z_\mu^W(s) + Z_\mu^H(s). \quad (2.52)$$

All vertices have three components in our LQD basis.

2.3.1 Scalar form factors

Now we construct the $24 = (4 : B = A, Z, H, W \text{-virtual}) \otimes (3 : L, Q, D) \otimes (2 : \gamma, Z \text{-incoming})$ scalar form factors, originating from the diagrams of Fig. 5. They are derived from the following six equations — three projections for $\gamma f \bar{f}$ vertices:

$$F_L^{\gamma B}(s) = \frac{2}{s_w I_f^{(3)}} \left\{ G_\mu^B(s) [i g^3 \gamma_\mu \gamma_+] + s_w Q_f F_L^{\gamma, ct} \right\}, \quad (2.53)$$

$$F_Q^{\gamma B}(s) = \frac{1}{s_w Q_f} \left\{ G_\mu^B(s) [i g^3 \gamma_\mu] + s_w Q_f F_Q^{\gamma, ct} \right\}, \quad (2.54)$$

$$F_D^{\gamma B}(s) = \frac{2}{s_w I_f^{(3)}} G_\mu^B(s) [g^3 m_t I D_\mu], \quad (2.55)$$

and three projections for $Z f \bar{f}$ vertices:

$$F_L^{z B}(s) = \frac{2c_w}{I_f^{(3)}} \left\{ Z_\mu^B(s) [i g^3 \gamma_\mu \gamma_+] + \frac{1}{c_w} F_L^{z, ct} \right\}, \quad (2.56)$$

$$F_Q^{z B}(s) = \frac{2c_w}{\delta_f} \left\{ Z_\mu^B(s) [i g^3 \gamma_\mu] + \frac{1}{c_w} F_Q^{z, ct} \right\}, \quad (2.57)$$

$$F_D^{z B}(s) = \frac{2c_w}{I_f^{(3)}} Z_\mu^B(s) [g^3 m_t I D_\mu]. \quad (2.58)$$

Here we introduce the symbol [...] for the definition of the procedure of the projection of $G_\mu(s)$ and $Z_\mu(s)$ to our basis. It has the same meaning as in form language [26], namely, e.g. $G_\mu^B(s) [i g^3 \gamma_\mu \gamma_+]$ means that only the coefficient of $[i g^3 \gamma_\mu \gamma_+]$ of the whole expression $G_\mu^B(s)$ is taken (*projected*).

The factors $1/(Q_f s_w)$, $2/(s_w I_f^{(3)})$ and $2c_w^2/(s_w I_f^{(3)})$ for $\gamma f \bar{f}$ vertices, and the factors $2c_w/I_f^{(3)}$, $2c_w/\delta_f$ and $2c_w/I_f^{(3)}$ for $Z f \bar{f}$ are due to the form factor definitions of Eq. (1.10).

The total $\gamma f \bar{f}$ and $Z f \bar{f}$ form factors are sums over four bosonic contributions $B = A, Z, W, H$. All 24 components of the total scalar form factors in the LQD basis look like:

$$F_{L,Q,D}^{\gamma(z)ff}(s) = F_{L,Q,D}^{\gamma(z)A}(s) + F_{L,Q,D}^{\gamma(z)Z}(s) + F_{L,Q,D}^{\gamma(z)W}(s) + F_{L,Q,D}^{\gamma(z)H}(s). \quad (2.59)$$

The quantities $F_{L,Q,D}^{\gamma(z)B}(s)$ originate from groups of diagrams, which we will call *clusters*.

2.4 Library of form factors for Bff clusters

Here we present a complete collection of scalar form factors $F_{L,Q,D}^{\gamma(z)B}(s)$ originating from a vertex diagram with a virtual vector boson, contribution of a scalar partner of this vector boson, and relevant counterterms.

Actually three gauge-invariant subsets of diagrams of this kind, A , Z and H , appear in our calculation. They may be termed *clusters*, since they are natural building blocks of the complete scalar form factors, which are the aim of our calculation. Again, in the spirit of our presentation, we write down their pole and finite parts.

The remaining vertices with virtual W and ϕ^+, ϕ^- with relevant counter-terms we also define as the W cluster. However, the latter diagrams do not form a gauge-invariant subset.

We note, that $F_L^{\gamma A}(s)$ and $F_L^{\gamma H}(s)$ are equal to zero.

2.4.1 Library of QED form factors for Att clusters

Up to the one-loop level, there are two diagrams that contribute to the A cluster, see Fig. 6.

Separating out pole contributions $1/\bar{\epsilon}$, we define finite (calligraphic) quantities. We note that, if a form factor $F_A^{ij}(s)$ has a pole, then the corresponding finite part $\mathcal{F}_A^{ij}(s)$ is μ -dependent.

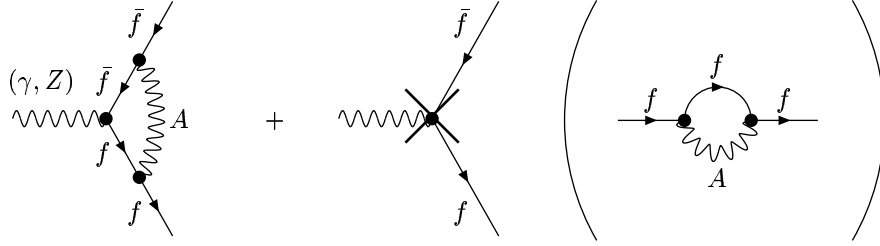


Figure 6: A cluster. The fermionic self-energy diagram in brackets gives rise to the counter term contribution depicted by the solid cross.

Since the scalar form factors of A cluster become UV-finite after wave function renormalization, for all form factors, which are also separately gauge-invariant, we have:

$$F_{L,Q,D}^{\gamma(z)A} = \mathcal{F}_{L,Q,D}^{\gamma(z)A}. \quad (2.60)$$

Individual components are:

$$\mathcal{F}_L^{\gamma A} = 0,$$

$$\mathcal{F}_Q^{\gamma A} = Q_f^2 s_w^2 \left\{ 2(s - 2m_f^2) C_0(-m_f^2, -m_f^2, -s; m_f, 0, m_f) - 3B_0^F(-s; m_f, m_f) + 3B_0^F(-m_f^2; m_f, 0) - 4m_f^2 B_{0p}^F(-m_f^2; 0, m_f) \right\},$$

$$\mathcal{F}_D^{\gamma A} = -\frac{Q_f^3 s_w^2}{I_f^{(3)}} \frac{4}{\Delta_{3r}} \left[B_0^F(-s; m_f, m_f) - B_0^F(-m_f^2; m_f, 0) \right],$$

$$\begin{aligned}
\mathcal{F}_L^{zA} &= \mathcal{F}_Q^{\gamma A} + Q_f^2 s_w^2 \frac{8m_f^2}{\Delta_{3r}} \left[B_0^F(-s; m_f, m_f) - B_0^F(-m_f^2; m_f, 0) \right], \\
\mathcal{F}_Q^{zA} &= \mathcal{F}_Q^{\gamma A} - Q_f^2 s_w^2 \frac{8m_f^2}{\Delta_{3r}} \frac{I_f^{(3)}}{\delta_f} \left[B_0^F(-s; m_f, m_f) - B_0^F(-m_f^2; m_f, 0) \right], \\
\mathcal{F}_D^{zA} &= -\frac{Q_f^2 s_w^2}{I_f^{(3)}} \frac{2v_f}{\Delta_{3r}} \left[B_0^F(-s; m_f, m_f) - B_0^F(-m_f^2; m_f, 0) \right], \quad (2.61)
\end{aligned}$$

with

$$\Delta_{3r} = 4m_f^2 - s. \quad (2.62)$$

2.4.2 Form factors of the Z cluster

The diagrams shown in Fig. 7 contribute to the Z cluster.

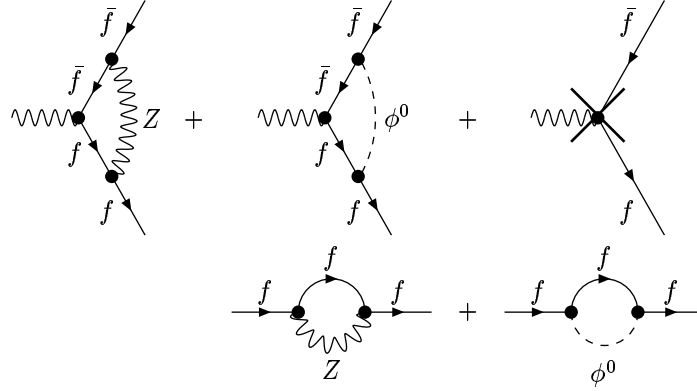


Figure 7: Z cluster. The two fermionic self-energy diagrams in the second row give rise to the counterterm contribution depicted by the solid cross in the last diagram of the first row.

Separating out pole contributions $1/\varepsilon$, we define finite quantities:

$$\begin{aligned}
F_L^{\gamma Z}(s) &= \mathcal{F}_L^{\gamma Z}(s), \\
F_Q^{\gamma Z}(s) &= \mathcal{F}_Q^{\gamma Z}(s), \\
F_D^{\gamma Z}(s) &= \mathcal{F}_D^{\gamma Z}(s), \\
F_L^{zZ}(s) &= -\frac{1}{4} r_{fw} \frac{1}{\varepsilon} + \mathcal{F}_L^{zZ}(s), \\
F_Q^{zZ}(s) &= -\frac{1}{16} \frac{1}{|Q_f| s_w^2} r_{fw} \frac{1}{\varepsilon} + \mathcal{F}_Q^{zZ}(s), \\
F_D^{zZ}(s) &= \mathcal{F}_D^{zZ}(s). \quad (2.63)
\end{aligned}$$

Here the finite parts are:

$$\begin{aligned} \mathcal{F}_L^{\gamma z}(s) = & \frac{1}{c_w^2} Q_f v_f \left\{ 2 \left(2 + \frac{1}{R_z} \right) M_z^2 C_0(-m_f^2, -m_f^2, -s; m_f, M_z, m_f) \right. \\ & - 3B_0^F(-s; m_f, m_f) + 2B_0^F(-m_f^2; m_f, M_z) - L_\mu(m_f^2) \quad (2.64) \\ & \left. + B_{d1}^F(-m_f^2; m_f, M_z) - 2(1 + 4r_{fz}) \frac{M_z^2}{\Delta_{3r}} L_{ab}(m_f, m_f, M_z) \right\}, \end{aligned}$$

$$\begin{aligned} \mathcal{F}_Q^{\gamma z}(s) = & \frac{1}{4c_w^2} \left\{ \delta_f^2 \left[\left(4(1 - r_{fz}) + \frac{2}{R_z} \right) M_z^2 C_0(-m_f^2, -m_f^2, -s; m_f, M_z, m_f) \right. \right. \\ & - 3B_0^F(-s; m_f, m_f) + 4B_0^F(-m_f^2; m_f, M_z) + L_\mu(M_z^2) - \frac{5}{2} \\ & \left. - r_{fz} B_{d2}^F(-m_f^2; m_f, M_z) - 2(1 + 2r_{fz}) M_z^2 B_{0p}(-m_f^2; m_f, M_z) \right] \\ & + 2v_f a_f r_{fz} \left[-4M_z^2 C_0(-m_f^2, -m_f^2, -s; m_f, M_z, m_f) \right. \\ & + 2(L_\mu(m_f^2) - L_\mu(M_z^2)) - 2(1 - r_{fz}) B_{d2}^F(-m_f^2; m_f, M_z) + 1 \\ & \left. - \frac{2}{r_{fz}} \left((1 + 2r_{fz}) M_z^2 B_{0p}(-m_f^2; m_f, M_z) + \frac{1}{2} \right) \right] \\ & + 2a_f^2 r_{fz} \left[B_0^F(-s; m_f, m_f) + L_\mu(M_z^2) - r_{fz} B_{d2}^F(-m_f^2; m_f, M_z) \right. \\ & \left. + 6M_z^2 B_{0p}(-m_f^2; m_f, M_z) - \frac{5}{2} \right] \\ & \left. - 4 \left[\frac{\delta_f^2}{2} - (4v_f a_f - a_f^2) r_{fz} \right] \frac{M_z^2}{\Delta_{3r}} L_{ab}(m_f, m_f, M_z) \right\}, \quad (2.65) \end{aligned}$$

$$\begin{aligned} \mathcal{F}_D^{\gamma z}(s) = & -\frac{2Q_f}{I_f^{(3)} c_w^2} \frac{1}{\Delta_{3r}} \left\{ \frac{v_f^2 + a_f^2}{2} \left[-4M_z^2 C_0(-m_f^2, -m_f^2, -s; m_f, M_z, m_f) \right. \right. \\ & + B_0^F(-s; m_f, m_f) - 2B_0^F(-m_f^2; m_f, M_z) - L_\mu(m_f^2) \\ & \left. + B_{d1}^F(-m_f^2; m_f, M_z) + 2 + 6 \frac{M_z^2}{\Delta_{3r}} L_{ab}(m_f, m_f, M_z) \right] \\ & + a_f^2 \left[2 \left(3r_{fz} - \frac{1}{R_z} \right) M_z^2 C_0(-m_f^2, -m_f^2, -s; m_f, M_z, m_f) \right. \\ & + B_0^F(-m_f^2; m_f, M_z) + L_\mu(M_z^2) - 1 \\ & \left. - r_{fz} \left[B_0^F(-s; m_f, m_f) + L_\mu(m_f^2) - 2 \right] \right. \\ & \left. \left. - 2 \left(2 - 3 \frac{m_f^2}{\Delta_{3r}} \right) L_{ab}(m_f, m_f, M_z) \right] \right\}, \quad (2.66) \end{aligned}$$

$$\begin{aligned}
\mathcal{F}_L^{zz}(s) = & \frac{1}{4c_w^2} \left\{ \frac{3v_f^2 + a_f^2}{3} \left[2 \left(3 \left(2 + \frac{1}{R_z} \right) - 2r_{fz} \right) \right. \right. \\
& \times M_z^2 C_0(-m_f^2, -m_f^2, -s; m_f, M_z, m_f) \\
& - 9B_0^F(-s; m_f, m_f) + 8B_0^F(-m_f^2; m_f, M_z) - L_\mu(m_f^2) - 2 \\
& \left. \left. + B_{d1}^F(-m_f^2; m_f, M_z) - 2(1 + 2r_{fz}) M_z^2 B_{0p}(-m_f^2; m_f, M_z) \right] \right. \\
& - \frac{2}{3} a_f^2 \left[4m_f^2 C_0(-m_f^2, -m_f^2, -s; m_f, M_z, m_f) \right. \\
& + 3r_{fz} \left[B_0^F(-s; m_f, m_f) + L_\mu(m_f^2) \right] + B_0^F(-m_f^2; m_f, M_z) \\
& + 3L_\mu(M_z^2) + 2L_\mu(m_f^2) - 1 + 2B_{d1}^F(-m_f^2; m_f, M_z) \\
& \left. + 2(1 - 7r_{fz}) M_z^2 B_{0p}(-m_f^2; m_f, M_z) \right] \\
& \left. - 2 \left[(3v_f^2 + a_f^2)(1 + 4r_{fz}) - 2a_f^2 r_{fz} \right] \frac{M_z^2}{\Delta_{3r}} L_{ab}(m_f, m_f, M_z) \right\}, \tag{2.67}
\end{aligned}$$

$$\begin{aligned}
\mathcal{F}_Q^{zz}(s) = & \frac{1}{c_w^2} \left\{ \frac{1}{4} \delta_f^2 \left[2 \left(2 - 2r_{fz} + \frac{1}{R_z} \right) M_z^2 C_0(-m_f^2, -m_f^2, -s; m_f, M_z, m_f) \right. \right. \\
& - 3B_0^F(-s; m_f, m_f) + 4B_0^F(-m_f^2; m_f, M_z) + L_\mu(m_f^2) - 2 \\
& - B_{d1}^F(-m_f^2; m_f, M_z) - 2(1 + 2r_{fz}) M_z^2 B_{0p}(-m_f^2; m_f, M_z) \\
& \left. - 2 \frac{M_z^2}{\Delta_{3r}} L_{ab}(m_f, m_f, M_z) \right] \\
& + a_f r_{fz} \left(v_f \left[-2M_z^2 C_0(-m_f^2, -m_f^2, -s; m_f, M_z, m_f) \right. \right. \\
& \left. \left. + \frac{1}{r_{fz}} \left[B_0^F(-m_f^2; m_f, M_z) + L_\mu(m_f^2) - 1 - B_{d1}^F(-m_f^2; m_f, M_z) \right. \right. \right. \\
& \left. \left. - (1 + 2r_{fz}) M_z^2 B_{0p}(-m_f^2; m_f, M_z) \right] + 6 \frac{M_z^2}{\Delta_{3r}} L_{ab}(m_f, m_f, M_z) \right] \\
& - \frac{1}{2} a_f \left[8M_z^2 C_0(-m_f^2, -m_f^2, -s; m_f, M_z, m_f) \right. \\
& - B_0^F(-s; m_f, m_f) - L_\mu(m_f^2) + 2 + B_{d1}^F(-m_f^2; m_f, M_z) \\
& \left. - 6M_z^2 B_{0p}(-m_f^2; m_f, M_z) - 10 \frac{M_z^2}{\Delta_{3r}} L_{ab}(m_f, m_f, M_z) \right] \\
& - \frac{a_f^2}{\delta_f} \left[4M_z^2 C_0(-m_f^2, -m_f^2, -s; m_f, M_z, m_f) \right. \\
& \left. \left. - B_0^F(-s; m_f, m_f) + 1 - 6 \frac{M_z^2}{\Delta_{3r}} L_{ab}(m_f, m_f, M_z) \right] \right\}, \tag{2.68}
\end{aligned}$$

$$\begin{aligned}
\mathcal{F}_D^{zz}(s) = & -\frac{1}{2I_f^{(3)}c_W^2\Delta_{3r}}\left\{(3a_f^2+v_f^2)v_f\right. \\
& \times \left[-4M_z^2C_0(-m_f^2,-m_f^2,-s;m_f,M_z,m_f)\right. \\
& + B_0^F(-s;m_f,m_f) - 2B_0^F(-m_f^2;m_f,M_z) - L_\mu(m_f^2) + 2 \\
& + B_{d1}^F(-m_f^2;m_f,M_z) + 6\frac{M_z^2}{\Delta_{3r}}L_{ab}(m_f,m_f,M_z)\left. \right] \\
& + 2v_f a_f^2 \left[2 \left(7r_{fz} - 2\frac{1}{R_z} \right) M_z^2 C_0(-m_f^2,-m_f^2,-s;m_f,M_z,m_f) \right. \\
& + B_0^F(-m_f^2;m_f,M_z) + L_\mu(M_z^2) - 1 \\
& - r_{fz} \left[B_0^F(-s;m_f,m_f) + L_\mu(m_f^2) - 2 \right] \\
& \left. \left. - 2 \left(4 - 3\frac{m_f^2}{\Delta_{3r}} \right) L_{ab}(m_f,m_f,M_z) \right] \right\}. \tag{2.69}
\end{aligned}$$

In Eq. (2.65) the ‘once and twice subtracted’ functions B_{d1}^F and B_{d2}^F are met:

$$\begin{aligned}
B_{d1}^F(-m_f^2;m_f,M_z) &= \frac{1}{r_{fz}} \left[B_0^F(-m_f^2;m_f,M_z) + L_\mu(M_z^2) - 1 \right], \tag{2.70} \\
B_{d2}^F(-m_f^2;m_f,M_z) &= \frac{1}{r_{fz}^2} \left[B_0^F(-m_f^2;m_f,M_z) + L_\mu(M_z^2) - 1 \right. \\
&\quad \left. - r_{fz} \left(L_\mu(m_f^2) - L_\mu(M_z^2) + \frac{1}{2} \right) \right].
\end{aligned}$$

They remain finite in the limit $m_f \rightarrow 0$.

We note that, for the Z cluster, all the six scalar form factors $F_{L,Q,D}^{\gamma(z)Z}(s)$ are *separately* gauge-invariant.

2.4.3 Form factors of the H cluster

The diagrams of Fig. 8 contribute to the H cluster. Separating UV poles, we have:

$$\begin{aligned}
F_Q^{\gamma H}(s) &= \mathcal{F}_Q^{\gamma H}(s), \\
F_D^{\gamma H}(s) &= \mathcal{F}_D^{\gamma H}(s), \\
F_L^{zH}(s) &= \frac{1}{4}r_{fw}\frac{1}{\bar{\epsilon}} + \mathcal{F}_L^{zH}(s), \\
F_Q^{zH}(s) &= \frac{1}{16}\frac{1}{|Q_f|}r_{fw}\frac{1}{s_W^2}\frac{1}{\bar{\epsilon}} + \mathcal{F}_Q^{zH}(s), \\
F_D^{zH}(s) &= \mathcal{F}_D^{zH}(s), \tag{2.71}
\end{aligned}$$

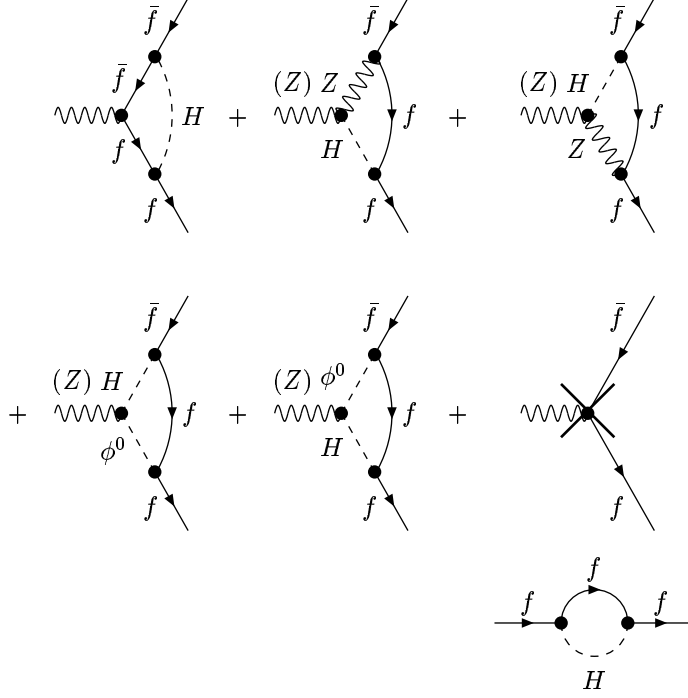


Figure 8: H cluster: the vertices and the counterterm.

with the finite parts:

$$\begin{aligned}
\mathcal{F}_Q^{\gamma H}(s) = & \frac{1}{8} r_{fw} \left\{ 8m_f^2 C_0(-m_f^2, -m_f^2, -s; m_f, M_H, m_f) \right. \\
& + B_0^F(-s; m_f, m_f) + L_\mu(m_f^2) - 2 - B_{d1}^F(-m_f^2; m_f, M_H) \\
& - 2(1 - 4r_{fH}) M_H^2 B_{0p}(-m_f^2; m_f, M_H) \\
& \left. - 2 \frac{M_H^2}{\Delta_{3r}} L_{ab}(m_f, m_f, M_H) \right\}, \quad (2.72)
\end{aligned}$$

$$\begin{aligned}
\mathcal{F}_D^{\gamma H}(s) = & - \frac{Q_t}{2I_f^{(3)}} \frac{r_{fw}}{\Delta_{3r}} \left\{ -6M_H^2 C_0(-m_f^2, -m_f^2, -s; m_f, M_H, m_f) \right. \\
& + 3B_0^F(-s; m_f, m_f) - 4B_0^F(-m_f^2; m_f, M_H) - L_\mu(m_f^2) \\
& \left. + 2 + B_{d1}^F(-m_f^2; m_f, M_H) + 6 \frac{M_H^2}{\Delta_{3r}} L_{ab}(m_f, m_f, M_H) \right\}, \quad (2.73)
\end{aligned}$$

$$\begin{aligned}
\mathcal{F}_L^{zH}(s) = & \frac{1}{4} r_{fw} \left\{ 4m_f^2 C_0(-m_f^2, -m_f^2, -s; m_f, M_H, m_f) \right. \\
& + \left[4(1-r_{fz}) + (1-r_{Hz})^2 R_z \right] \\
& \quad \times M_z^2 C_0(-m_f^2, -m_f^2, -s; M_H, m_f, M_z) \\
& + 2B_0^F(-s; M_z, M_H) - \frac{1}{2} B_0^F(-s; m_f, m_f) + \frac{1}{2} L_\mu(m_f^2) + 2 \\
& - \frac{1}{2} B_{d1}^F(-m_f^2; m_f, M_H) - (1-4r_{fH}) M_H^2 B_{0p}(-m_f^2; m_f, M_H) \\
& + (1-r_{Hz}) R_z \left[B_0^F(-m_f^2; M_z, m_f) - B_0^F(-m_f^2; m_f, M_H) \right] \\
& + \frac{M_z^2}{\Delta_{3r}} \left[(r_{Hz} - 8r_{fz}) L_{ab}(m_f, m_f, M_H) \right. \\
& \left. - 2(3-r_{Hz} + 4r_{fz}) L_{Hi}(m_f, M_H, M_z) \right] \left. \right\}, \tag{2.74}
\end{aligned}$$

$$\begin{aligned}
\mathcal{F}_Q^{zH}(s) = & r_{fw} \left\{ m_f^2 C_0(-m_f^2, -m_f^2, -s; m_f, M_H, m_f) \right. \\
& + \left[1 + (1-r_{Hz}) R_z \right] M_z^2 C_0(-m_f^2, -m_f^2, -s; M_H, m_f, M_z) \\
& + \frac{1}{8} \left[B_0^F(-s; m_f, m_f) + L_\mu(m_f^2) - 2 \right] \\
& + R_z \left[B_0^F(-m_f^2; M_z, m_f) - B_0^F(-m_f^2; m_f, M_H) \right] \\
& - \frac{1}{8} B_{d1}^F(-m_f^2; m_f, M_H) - \frac{1}{4} (1-4r_{fH}) M_H^2 B_{0p}(-m_f^2; m_f, M_H) \\
& - \frac{1}{4} \frac{M_H^2}{\Delta_{3r}} L_{ab}(m_f, m_f, M_H) \\
& + \frac{1}{4} \frac{a_f}{\delta_f} \left(\left[4r_{fz} + (3+r_{Hz})(1-r_{Hz}) R_z \right] \right. \\
& \quad \left. \times M_z^2 C_0(-m_f^2, -m_f^2, -s; M_H, m_f, M_z) \right. \\
& + B_0^F(-s; m_f, m_f) - 2B_0^F(-s; M_z, M_H) - 3 \\
& + (3+r_{Hz}) R_z \left[B_0^F(-m_f^2; M_z, m_f) - B_0^F(-m_f^2; m_f, M_H) \right] \\
& - 2 \frac{M_z^2}{\Delta_{3r}} \left[(1-4r_{fH}) r_{Hz} L_{ab}(m_f, m_f, M_H) \right. \\
& \left. \left. - (3-r_{Hz} + 4r_{fz}) L_{Hi}(m_f, M_H, M_z) \right] \right) \left. \right\}, \tag{2.75}
\end{aligned}$$

$$\begin{aligned}
\mathcal{F}_D^{zH}(s) = & -\frac{v_f}{2I_f^{(3)}c_W^2\Delta_{3r}} \left\{ -3r_{fz}M_H^2C_0(-m_f^2, -m_f^2, -s; m_f, M_H, m_f) \right. \\
& + 2 \left[2(r_{Hz} - 1) \frac{m_f^2}{s} - r_{Hz} + 2r_{fz} \right] \\
& \quad \times M_Z^2C_0(-m_f^2, -m_f^2, -s; M_H, m_f, M_Z) \\
& - 4 \frac{m_f^2}{s} \left[B_0^F(-m_f^2; M_Z, m_f) - B_0^F(-m_f^2; m_f, M_H) \right] \\
& - 2B_0^F(-s; M_Z, M_H) + 2B_0^F(-m_f^2; M_Z, m_f) \\
& + \frac{3}{2}r_{fz} \left[B_0^F(-s; m_f, m_f) - B_0^F(-m_f^2; m_f, M_H) \right] \\
& + \frac{1}{2}r_{Hz} \left[B_0^F(-m_f^2; m_f, M_H) + L_\mu(M_H^2) - 1 \right] \\
& - \frac{1}{2}r_{fz} \left[B_0^F(-m_f^2; m_f, M_H) + L_\mu(m_f^2) - 2 \right] \\
& \left. + 3r_{fz} \frac{M_H^2}{\Delta_{3r}} L_{ab}(m_f, m_f, M_H) \right\}. \tag{2.76}
\end{aligned}$$

Again, the five (one does not exist) scalar form factors in Eq. (2.71) are *separately* gauge-invariant. Note also that UV poles persisting in the scalar form factors of the H cluster cancel exactly the corresponding poles of the Z cluster. In other words, the form factors of the ‘neutral sector’ cluster ($Z+H$) are UV finite.

In total, we have 11 separately gauge-invariant *building blocks* that originate from Z and H clusters.

2.4.4 Form factors of the W cluster

Finally, the W cluster is made of the diagrams shown in Fig. 9.

In the formulae below, we present contributions to scalar form factors from all the diagrams of the W cluster, not subdividing them into abelian and non-abelian contributions. To some extent two sub-clusters are automatically marked by the type of arguments of C_0 functions and typical coupling constants. Separating poles, we have:

$$\begin{aligned}
F_L^{\gamma W}(s) &= 2\frac{1}{\bar{\epsilon}} + \mathcal{F}_L^{\gamma W}(s), \\
F_Q^{\gamma W}(s) &= \mathcal{F}_Q^{\gamma W}(s), \\
F_D^{\gamma W}(s) &= \mathcal{F}_D^{\gamma W}(s), \\
F_L^{zW}(s) &= 2c_W^2\frac{1}{\bar{\epsilon}} + \mathcal{F}_L^{zW}(s), \\
F_Q^{zW}(s) &= \mathcal{F}_Q^{zW}(s), \\
F_D^{zW}(s) &= \mathcal{F}_D^{zW}(s). \tag{2.77}
\end{aligned}$$

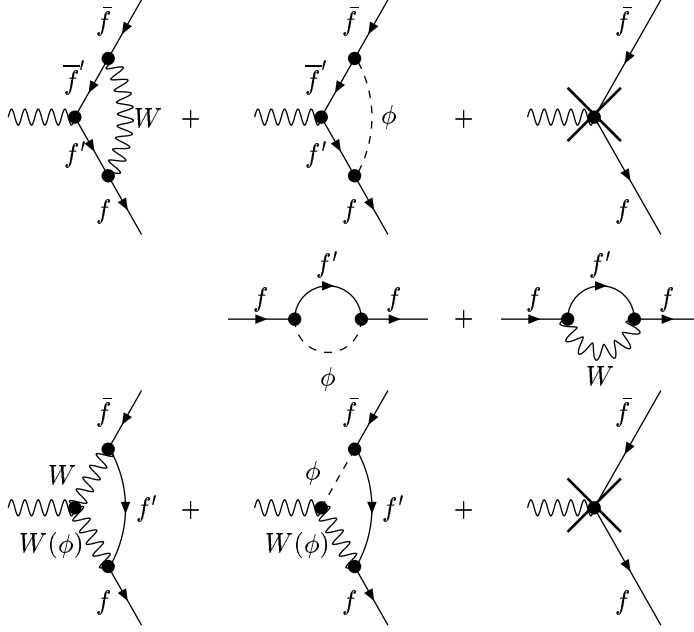


Figure 9: W cluster: the first row shows the abelian diagrams of the cluster, the last row the non-abelian diagrams; the second row shows diagrams that contribute to both counterterm crosses (last diagrams in first and third rows).

Here the finite parts are:

$$\begin{aligned}
\mathcal{F}_L^{\gamma W} = & \frac{Q_{f'}}{2I_f^{(3)}} \left\{ \left[3 + (1+r^-)^2 + \frac{2}{R_W} \right] M_W^2 C_0(-m_f^2, -m_f^2, -s; m_{f'}, M_W, m_{f'}) \right. \\
& - \frac{1}{2} (6+r^-) \left[B_0^F(-s; m_{f'}, m_{f'}) - B_0^F(-m_f^2; m_{f'}, M_W) \right] \\
& + \frac{1}{2} (2-r^-) \left[B_{dW}^F(-m_f^2; m_{f'}, M_W) - 1 \right] \\
& + \left[4 - (2+r^-)(3+3r_{fW} + r_{f'W}) \right] \frac{M_W^2}{\Delta_{3r}} L_{ab}(m_f, m_{f'}, M_W) \left. \right\} \\
& - r_{f'W} (2-r^-) M_W^2 C_0(-m_f^2, -m_f^2, -s; M_W, m_{f'}, M_W) \\
& + \frac{1}{2} (6-r^-) \left[B_0^F(-s; M_W, M_W) - B_0^F(-m_f^2; m_{f'}, M_W) \right] \\
& + 2B_0^F(-m_f^2; m_{f'}, M_W) + \frac{1}{2} (2-3r^-) \left[B_{dW}^F(-m_f^2; m_{f'}, M_W) + 1 \right] \\
& - \left(4 - \left[2 + r_{fW}(13+r_{fW}) - r_{f'W}(1+r_{f'W}) \right] \frac{M_W^2}{\Delta_{3r}} \right) \\
& \quad \quad \quad \times L_{na}(m_f, m_{f'}, M_W) \\
& - \frac{Q_f}{4I_f^{(3)}} (\Delta_{\mathcal{F}_{\text{Im}}} - 3) i \text{Im} B_0^F(-m_f^2; M_W, m_{f'}), \tag{2.78}
\end{aligned}$$

where $\Delta_{\mathcal{F}_{\text{im}}} = (1 - r_{f'w}) \frac{(2 + r_{f'w})}{r_{f'w}} + r_{f'w}$.

The last term in Eq. (2.78) is due to a non-cancellation of the imaginary part of the function $B_0^F(-m_f^2; M_W, m_{f'})$ which appear in real counterterms and complex-valued vertices.

$$\begin{aligned}
\mathcal{F}_Q^{\gamma W} = & \frac{r_{f'w}}{4Q_f} \left\{ Q_{f'} \left[-4M_W^2 C_0(-m_f^2, -m_f^2, -s; m_{f'}, M_W, m_{f'}) \right. \right. \\
& + B_0^F(-s; m_{f'}, m_{f'}) - B_0^F(-m_f^2; m_{f'}, M_W) - 1 \\
& - \frac{2 + r_{f'w}}{r_{f'w}} B_{dw}^F(-m_f^2; m_{f'}, M_W) \\
& - \left(\frac{(1 - r_{f'w})(2 + r_{f'w})}{r_{f'w}} - 1 - r_{f'w} + 2r_{f'w} \right) \\
& \quad \left. \times M_W^2 B_{0p}(-m_f^2; m_{f'}, M_W) \right. \\
& + 2(3 + r^-) \frac{M_W^2}{\Delta_{3r}} L_{ab}(m_f, m_{f'}, M_W) \left. \right] \\
& - 2I_f^{(3)} \left[2m_{f'}^2 C_0(-m_f^2, -m_f^2, -s; M_W, m_{f'}, M_W) \right. \\
& - B_0^F(-s; M_W, M_W) + B_0^F(-m_f^2; m_{f'}, M_W) - 1 \\
& + \frac{2 + r_{f'w}}{r_{f'w}} B_{dw}^F(-m_f^2; m_{f'}, M_W) \\
& + \left(\frac{2 - r_{f'w}(1 + r_{f'w})}{r_{f'w}} - 1 - r_{f'w} + 2r_{f'w} \right) \\
& \quad \left. \times M_W^2 B_{0p}(-m_f^2; m_{f'}, M_W) + 2(7 + r^+) \frac{M_W^2}{\Delta_{3r}} L_{na}(m_f, m_{f'}, M_W) \right] \left. \right\} \\
& + \frac{1}{4} \Delta_{\mathcal{F}_{\text{im}}} i \text{Im} B_0^F(-m_f^2; M_W, m_{f'}), \tag{2.79}
\end{aligned}$$

$$\begin{aligned}
\mathcal{F}_D^{\gamma W} = & -\frac{1}{\Delta_{3r}} \left\{ \frac{Q_{f'}}{2I_f^{(3)}} \left(-2 \left[8 + r^{-2} - 6r_{f'w} + \frac{2}{R_W} \right] \right. \right. \\
& \times M_W^2 C_0(-m_f^2, -m_f^2, -s; m_{f'}, M_W, m_{f'}) \\
& + (10 + r_{f'w} - 3r_{f'w}) \left[B_0^F(-s; m_{f'}, m_{f'}) - B_0^F(-m_f^2; m_{f'}, M_W) \right] \\
& + (2 + r^+) \left[B_{dw}^F(-m_f^2; m_{f'}, M_W) + 1 \right] \\
& + 6 \left[(1 + r_{f'w})(2 + r_{f'w}) - r_{f'w}(1 + r_{f'w}) \right] \frac{M_W^2}{\Delta_{3r}} L_{ab}(m_f, m_{f'}, M_W) \\
& + 2 \left[(1 - r^+)(2 - r_{f'w}) - r_{f'w} \left(1 - 4r_{f'w} - \frac{1}{R_W} \right) \right] \\
& \quad \left. \times M_W^2 C_0(-m_f^2, -m_f^2, -s; M_W, m_{f'}, M_W) \right.
\end{aligned}$$

$$\begin{aligned}
& + (6 - r_{fW} - 5r_{f'W}) \left[B_0^F(-s; M_W, M_W) - B_0^F(-m_f^2; m_{f'}, M_W) \right] \\
& + (2 + r^+) \left[B_{dW}^F(-m_f^2; m_{f'}, M_W) - 1 \right] \\
& - 6 \left[(1 - r_{fW})(2 + r_{fW}) - r_{f'W}(1 + 2r_{fW} + r_{f'W}) \right] \\
& \times \frac{M_W^2}{\Delta_{3r}} L_{na}(m_f, m_{f'}, M_W) \left. \right\}, \tag{2.80} \\
\mathcal{F}_L^{zW} = & \frac{\sigma_{f'}}{4I_f^{(3)}} \left\{ \left[3 + (1 + r^-)^2 + \frac{2}{R_W} \right] M_W^2 C_0(-m_f^2, -m_f^2, -s; m_{f'}, M_W, m_{f'}) \right. \\
& - \frac{1}{2} (6 + r^-) \left[B_0^F(-s; m_{f'}, m_{f'}) - B_0^F(-m_f^2; m_{f'}, M_W) \right] \\
& + \frac{1}{2} (2 - r^-) \left[B_{dW}^F(-m_f^2; m_{f'}, M_W) - 1 \right] \\
& + \left[4 - (2 + r^-)(3 + 3r_{fW} + r_{f'W}) \right] \frac{M_W^2}{\Delta_{3r}} L_{ab}(m_f, m_{f'}, M_W) \left. \right\} \\
& + r_{f'W} M_W^2 C_0(-m_f^2, -m_f^2, -s; m_{f'}, M_W, m_{f'}) \\
& + \frac{1}{4} \left\{ r^- B_0^F(-s; M_W, M_W) - r_{fW} \left[B_0^F(-m_f^2; m_{f'}, M_W) - 1 \right] \right. \\
& + r_{f'W} \left[B_0^F(-s; m_{f'}, m_{f'}) - 2 \right] - (2 + r_{f'W}) B_{dW}^F(-m_f^2; m_{f'}, M_W) \\
& - \left[(1 - r_{fW})(2 + r_{fW}) - r_{f'W}(1 - 2r_{fW} + r_{f'W}) \right] \\
& \times M_W^2 B_{0p}(-m_f^2; m_{f'}, M_W) \\
& - 2r_{f'W}(1 + r^-) \frac{M_W^2}{\Delta_{3r}} L_{ab}(m_f, m_{f'}, M_W) \left. \right\} \\
& - c_W^2 \left\{ \left(4(1 - r_{fW}) + \frac{1}{2} r_{f'W} \left[4 + \frac{s_W^2 - c_W^2}{c_W^2} (4 + r^-) \right] \right) \right. \\
& \times M_W^2 C_0(-m_f^2, -m_f^2, -s; M_W, m_{f'}, M_W) \\
& + \frac{1}{2} (2 + r^-) \left[B_0^F(-m_f^2; M_W, M_W) - B_0^F(-m_f^2; m_{f'}, M_W) \right] \\
& - \frac{1}{2} (2 - r^-) \left[B_{dW}^F(-m_f^2; m_{f'}, M_W) + 1 \right] - 2B_0^F(-m_f^2; m_{f'}, M_W) \\
& - \frac{1}{2} \left(4 + 12r_{fW} - \frac{s_W^2 - c_W^2}{c_W^2} r_{fW} (7 + r_{fW}) \right. \\
& \left. \left. - r_{f'W} \left[4 + \frac{s_W^2 - c_W^2}{c_W^2} (1 - r_{f'W}) \right] \right) \frac{M_W^2}{\Delta_{3r}} L_{na}(m_f, m_{f'}, M_W) \left. \right\}
\end{aligned}$$

$$+ \frac{1}{8I_f^{(3)}} \left(3\sigma_f - \delta_f \Delta_{\mathcal{F}_{\text{Im}}} \right) i \text{Im} B_0^F(-m_f^2; M_W, m_{f'}) , \quad (2.81)$$

$$\begin{aligned} \mathcal{F}_Q^{zw} = & -\frac{r_{f'w}}{4} \frac{\sigma_{f'}}{\delta_t} \left\{ 4M_W^2 C_0(-m_f^2, -m_f^2, -s; m_{f'}, M_W, m_{f'}) \right. \\ & - B_0^F(-s; m_{f'}, m_{f'}) + B_0^F(-m_f^2; m_{f'}, M_W) + 1 \\ & \left. - 2(3+r^-) \frac{M_W^2}{\Delta_{3r}} L_{ab}(m_f, m_{f'}, M_W) \right\} \\ & - \frac{1}{4} (2+r_{f'w}) B_{dw}^F(-m_f^2; m_{f'}, M_W) \\ & - \frac{1}{4} \left[(1-r_{f'w})(2+r^-) + r_{f'w} r^- \right] M_W^2 B_{0p}(-m_f^2; m_{f'}, M_W) \\ & + I_f^{(3)} c_w^2 \frac{r_{f'w}}{\delta_t} \left\{ \frac{s_w^2 - c_w^2}{c_w^2} \left(r_{f'w} M_W^2 C_0(-m_f^2, -m_f^2, -s; M_W, m_{f'}, M_W) \right. \right. \\ & \left. \left. - \frac{1}{2} \left[B_0^F(-s; M_W, M_W) - B_0^F(-m_f^2; m_{f'}, M_W) + 1 \right] \right) \right. \\ & \left. - \left[8 - \frac{s_w^2 - c_w^2}{c_w^2} (3+r_{f'w} + r_{f'w}) \right] \frac{M_W^2}{\Delta_{3r}} L_{na}(m_f, m_{f'}, M_W) \right\} \\ & + \frac{1}{4} \Delta_{\mathcal{F}_{\text{Im}}} i \text{Im} B_0^F(-m_f^2; M_W, m_{f'}) , \quad (2.82) \end{aligned}$$

$$\begin{aligned} \mathcal{F}_D^{zw} = & \frac{1}{\Delta_{3r}} \left\{ \frac{\sigma_{f'}}{2I_f^{(3)}} \left(\left[8 + (r^-)^2 - 6r_{f'w} + \frac{2}{R_w} \right] \right. \right. \\ & \times M_W^2 C_0(-m_f^2, -m_f^2, -s; m_{f'}, M_W, m_{f'}) \\ & - \frac{1}{2} (10+r_{f'w} - 3r_{f'w}) \left[B_0^F(-s; m_{f'}, m_{f'}) - B_0^F(-m_f^2; m_{f'}, M_W) \right] \\ & - \frac{1}{2} (2+r^+) \left[B_{dw}^F(-m_f^2; m_{f'}, M_W) + 1 \right] \\ & \left. - 3 \left[(1+r_{f'w})(2+r_{f'w}) - r_{f'w}(1+r_{f'w}) \right] \frac{M_W^2}{\Delta_{3r}} L_{ab}(m_f, m_{f'}, M_W) \right) \\ & + r_{f'w} \left(M_W^2 C_0(-m_f^2, -m_f^2, -s; m_{f'}, M_W, m_{f'}) \right. \\ & \left. + \frac{1}{2} \left[B_0^F(-s; m_{f'}, m_{f'}) - B_0^F(-m_f^2; m_{f'}, M_W) - 1 \right] \right. \\ & \left. - \frac{1}{2} B_{dw}^F(-m_f^2; m_{f'}, M_W) - 3(1+r^-) \frac{M_W^2}{\Delta_{3r}} L_{ab}(m_f, m_{f'}, M_W) \right) \\ & - c_w^2 \left(\left[4r_{f'w} - \frac{s_w^2 - c_w^2}{c_w^2} \right] \left((1-r_{f'w})(2-r_{f'w}) \right. \right. \end{aligned}$$

$$\begin{aligned}
& - r_{f'w} \left(5 - r_{fw} - 4r_{f'w} - \frac{1}{R_z} \right) \Big] \\
& \times M_w^2 C_0(-m_f^2, -m_f^2, -s; M_w, m_{f'}, M_w) \\
& + \frac{1}{2} \left[4 - \frac{s_w^2 - c_w^2}{c_w^2} (4 - r_{fw} - 5r_{f'w}) \right] \\
& \times \left[B_0^F(-s; M_w, M_w) - B_0^F(-m_f^2; m_{f'}, M_w) \right] \\
& + \frac{1}{2} \left(4 - \frac{s_w^2 - c_w^2}{c_w^2} r_{tb}^+ \right) \left[B_{dw}^F(-m_f^2; m_{f'}, M_w) - 1 \right. \\
& \left. - 6(1 - r^+) \frac{M_w^2}{\Delta_{3r}} L_{na}(m_f, m_{f'}, M_w) \right] \Big\}. \tag{2.83}
\end{aligned}$$

Here we introduce more ratios, which were not given in Eq. (2.10):

$$r^\pm = r_{fw} \pm r_{f'w}. \tag{2.84}$$

Furthermore, we used one more ‘subtracted’ function:

$$\begin{aligned}
B_{dw}^F(-m_f^2; m_{f'}, M_w) &= \frac{1}{r_{f'w}} \left\{ (1 - r_{f'w}) \left[B_0^F(-m_f^2; m_{f'}, M_w) \right. \right. \\
& \left. \left. + L_\mu(M_w^2) - 1 \right] - r_{f'w} \left[L_\mu(m_{f'}^2) - L_\mu(M_w^2) \right] \right\}, \tag{2.85}
\end{aligned}$$

and the three auxiliary functions:

$$\begin{aligned}
L_{ab}(M_1, M_2, M_3) &= (M_3^2 + M_1^2 - M_2^2) C_0(-m_f^2, -m_f^2, -s; M_2, M_3, M_2) \\
& - B_0^F(-s; M_2, M_2) + B_0^F(-m_f^2; M_2, M_3), \tag{2.86}
\end{aligned}$$

$$\begin{aligned}
L_{na}(M_1, M_2, M_3) &= (M_3^2 - M_1^2 - M_2^2) C_0(-m_f^2, -m_f^2, -s; M_3, M_2, M_3) \\
& + B_0^F(-s; M_3, M_3) - B_0^F(-m_f^2; M_3, M_2), \tag{2.87}
\end{aligned}$$

$$\begin{aligned}
L_{Hi}(M_1, M_2, M_3) &= \left[\frac{1}{2} (M_2^2 + M_3^2) - 2M_1^2 \right] \\
& \times C_0(-m_f^2, -m_f^2, -s; M_2, M_1, M_3) + B_0^F(-s; M_3, M_2) \\
& - \frac{1}{2} B_0^F(-m_f^2; M_1, M_2) - \frac{1}{2} B_0^F(-m_f^2; M_3, M_1). \tag{2.88}
\end{aligned}$$

Four scalar form factors, $\mathcal{F}_{Q,D}^{\gamma(z)W}$, as follows from calculations, are both gauge-invariant and finite, thus enlarging the number of gauge-invariant *building blocks* to 15. On the contrary, two form factors, $\mathcal{F}_L^{\gamma(z)W}$, are neither gauge-invariant nor finite. Gauge dependence on ξ , as well as UV poles, of L form factors cancel in the sum with the WW box and the self-energy contributions.

2.5 Library of scalar form factors in the limit $m_f = 0$

In the limit $m_f = 0$ only nine scalar form factors of vertex clusters give non-zero contributions: $F_Q^{\gamma A}$, $F_{L,Q}^{zA}$, $F_{L,Q}^{\gamma Z}$, $F_{L,Q}^{zZ}$ and $F_L^{\gamma,zW}$, which, in turn, may be expressed in terms of three auxiliary functions F_{lim}^A , F_{lim}^Z and F_{lim}^W . These nine form factors are:

$$\begin{aligned}
F_{Q\text{lim}}^{\gamma A} &= F_{L\text{lim}}^{zA} = F_{Q\text{lim}}^{zA} = Q_f^2 s_w^2 F_{\text{lim}}^A, \\
F_{L\text{lim}}^{\gamma Z} &= \frac{1}{c_w^2} 2Q_f v_f a_f F_{\text{lim}}^Z, \\
F_{Q\text{lim}}^{\gamma Z} &= F_{Q\text{lim}}^{zZ} = \frac{1}{4c_w^2} \delta_f^2 F_{\text{lim}}^Z, \\
F_{L\text{lim}}^{zZ} &= \frac{1}{4I_f^{(3)} c_w^2} (3v_f^2 + a_f^2) a_f F_{\text{lim}}^Z, \\
F_{L\text{lim}}^{\gamma W} &= \frac{Q_{f'}}{2I_f^{(3)}} F_{\text{lim}}^W - \left[r_{f'w}(2 + r_{f'w}) + 4d_w + d_w^2(2 + r_{f'w})R_w \right] \\
&\quad \times M_w^2 C_0(0, 0, -s; M_w, m_f, M_w) \\
&\quad - \left[1 - \frac{1}{2}r_{f'w} + d_w(2 + r_{f'w})R_w \right] \\
&\quad \times \left[B_0^F(-s; M_w, M_w) + L_\mu(m_{f'}^2) - 1 \right] \\
&\quad - \left[\frac{3}{2d_w^2} + \frac{1}{2d_w} + 1 + (2 + r_{f'w})R_w \right] \left[L_\mu(m_{f'}^2) - L_\mu(M_w^2) \right] \\
&\quad - 2L_\mu(m_{f'}^2) + \frac{3}{2d_w} + 2 + \frac{r_{f'w}}{4}, \\
F_{L\text{lim}}^{zW} &= \frac{\sigma_{f'}}{4I_f^{(3)}} F_{\text{lim}}^W \\
&\quad + \frac{r_{f'w}}{2} \left\{ (2 + d_w^2 R_w) M_w^2 C_0(-m_f^2, -m_f^2, -s; m_f, M_w, m_f) \right. \\
&\quad - \frac{1}{2} \left[B_0^F(-s; M_w, M_w) - B_0^F(-s; m_f, m_f) + 2 \right] \\
&\quad - R_w \left[B_0^F(-s; m_f, m_f) + L_\mu(M_w^2) - 1 \right. \\
&\quad \left. \left. - r_{f'w} (B_0^F(-s; m_f, m_f) + L_\mu(m_{f'}^2) - 1) \right] \right\} \\
&\quad - c_w^2 \left\{ \left[4 + \frac{r_{f'w}}{2} [4 + (4 - r_{f'w})t_w] + \left(2 - \frac{r_{f'w}}{2} (4 + d_w t_w) \right) \right. \right. \\
&\quad \left. \left. \times d_w R_w \right] M_w^2 C_0(-m_f^2, -m_f^2, -s; M_w, m_f, M_w) \right.
\end{aligned}$$

$$\begin{aligned}
& + \frac{1}{2} \left(2 - r_{f'W} + [4 - r_{f'W}(4 + d_W t_W)] R_W \right) \\
& \times \left[B_0^F(-s; M_W, M_W) + L_\mu(M_W^2) - 1 \right] \\
& - \left(\frac{3}{2d_W^2} + \frac{1}{2d_W} - 2 + \frac{1}{2} r_{f'W} [1 + (4 - r_{f'W} t_W) R_W] \right) \\
& \times \left[L_\mu(m_{f'}^2) - L_\mu(M_W^2) \right] \\
& + 2L_\mu(M_W^2) - \frac{3}{2d_W} - 2 - \frac{1}{4} r_{f'W} \Big\}, \tag{2.89}
\end{aligned}$$

while the three auxiliary functions read:

$$\begin{aligned}
F_{\text{lim}}^A &= 2s C_0(-m_f^2, -m_f^2, -s; m_f, \lambda, m_f) \\
&\quad - 3B_0^F(-s; 0, 0) - 3L_\mu(m_f^2) + 2L_\lambda(m_f^2) + 2, \\
F_{\text{lim}}^Z &= \frac{2(1 + R_Z)^2}{R_Z} M_Z^2 C_0(0, 0, -s; 0, M_Z, 0) \\
&\quad - (3 + 2R_Z) \left[B_0^F(-s; 0, 0) + L_\mu(M_Z^2) - 1 \right] - \frac{1}{2}, \\
F_{\text{lim}}^W &= \left(\frac{2}{R_W} + 3 + d_W^2 [1 + (2 + r_{f'W}) R_W] \right) \\
&\quad \times M_W^2 C_0(0, 0, -s; m_f, M_W, m_f) \\
&\quad - \frac{1}{2} [6 - r_{f'W} + 2d_W(2 + r_{f'W}) R_W] \\
&\quad \times \left[B_0^F(-s; m_f, m_f) + L_\mu(m_{f'}^2) - 1 \right] \\
&\quad + \frac{1}{2} \left[\frac{3}{d_W^2} + \frac{1}{d_W} + 2 + 2(2 + r_{f'W}) R_W \right] \left[L_\mu(m_{f'}^2) - L_\mu(M_W^2) \right] \\
&\quad + \frac{3}{2d_W} - 2 - \frac{3}{4} r_{f'W}, \tag{2.90}
\end{aligned}$$

where

$$\begin{aligned}
L_\lambda(m_f^2) &= \ln \frac{m_f^2}{\lambda^2}, \\
d_W &= 1 - r_{f'W}, \tag{2.91}
\end{aligned}$$

with λ being the photon mass.

The formulae, presented in this subsection, are useful to compute the one-loop corrections for the channels with massless or light final state fermions f and heavy virtual fermions f' .

2.6 Library of scalar form factors for electron vertex

Besides Btt clusters, we need also Bee clusters, which can, in principle, be taken from [5] or derived from the formulae of previous subsection in the limit $m_{f'} \rightarrow 0$ and $m_f = m_e$. Here we simply list the results:

$$\begin{aligned}
\mathcal{F}_L^{\gamma ee}(s) &= -\frac{2}{c_w^2} Q_e v_e a_e \mathcal{F}^{z,e}(s) + \mathcal{F}^{wna,e}(s), \\
\mathcal{F}_Q^{\gamma ee}(s) &= \mathcal{F}^{A,e}(s) + \frac{1}{4c_w^2} \delta_e^2 \mathcal{F}^{z,e}(s), \\
\mathcal{F}_L^{zee}(s) &= \mathcal{F}^{A,e}(s) - \frac{1}{2c_w^2} (3v_e^2 + a_e^2) a_e \mathcal{F}^{z,e}(s) + \mathcal{F}^{w,e}(s), \\
\mathcal{F}_Q^{zee}(s) &= \mathcal{F}^{A,e}(s) + \frac{1}{4c_w^2} \delta_e^2 \mathcal{F}^{z,e}(s),
\end{aligned} \tag{2.92}$$

with

$$\mathcal{F}^{w,e}(s) = -\mathcal{F}^{wab,e}(s) + c_w^2 \mathcal{F}^{wna,e}(s). \tag{2.93}$$

In Eq. (2.92) we use four more auxiliary functions:

$$\begin{aligned}
\mathcal{F}^{A,e}(s) &= Q_e^2 s_w^2 \left[2s C_0(-m_e^2, -m_e^2, -s; m_e, \lambda, m_e) \right. \\
&\quad \left. - 3B_0^F(-s; 0, 0) - 3L_\mu(m_e^2) + 2L_\lambda(m_e^2) + 2 \right],
\end{aligned} \tag{2.94}$$

$$\begin{aligned}
\mathcal{F}^{z,e}(s) &= 2 \frac{(1+R_z)^2}{R_z} M_z^2 C_0(0, 0, -s; 0, M_z, 0) \\
&\quad - 3 \left[B_0^F(-s; 0, 0) + L_\mu(M_z^2) \right] \\
&\quad + \frac{5}{2} - 2R_z \left[B_0^F(-s; 0, 0) + L_\mu(M_z^2) - 1 \right],
\end{aligned} \tag{2.95}$$

$$\begin{aligned}
\mathcal{F}^{wna,e}(s) &= -2R_w \left[M_w^2 C_0(0, 0, -s; M_w, 0, M_w) \right. \\
&\quad \left. + B_0^F(-s; M_w, M_w) + L_\mu(M_w^2) - 1 \right] \\
&\quad - 4M_w^2 C_0(0, 0, -s; M_w, 0, M_w) \\
&\quad - B_0^F(-s; M_w, M_w) - 3L_\mu(M_w^2) + \frac{9}{2},
\end{aligned} \tag{2.96}$$

$$\begin{aligned}
\mathcal{F}^{wab,e}(s) &= \sigma_\nu \left\{ \frac{(1+R_w)^2}{R_w} M_w^2 C_0(0, 0, -s; 0, M_w, 0) \right. \\
&\quad - \frac{3}{2} \left[B_0^F(-s; 0, 0) + L_\mu(M_w^2) \right] \\
&\quad \left. + \frac{5}{4} - R_w \left[B_0^F(-s; 0, 0) + L_\mu(M_w^2) - 1 \right] \right\},
\end{aligned} \tag{2.97}$$

where $L_\lambda(m_e^2) = \ln(m_e^2/\lambda^2)$.

2.7 Amplitudes of boxes

The contributions of QED AA and ZA boxes form gauge-invariant and UV-finite subsets. In terms of six structures $(L, R) \otimes (L, R, D)$ they read:

$$\begin{aligned} \left(B^{LK} \right)^{d+c} = k^{LK} \frac{g^4}{s} & \left[[\gamma_\mu \gamma_+ \otimes \gamma_\mu \gamma_+] \mathcal{F}_{LL}^{LK}(s, t, u) \right. \\ & + [\gamma_\mu \gamma_+ \otimes \gamma_\mu \gamma_-] \mathcal{F}_{LR}^{LK}(s, t, u) \\ & + [\gamma_\mu \gamma_- \otimes \gamma_\mu \gamma_+] \mathcal{F}_{RL}^{LK}(s, t, u) \\ & + [\gamma_\mu \gamma_- \otimes \gamma_\mu \gamma_-] \mathcal{F}_{RR}^{LK}(s, t, u) \\ & + [\gamma_\mu \gamma_+ \otimes (-im_f ID_\mu)] \mathcal{F}_{LD}^{LK}(s, t, u) \\ & \left. + [\gamma_\mu \gamma_- \otimes (-im_f ID_\mu)] \mathcal{F}_{RD}^{LK}(s, t, u) \right], \end{aligned} \quad (2.98)$$

where $LK = AA, ZA, ZZ$ and for shortening of presentation we factorize out normalization factors:

$$k^{AA} = s_W^4 Q_e^2 Q_f^2, \quad k^{ZA} = \frac{s_W^2 Q_e Q_f}{c_W^2}, \quad k^{ZZ} = \frac{1}{32 c_W^4}. \quad (2.99)$$

2.7.1 AA box contribution

There are only two AA diagrams, *direct* and *crossed*:

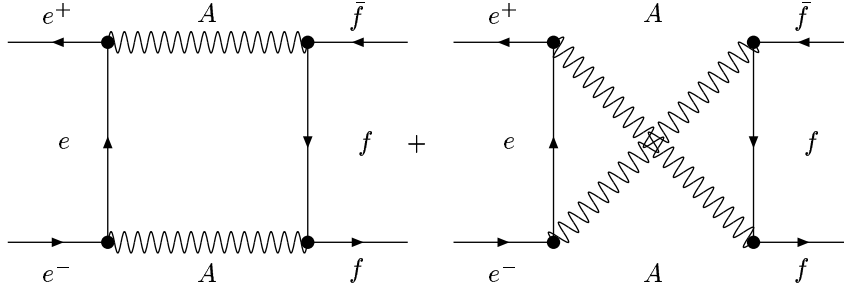


Figure 10: Direct and crossed AA boxes.

The six form factors of AA boxes might be expressed in terms of four auxiliary functions \mathcal{F}_1 and $\mathcal{H}_{1,2,3}$:

$$\begin{aligned} \mathcal{F}_{LL}^{AA}(s, t, u) = \mathcal{F}_{RR}^{AA}(s, t, u) &= \mathcal{H}_1(s, t) - \mathcal{H}_1(s, u) + \mathcal{H}_2(s, t) + \mathcal{H}_3(s, u), \\ \mathcal{F}_{LR}^{AA}(s, t, u) = \mathcal{F}_{RL}^{AA}(s, t, u) &= \mathcal{H}_1(s, t) - \mathcal{H}_1(s, u) - \mathcal{H}_2(s, u) - \mathcal{H}_3(s, t), \\ \mathcal{F}_{LD}^{AA}(s, t, u) = \mathcal{F}_{RD}^{AA}(s, t, u) &= \mathcal{F}_1(s, t) - \mathcal{F}_1(s, u). \end{aligned} \quad (2.100)$$

The auxiliary functions are rather short:

$$\begin{aligned}
\mathcal{F}_1(s, t) = & -\frac{1}{2} \frac{s}{\Delta_{4r}} \left\{ \frac{1}{\Delta_{4r}} \left[-t_-^3 J_{AA}(-s, -t; m_e, m_f) \right. \right. \\
& + t s^2 C_0(-m_e^2, -m_e^2, -s; 0, m_e, 0) \\
& + t \left[\frac{4m_f^2}{\Delta_{3r}} + \frac{s(s-2m_f^2)}{\Delta_{4r}} \right] C_0(-m_f^2, -m_f^2, -s; 0, m_f, 0) \\
& - 2 \frac{t}{\Delta_{3r}} \left[B_0^F(-s; 0, 0) - B_0^F(-m_f^2; m_f, 0) \right] \\
& \left. \left. + 2 \frac{t}{t_-} \left[B_0^F(-t; m_e, m_f) - B_0^F(-m_f^2; m_f, 0) \right] \right\}, \quad (2.101)
\end{aligned}$$

$$\begin{aligned}
\mathcal{H}_1(s, t) = & -\frac{t_-}{4} \left[2 - \left(t + \frac{t_+ t_-^2}{\Delta_{4r}} \right) \frac{s}{\Delta_{4r}} \right] J_{AA}(-s, -t; m_e, m_f) \\
& + t_- C_0(-m_e^2, -m_f^2, -t; m_e, 0, m_f) \quad (2.102) \\
& + \frac{s m_f^2}{2 \Delta_{4r}} \left(1 - 2 \frac{t}{t_-} \right) \left[B_0^F(-t; m_e, m_f) - B_0^F(-m_f^2; m_f, 0) \right],
\end{aligned}$$

$$\begin{aligned}
\mathcal{H}_2(s, t) = & \frac{s}{4 \Delta_{4r}} \left\{ (s + 2t_-) \left(1 - t_+ \frac{s}{\Delta_{4r}} \right) s C_0(-m_e^2, -m_e^2, -s; 0, m_e, 0) \right. \\
& - \left[2m_f^2 s - (s - 4m_f^2) \left(s + 2t_- - (st_+ + 2tt_-) \frac{s}{\Delta_{4r}} \right) \right] \\
& \quad \times C_0(-m_f^2, -m_f^2, -s; 0, m_f, 0) \\
& + 2t_- \left[B_0^F(-s; 0, 0) - B_0^F(-t; m_e, m_f) \right] \\
& \left. - 4m_f^2 \left[B_0^F(-t; m_e, m_f) - B_0^F(-m_f^2; m_f, 0) \right] \right\}, \quad (2.103)
\end{aligned}$$

$$\mathcal{H}_3(s, t) = \frac{s}{4 \Delta_{4r}^2} (s + 2t_-) t_-^3 J_{AA}(-s, -t; m_e, m_f). \quad (2.104)$$

Here

$$\Delta_{4r} = -tu + m_f^4, \quad (2.105)$$

and $J_{AA}(Q^2, P^2; M_1, M_2)$ is due to a procedure of disentangling of the infrared divergences from D_0 . Its explicit expression reads ($P^2 > 0, Q^2 < 0$, and M_1 is ignored everywhere but for the arguments of \ln):

$$\begin{aligned}
J_{AA}(Q^2, P^2; M_1, M_2) &= \frac{1}{\Delta_P} \left\{ \ln \frac{\Delta_P^2}{-Q^2 P^2} \ln \left(\frac{P^2}{-Q^2} \right) - \frac{1}{2} \ln^2 \left(\frac{M_1^2}{-Q^2} \right) \right. \\
&\quad \left. - \frac{1}{2} \ln^2 \left(\frac{M_2^2}{-Q^2} \right) + \ln^2 \left(1 + \frac{M_2^2}{P^2} \right) - 2\text{Li}_2 \left(\frac{P^2}{\Delta_P} \right) + i\pi \ln \left[\frac{\Delta_P^2}{M_1^2 M_2^2} \right] \right\}.
\end{aligned} \tag{2.106}$$

Furthermore, the relevant infrared divergent C_0 function (again $P^2 > 0$), is

$$\begin{aligned}
C_0^{\text{IR}}(-M_1^2, -M_2^2, P^2; M_1, \lambda, M_2) &= \frac{1}{2\Delta_P} \left\{ \ln \left[\frac{\Delta_P^2}{M_1^2 M_2^2} \right] \ln \frac{P^2}{\lambda^2} \right. \\
&\quad \left. - 2\text{Li}_2 \left(\frac{P^2}{\Delta_P} \right) - \frac{1}{2} \ln^2 \left(\frac{M_1^2}{P^2} \right) - \frac{1}{2} \ln^2 \left(\frac{M_2^2}{P^2} \right) + \ln^2 \left(1 + \frac{M_2^2}{P^2} \right) \right\},
\end{aligned} \tag{2.107}$$

where $\Delta_P = P^2 + M^2$.

2.7.2 ZA box contribution

In R_ξ gauge there are eight ZA boxes; however, since the electron mass is ignored, only four diagrams without ϕ_0 contribute, see Fig. 11.

The six relevant scalar form factors are conveniently presentable in the form of differences of f - and u - dependent functions:

$$\mathcal{F}_{IJ}^{ZA}(s, t, u) = \mathcal{F}_{IJ}^{ZA}(s, t) - \mathcal{F}_{IJ}^{ZA}(s, u), \tag{2.108}$$

where the index IJ is any pair of $L, R \otimes L, R, D$. The 12 \mathcal{F}_{IJ}^{ZA} functions depend on 6 auxiliary functions by means of equations where the coupling constants are factored out:

$$\begin{aligned}
\mathcal{F}_{LL}^{ZA}(s, t) &= \sigma_e \sigma_f \mathcal{G}_1(s, t) + \sigma_e \delta_f \mathcal{G}_2(s, t), \\
\mathcal{F}_{LL}^{ZA}(s, u) &= \sigma_e \delta_f \mathcal{H}_1(s, u) + \sigma_e \sigma_f \mathcal{H}_2(s, u), \\
\mathcal{F}_{RR}^{ZA}(s, t) &= \delta_e \delta_f \mathcal{G}_1(s, t) + \delta_e \sigma_f \mathcal{G}_2(s, t), \\
\mathcal{F}_{RR}^{ZA}(s, u) &= \delta_e \sigma_f \mathcal{H}_1(s, u) + \delta_e \delta_f \mathcal{H}_2(s, u), \\
\mathcal{F}_{LR}^{ZA}(s, t) &= \sigma_e \sigma_f \mathcal{H}_1(s, t) + \sigma_e \delta_f \mathcal{H}_2(s, t), \\
\mathcal{F}_{LR}^{ZA}(s, u) &= \sigma_e \delta_f \mathcal{G}_1(s, u) + \sigma_e \sigma_f \mathcal{G}_2(s, u), \\
\mathcal{F}_{RL}^{ZA}(s, t) &= \delta_e \delta_f \mathcal{H}_1(s, t) + \delta_e \sigma_f \mathcal{H}_2(s, t), \\
\mathcal{F}_{RL}^{ZA}(s, u) &= \delta_e \sigma_f \mathcal{G}_1(s, u) + \delta_e \delta_f \mathcal{G}_2(s, u), \\
\mathcal{F}_{LD}^{ZA}(s, t) &= \sigma_e \sigma_f \mathcal{F}_1(s, t) + \sigma_e \delta_f \mathcal{F}_2(s, t), \\
\mathcal{F}_{LD}^{ZA}(s, u) &= \sigma_e \delta_f \mathcal{F}_1(s, u) + \sigma_e \sigma_f \mathcal{F}_2(s, u), \\
\mathcal{F}_{RD}^{ZA}(s, t) &= \delta_e \delta_f \mathcal{F}_1(s, t) + \delta_e \sigma_f \mathcal{F}_2(s, t), \\
\mathcal{F}_{RD}^{ZA}(s, u) &= \delta_e \sigma_f \mathcal{F}_1(s, u) + \delta_e \delta_f \mathcal{F}_2(s, u).
\end{aligned} \tag{2.109}$$

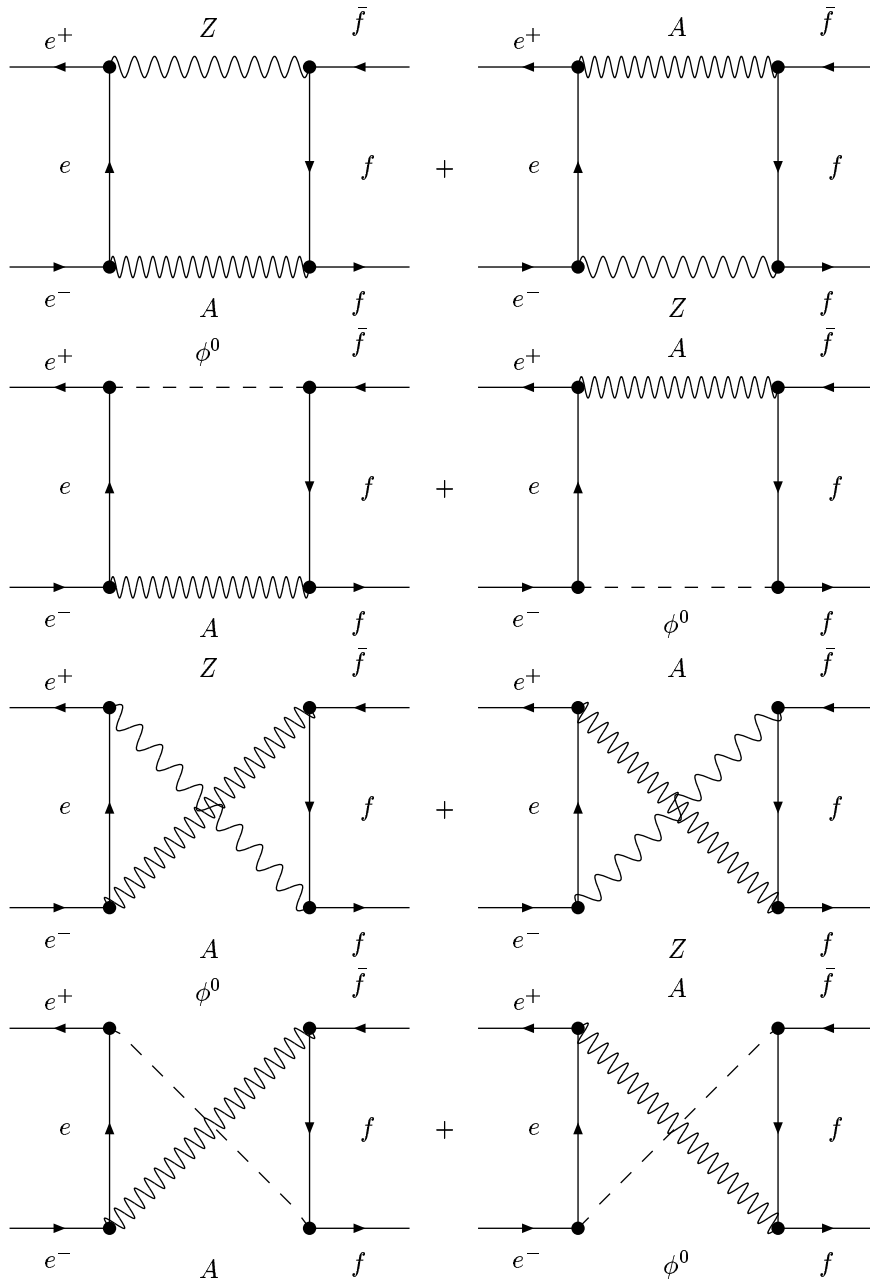


Figure 11: Direct and crossed $Z A$ boxes.

Finally, we present these 6 auxiliary functions:

$$\begin{aligned}
\mathcal{F}_1(s, t) = & -\frac{1}{8} \frac{s}{\Delta_{4r}} \left\{ t_- \left(R_z + \frac{t_-}{s} - 2 + 2t \frac{s_-}{\Delta_{4r}} \right) J_{Az}(-s, -t; m_e, m_f) \right. \\
& - \left(s_+ + 2 \frac{s_- t_-^2}{\Delta_{4r}} \right) C_0(-m_e^2, -m_e^2, -s; M_z, m_e, 0) \\
& - 2 \left(t + 2t_- + \frac{t M_z^2}{t_-} - 2 \frac{s_- t t_-}{\Delta_{4r}} \right) \\
& \quad \times C_0(-m_f^2, -m_e^2, -t; m_f, M_z, m_e) \\
& - \left[2 \frac{t_+}{\Delta_{3r}} (M_z^2 - 4m_f^2) + s_- \left(1 + 2 \frac{t_- t_+}{\Delta_{4r}} \right) \right] \\
& \quad \times C_0(-m_f^2, -m_f^2, -s; M_z, m_f, 0) \\
& + 2 \frac{t}{t_-} \left[2B_0^F(-t; m_e, m_f) \right. \\
& \quad \left. - B_0^F(-m_f^2; M_z, m_f) - B_0^F(-m_f^2; m_f, 0) \right] \\
& - 2 \frac{t_+}{\Delta_{3r}} \left[2B_0^F(-s; M_z, 0) \right. \\
& \quad \left. - B_0^F(-m_f^2; M_z, m_f) - B_0^F(-m_f^2; m_f, 0) \right] \left. \right\}, \\
\mathcal{F}_2(s, t) = & \frac{1}{8} \frac{s}{\Delta_{4r}} \left[\frac{t_-^2}{s} J_{Az}(-s, -t; m_e, m_f) \right. \\
& \left. - 2t C_0(-m_f^2, -m_e^2, -t; m_f, M_z, m_e) \right], \tag{2.110}
\end{aligned}$$

$$\begin{aligned}
\mathcal{H}_1(s, t) = & -\frac{sm_f^2}{8} \left\{ \left(\frac{1}{s} - \left[t - t_- \left(R_z - 2 + \frac{s_- t_+}{\Delta_{4r}} \right) \right] \frac{1}{\Delta_{4r}} \right) \right. \\
& \quad \times J_{Az}(-s, -t; m_e, m_f) \\
& - 2 \left(\frac{R_z}{t_-} + \left[t - t_- \left(R_z - 2 + \frac{s_- t_+}{\Delta_{4r}} \right) \right] \frac{1}{\Delta_{4r}} \right) \\
& \quad \times C_0(-m_f^2, -m_e^2, -t; m_f, M_z, m_e) \\
& - \frac{1}{\Delta_{4r}} \left(\left[s_+ + s_- (s + 2t_-) \frac{t_-}{\Delta_{4r}} \right] C_0(-m_e^2, -m_e^2, -s; M_z, m_e, 0) \right. \\
& \quad \left. + \left[s_- - 2t_+ - s_- (s - 4m_f^2) \frac{t_-}{\Delta_{4r}} \right] \right. \\
& \quad \times C_0(-m_f^2, -m_f^2, -s; M_z, m_f, 0) \\
& + 2 \left[B_0^F(-s; M_z, 0) - B_0^F(-t; m_e, m_f) \right] \\
& \left. - 2 \frac{m_f^2}{t_-} \left[2B_0^F(-t; m_e, m_f) \right. \right. \\
& \quad \left. \left. - B_0^F(-m_f^2; M_z, m_f) - B_0^F(-m_f^2; m_f, 0) \right] \right\}, \tag{2.111}
\end{aligned}$$

$$\begin{aligned}
\mathcal{H}_2(s, t) &= \frac{s}{4} \left\{ \left[-\frac{t_-}{s_-} + \frac{m_f^2}{2} \left(\frac{1}{s} - \frac{m_f^2}{\Delta_{4r}} \right) \right] J_{AZ}(-s, -t; m_e, m_f) \right. \\
&\quad + \frac{t_-}{s_-} C_0(-m_e^2, -m_f^2, -t; m_e, 0, m_f) \\
&\quad \left. - \left(\frac{t_-}{s_-} + \frac{m_t^4}{\Delta_{4r}} \right) C_0(-m_f^2, -m_e^2, -t; m_f, M_Z, m_e) \right\}, \\
\mathcal{G}_1(s, t) &= \frac{s}{4} \left\{ \left(-\frac{t_-}{s_-} - \frac{m_f^2}{2s} + \frac{1}{2\Delta_{4r}} \left[m_f^4 + t_- \left(2t_+ - m_f^2 R_Z \right) - \frac{s_- t t_- t_+}{\Delta_{4r}} \right] \right) \right. \\
&\quad \times J_{AZ}(-s, -t; m_e, m_f) + \frac{t_-}{s_-} C_0(-m_e^2, -m_f^2, -t; m_e, 0, m_f) \\
&\quad - \left[\frac{t_-}{s_-} - \frac{1}{\Delta_{4r}} \left(m_f^4 + 2t_- t_+ + \frac{m_f^2 M_Z^2 t}{t_-} - \frac{s_- t t_- t_+}{\Delta_{4r}} \right) \right] \\
&\quad \quad \times C_0(-m_f^2, -m_e^2, -t; m_f, M_Z, m_e) \\
&\quad + \frac{1}{2\Delta_{4r}} \left[\left(t s_+ + \frac{s_- t_-^2 t_+}{\Delta_{4r}} \right) C_0(-m_e^2, -m_e^2, -s; M_Z, m_e, 0) \right. \\
&\quad \left. - \left(2m_f^2 t_- - t(s_+ - 4m_f^2) - \frac{s_- t_- t_+^2}{\Delta_{4r}} \right) \right. \\
&\quad \quad \left. \times C_0(-m_f^2, -m_f^2, -s; M_Z, m_f, 0) \right. \\
&\quad + 2t \left(B_0^F(-s; M_Z, 0) - B_0^F(-t; m_e, m_f) \right. \\
&\quad \left. - \frac{m_f^2}{t_-} \left[2B_0^F(-t; m_e, m_f) \right. \right. \\
&\quad \quad \left. \left. - B_0^F(-m_f^2; M_Z, m_f) - B_0^F(-m_f^2; m_f, 0) \right] \right) \left. \right\}, \tag{2.112}
\end{aligned}$$

$$\begin{aligned}
\mathcal{G}_2(s, t) &= \frac{s m_f^2}{8} \left[\left(\frac{1}{s} - \frac{t}{\Delta_{4r}} \right) J_{AZ}(-s, -t; m_e, m_f) \right. \\
&\quad \left. - 2 \frac{t}{\Delta_{4r}} C_0(-m_f^2, -m_e^2, -t; m_f, M_Z, m_e) \right], \tag{2.113}
\end{aligned}$$

where a new notation were introduced for the invariants:

$$s_{\pm} = s \pm M_Z^2, \quad t_{\pm} = t \pm m_f^2, \tag{2.114}$$

and for the new function $J_{I,J}(Q^2, P^2; M_1, M_2)$:

$$J_{AZ}(Q^2, P^2; M_1, M_2) = \frac{1}{P^2 + M_2^2} \ln \left(\frac{Q^2 + M_Z^2}{M_Z^2} \right) \ln \left[\frac{M_1^2 M_2^2}{(P^2 + M_2^2)^2} \right]. \tag{2.115}$$

2.7.3 The WW box

There is only one, *direct* or *crossed*, WW diagram contributing to our process, see Fig. 12.

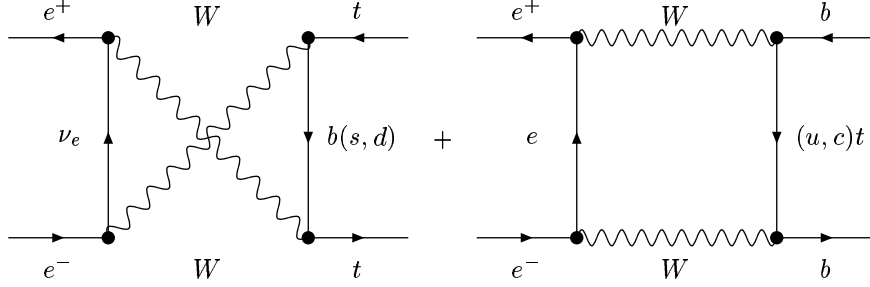


Figure 12: Crossed and direct WW boxes.

Here we give the contribution of this diagram to the scalar form factor LL :

$$\left(\mathcal{B}^{WW}\right)^c = (2\pi)^4 i \frac{g^4}{16\pi^2} \frac{1}{s} \gamma_\mu \gamma_+ \otimes \gamma_\mu \gamma_+ \mathcal{F}_{LL}^{WW}(s, u), \quad (2.116)$$

where

$$\begin{aligned} \mathcal{F}_{LL}^{WW}(s, u) = \frac{s}{I_t^{(3)}} & \left[(u - m_b^2) D_0(0, 0, -m_t^2, -m_t^2, -s, -u; M_W, 0, M_W, m_b) \right. \\ & \left. + C_0(-m_t^2, -m_t^2, -s; M_W, 0, M_W) + C_0(0, 0, -s; M_W, 0, M_W) \right], \end{aligned} \quad (2.117)$$

with s , t , and u being the usual Mandelstamm variables satisfying

$$s + t + u = 2m_f^2, \quad f = t \text{ or } b. \quad (2.118)$$

For the processes, where the direct box contributes, we have:

$$\begin{aligned} \mathcal{F}_{LL}^{WW} = \frac{s}{2I_b^{(3)}} & \left\{ \left[-(2 - K_2) t'_- + \left(2M_W^4 t_+ + K_1 (m_b^2 t'_- - m_t^2 t_+) \right) \frac{t_-}{t} \right] \frac{1}{\Delta_{4r}} \right. \\ & \left. - K_1^2 t_+ t_-^2 \frac{1}{\Delta_{4r}^2} \right] D_0(0, 0, -m_b^2, -m_b^2, -s, -t; M_W, 0, M_W, m_t) \\ & - \left(K_2 + \left[K_2 t_+ t_- - K_1 \left(\frac{m_b^4}{t} + t \right) \right] \frac{1}{\Delta_{4r}} + K_1 \frac{t_+^2 t_-^2}{t} \frac{1}{\Delta_{4r}^2} \right) \\ & \times C_0(-m_b^2, -m_b^2, -t; M_W, m_t, M_W) \\ & \left. + 2 \left(K_2 t + K_1 t_+ t_- \frac{1}{\Delta_{4r}} \right) t_- \frac{1}{\Delta_{4r}} C_0(0, -m_b^2, -t; 0, M_W, m_t) \right\} \end{aligned}$$

$$\begin{aligned}
& - \left[2 - K_2 + (K_2 t t_- - K_1 t_+) \frac{t_-}{t} \frac{1}{\Delta_{4r}} + K_1 \frac{t_+ t_-^2}{t} \frac{1}{\Delta_{4r}^2} \right] \\
& \quad \times C_0(0, 0, -s; M_w, 0, M_w) \\
& + 2t_- \frac{1}{\Delta_{4r}} \left[B_0^F(-s; M_w, M_w) - B_0^F(-m_b^2; M_w, m_t) \right] \\
& - 2t_+ \frac{1}{\Delta_{4r}} \left[B_0^F(-t; 0, m_t) - B_0^F(-m_b^2; M_w, m_t) \right] \Big\}, \quad (2.119)
\end{aligned}$$

$$\begin{aligned}
\mathcal{F}_{LQ}^{WW} = & \frac{s m_b^2}{4I_e^{(3)} s_w^2 Q_b} \left\{ - \left(m_t^2 \frac{t_-'}{t^2} - \frac{1}{2} \left[(t_-')^2 - 2K_1 t_+ - \left(m_b^2 \frac{t_-'}{t} - K_1 \right)^2 \right] \frac{1}{\Delta_{4r}} \right. \right. \\
& + K_1^2 t_+ t_- \frac{1}{\Delta_{4r}^2} \Big) D_0(0, 0, -m_b^2, -m_b^2, -s, -t; M_w, 0, M_w, m_t) \\
& + \left[\frac{m_t^2}{t^2} - \left(K_2 t_+ + K_1 \frac{m_b^2}{t} \right) \frac{1}{\Delta_{4r}} - K_1 \frac{t_+^2 t_-}{t} \frac{1}{\Delta_{4r}^2} \right] \\
& \quad \times C_0(-m_b^2, -m_b^2, -s; M_w, m_t, M_w) \\
& + 2 \left[\left(K_2 + \frac{K_1}{t_-} \right) t + K_1 t_+ t_- \frac{1}{\Delta_{4r}} \right] \frac{1}{\Delta_{4r}} C_0(0, -m_b^2, -t; 0, M_w, m_t) \\
& - \left[\frac{m_t^2}{t^2} + \left(K_2 t_- - K_1 \frac{m_b^2}{t} \right) \frac{1}{\Delta_{4r}} + K_1 \frac{t_+ t_-^2}{t} \frac{1}{\Delta_{4r}^2} \right] \\
& \quad \times C_0(0, 0, -s; M_w, 0, M_w) \\
& + 2 \frac{1}{\Delta_{4r}} \left[B_0^F(-s; M_w, M_w) - B_0^F(-m_b^2; M_w, m_t) \right] \\
& - \frac{2t_+}{t_-} \frac{1}{\Delta_{4r}} \left[B_0^F(-t; 0, m_t) - B_0^F(-m_b^2; M_w, m_t) \right] \Big\}, \quad (2.120)
\end{aligned}$$

$$\begin{aligned}
\mathcal{F}_{LD}^{WW} = & - \frac{s}{I_b^{(3)}} \frac{1}{\Delta_{4r}} \left\{ \left[2m_t^2 t_- + K_3 t_+ + K_1^2 t_- t \frac{1}{\Delta_{4r}} \right] \right. \\
& \times D_0(0, 0, -m_b^2, -m_b^2, -s, -t; M_w, 0, M_w, m_t) \\
& + \left[K_3 + 2 \left(\frac{m_b^2 t_+'}{t} - K_3 \right) t_+ \frac{1}{\Delta_{4r}} + K_1 t_- t_+ \frac{1}{\Delta_{4r}} \right] \frac{1}{\Delta_{4r}} \\
& \times C_0(-m_b^2, -m_b^2, -s; M_w, m_t, M_w) \\
& - t \left[\frac{t_+'}{t} + \frac{K_1}{t_-} + 2K_1 t_- \frac{1}{\Delta_{4r}} \right] C_0(0, -m_b^2, -t; 0, M_w, m_t) \\
& - \left(K_3 - K_1 t_-^2 \frac{1}{\Delta_{4r}} \right) C_0(0, 0, -s; M_w, 0, M_w) \\
& - 2t_+ \frac{1}{\Delta_{3r}} \left[B_0^F(-s; M_w, M_w) - B_0^F(-m_b^2; M_w, m_t) \right] \\
& + 2 \frac{t}{t_-} \left[B_0^F(-t; 0, m_t) - B_0^F(-m_b^2; M_w, m_t) \right] \Big\}, \quad (2.121)
\end{aligned}$$

where

$$\begin{aligned}
K_1 &= 2M_W^2 + \frac{t'_- t_-}{t}, \\
K_2 &= \frac{m_f^2 m_{f'}^2}{t^2} + 1 \\
K_3 &= 2M_W^2 - m_{f'}^2 \frac{t_-}{t}, \\
t'_- &= t - m_t^2, & t'_+ &= t + m_t^2, \\
t_- &= t - m_b^2, & t_+ &= t + m_b^2.
\end{aligned} \tag{2.122}$$

In the limit $m_b \rightarrow 0$, for F_{LL}^{WW} one has:

$$\begin{aligned}
F_{LL}^{WW} \lim &= \frac{s}{2I_b^{(3)}} \left\{ - \left[\left(\frac{1}{2} \frac{t'_-}{u} + 1 \right) t'_- - K_1^{\lim} \frac{t}{u} + \frac{(K_1^{\lim})^2}{u} \left(\frac{t}{u} + \frac{1}{2} \right) \right] \right. \\
&\quad \times D_0(0, 0, 0, 0, -s, -t; M_W, 0, M_W, m_t) \\
&\quad + \left[\frac{t}{u} - 1 - \frac{K_1^{\lim}}{u} \left(\frac{t}{u} + 1 \right) \right] \\
&\quad \times \left[C_0(0, 0, -s; M_W, 0, M_W) + C_0(0, 0, -s; M_W, m_t, M_W) \right] \\
&\quad - 2 \frac{t}{u} \left(1 - \frac{K_1^{\lim}}{u} \right) C_0(0, 0, -t; 0, M_W, m_t) \\
&\quad \left. - \frac{2}{u} \left[B_0^F(-s; M_W, M_W) - B_0^F(-t; 0, m_t) \right], \right.
\end{aligned} \tag{2.123}$$

where

$$K_1^{\lim} = 2M_W^2 + t'_-. \tag{2.124}$$

2.7.4 The ZZ box

There are four ZZ box diagrams, which form a gauge-invariant and UV finite subset, see Fig. 13.

First, we use three auxiliary functions $\mathcal{F}, \mathcal{H}, \mathcal{G}$:

$$\begin{aligned}
\mathcal{F}_{LD}^{ZZ}(s, t, u) &= \mathcal{F}(\sigma_e, \sigma_f, \delta_f, s, t) - \mathcal{F}(\sigma_e, \delta_f, \sigma_f, s, u), \\
\mathcal{F}_{RD}^{ZZ}(s, t, u) &= \mathcal{F}(\delta_e, \delta_f, \sigma_f, s, t) - \mathcal{F}(\delta_e, \sigma_f, \delta_f, s, u), \\
\mathcal{F}_{LR}^{ZZ}(s, t, u) &= \mathcal{H}(\sigma_e, \sigma_f, \delta_f, s, t) - \mathcal{G}(\sigma_e, \delta_f, \sigma_f, s, u), \\
\mathcal{F}_{RL}^{ZZ}(s, t, u) &= \mathcal{H}(\delta_e, \delta_f, \sigma_f, s, t) - \mathcal{G}(\delta_e, \sigma_f, \delta_f, s, u), \\
\mathcal{F}_{LL}^{ZZ}(s, t, u) &= \mathcal{G}(\sigma_e, \sigma_f, \delta_f, s, t) - \mathcal{H}(\sigma_e, \delta_f, \sigma_f, s, u), \\
\mathcal{F}_{RR}^{ZZ}(s, t, u) &= \mathcal{G}(\delta_e, \delta_f, \sigma_f, s, t) - \mathcal{H}(\delta_e, \sigma_f, \delta_f, s, u).
\end{aligned} \tag{2.125}$$

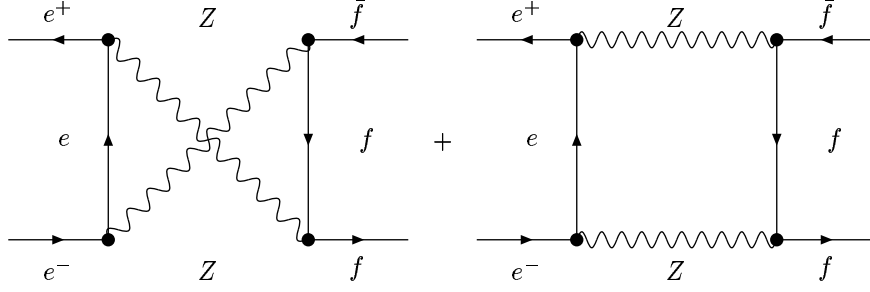


Figure 13: Crossed and direct ZZ boxes.

Separating out Z fermion coupling constants and some common factors, we introduce more auxiliary functions. For $\mathcal{F}(\sigma_e, \sigma_f, \delta_f, s, t)$ defined as

$$\mathcal{F}(\sigma_e, \sigma_f, \delta_f, s, t) = \frac{s}{\Delta_{4r}} \left[\sigma_e^2 \sigma_f^2 \mathcal{F}_1(s, t) + \sigma_e^2 \sigma_f \delta_f \mathcal{F}_2(s, t) \right], \quad (2.126)$$

there are two

$$\begin{aligned} \mathcal{F}_1(s, t) = & \left(t_+ M_Z^2 + t_-^2 + [(-s_z + 2M_Z^2) t_-^2 + 4t M_Z^4] \frac{t_-}{\Delta_{4r}} \right) \\ & \times D_0(0, 0, -m_f^2, -m_f^2, -s, -t; M_Z, 0, M_Z, m_f) \\ & - \left[m_f^2 - M_Z^2 - \frac{t_- (t_- t + 2M_Z^2 t_+) + s m_f^4}{\Delta_{4r}} + \frac{2t_+ (M_Z^2 - 2m_f^2)}{\Delta_{3r}} \right] \\ & \quad \times C_0(-m_f^2, -m_f^2, s; M_Z, m_f, M_Z) \\ & - 2 \left[t \left(1 + \frac{M_Z^2}{t_-} \right) + \frac{t^3 + 2t t_- M_Z^2 - m_f^2 (3t t_- + m_f^4)}{\Delta_{4r}} \right] \\ & \quad \times C_0(0, -m_f^2, t; 0, M_Z, m_f) \\ & - \left[M_Z^2 - m_f^2 + \frac{(t - 2t_- - 2M_Z^2) t_-^2 + s m_f^4}{\Delta_{4r}} \right] C_0(0, 0, s; M_Z, 0, M_Z) \\ & - \left(1 + \frac{s + 2t_-}{\Delta_{3r}} \right) \left[B_0(-s; M_Z, M_Z) - B_0(-m_f^2; M_Z, m_f) \right] \\ & + \frac{2t}{t_-} \left[B_0(t; m_f, 0) - B_0(-m_f^2; M_Z, m_f) \right], \quad (2.127) \end{aligned}$$

and

$$\begin{aligned} \mathcal{F}_2(s, t) = & - (t_-^2 + 2M_Z^2 t) D_0(0, 0, -m_f^2, -m_f^2, -s, -t; M_Z, 0, M_Z, m_f) \\ & - t_+ C_0(-m_f^2, -m_f^2, s; M_Z, m_f, M_Z) \\ & + 2t C_0(0, -m_f^2, t; 0, M_Z, m_f) - t_- C_0(0, 0, s; M_Z, 0, M_Z). \quad (2.128) \end{aligned}$$

For \mathcal{H} written out as

$$\mathcal{H}(\sigma_e, \sigma_f, \delta_f, s, t) = \frac{m_f^2 s}{\Delta_{4r}} \left[\sigma_e^2 \sigma_f^2 \mathcal{H}_1(s, t) + \sigma_e^2 \sigma_f \delta_f \mathcal{H}_2(s, t) \right] + \sigma_e^2 \delta_f^2 \mathcal{H}_3(s, t), \quad (2.129)$$

we need three auxiliary subfunctions:

$$\begin{aligned} \mathcal{H}_1(s, t) = & \left[\frac{st_-}{2} - (t_- + M_z^2)^2 - 2M_z^2 t - \frac{s_z^2 t_- t_+}{2\Delta_{4r}} \right] \\ & \times D_0(0, 0, -m_f^2, -m_f^2, -s, -t; M_z, 0, M_z, m_f) \\ & - \left(t_+ - \frac{s_z [t_+^2 + \Delta_{3r} m_f^2]}{2\Delta_{4r}} \right) C_0(-m_f^2, -m_f^2, s; M_z, m_f, M_z) \\ & + \left(2t + t_- + \frac{2M_z^2 t}{t_-} - \frac{s_z t_- t_+}{\Delta_{4r}} \right) C_0(0, 0, s; M_z, 0, M_z) \\ & - \left[t_- + \frac{s_z (sm_f^2 - t_-^2)}{2\Delta_{4r}} \right] C_0(0, -m_f^2, t; 0, M_z, m_f) \\ & - 2 \frac{m_f^2}{t_-} \left(B_0(t; m_f, 0) - B_0(-m_f^2; M_z, m_f) \right) \\ & - B_0(t; m_f, 0) + B_0(s; M_z, M_z), \end{aligned} \quad (2.130)$$

$$\begin{aligned} \mathcal{H}_2(s, t) = & [t_- (s+t_-) + 2m_f^2 M_z^2] D_0(0, 0, -m_f^2, -m_f^2, -s, -t; M_z, 0, M_z, m_f) \\ & - (s + t_- - 2m_f^2) C_0(-m_f^2, -m_f^2, s; M_z, m_f, M_z) \\ & - 2m_f^2 C_0(-m_f^2, -m_f^2, s; 0, M_z, m_f) \\ & + (s + t_-) C_0(0, 0, s; M_z, 0, M_z), \end{aligned} \quad (2.131)$$

and

$$\begin{aligned} \mathcal{H}_3(s, t) = & -s \left[t_- D_0(0, 0, -m_f^2, -m_f^2, -s, -t; M_z, 0, M_z, m_f) \right. \\ & \left. + C_0(-m_f^2, -m_f^2, s; M_z, m_f, M_z) + C_0(0, -m_f^2, t; M_z, 0, M_z) \right]. \end{aligned} \quad (2.132)$$

Finally, \mathcal{G} also, defined as follows:

$$\mathcal{G}(\sigma_e, \sigma_f, \delta_f, s, t) = \frac{s}{\Delta_{4r}} \left[\sigma_e^2 \sigma_f^2 \mathcal{G}_1(s, t) + \sigma_e^2 \sigma_f \delta_f \mathcal{G}_2(s, t) \right], \quad (2.133)$$

needs only two additional functions:

$$\begin{aligned}
\mathcal{G}_1(s, t) = & - \left[t_- t_+ \left(2M_z^2 + \frac{s_z^2 t}{2\Delta_{4r}} \right) - t_- \left(\frac{sm_f^2}{2} - t_- t \right) + tM_z^2 (2m_f^2 - M_z^2) \right] \\
& \times D_0(0, 0, -m_f^2, -m_f^2, -s, -t; M_z, 0, M_z, m_f) \\
& + \left[t_+ t + \frac{s_z}{2} \left(t - \frac{t_- t_+^2}{\Delta_{4r}} \right) \right] C_0(-m_f^2, -m_f^2, s; M_z, m_f, M_z) \\
& - \left[t_+ (t + t_-) + 2M_z^2 m_f^2 \frac{t}{t_-} - \frac{t_+ t_- t s_z}{\Delta_{4r}} \right] C_0(0, -m_f^2, -t; 0, M_z, m_f) \\
& - \left[t_- t + \frac{s_z}{2} \left(t - \frac{t_+ t_-^2}{\Delta_{4r}} \right) \right] C_0(0, 0, s; M_z, 0, M_z) \\
& + 2m_f^2 \left(1 + \frac{m_f^2}{t_-} \right) \left[B_0(t; m_f, 0) - B_0(-m_f^2; M_z, m_f) \right] \\
& - t \left[B_0(s; M_z, M_z) - B_0(t; m_f, 0) \right], \tag{2.134}
\end{aligned}$$

and

$$\begin{aligned}
\mathcal{G}_2(s, t) = & m_f^2 \left[\left(t_-^2 + 2M_z^2 t \right) D_0(0, 0, -m_f^2, -m_f^2, -s, -t; M_z, 0, M_z, m_f) \right. \\
& + t_+ C_0(-m_f^2, -m_f^2, s; M_z, m_f, M_z) - 2t C_0(0, -m_f^2, t; 0, M_z, m_f) \\
& \left. + t_- C_0(0, 0, s; M_z, 0, M_z) \right]. \tag{2.135}
\end{aligned}$$

We recall that $\Delta_{4r} = -tu + m_f^4$ together with Δ_{3r} of Eq. (2.84) denotes remnants of Gram determinants that remained after cancellation of factors s and 4, leading to a simplification of the expressions.

2.7.5 Transition to the L, Q, D basis

Since the ZZ box contribution is given in the L, R, D basis, while all the rest is in the L, Q, D basis, we should transfer one of them to a chosen basis. At this phase of the calculations there is not much difference which basis is chosen. For definiteness we choose the L, Q, D basis and transfer the ZZ box contribution to it. The transition formulae are simple:

$$\begin{aligned}
\tilde{\mathcal{F}}_{LL}^{ZZ}(s, t, u) &= \mathcal{F}_{LL}^{ZZ}(s, t, u) + \mathcal{F}_{RR}^{ZZ}(s, t, u) - \mathcal{F}_{LR}^{ZZ}(s, t, u) - \mathcal{F}_{RL}^{ZZ}(s, t, u), \\
\tilde{\mathcal{F}}_{QL}^{ZZ}(s, t, u) &= 2 \left[\mathcal{F}_{RL}^{ZZ}(s, t, u) - \mathcal{F}_{RR}^{ZZ}(s, t, u) \right], \\
\tilde{\mathcal{F}}_{LQ}^{ZZ}(s, t, u) &= 2 \left[\mathcal{F}_{LR}^{ZZ}(s, t, u) - \mathcal{F}_{RR}^{ZZ}(s, t, u) \right],
\end{aligned}$$

$$\begin{aligned}
\tilde{\mathcal{F}}_{Q^Z}^{ZZ}(s, t, u) &= 4\mathcal{F}_{RR}^{ZZ}(s, t, u), \\
\tilde{\mathcal{F}}_{LD}^{ZZ}(s, t, u) &= \mathcal{F}_{LD}^{ZZ}(s, t, u) - \mathcal{F}_{RD}^{ZZ}(s, t, u), \\
\tilde{\mathcal{F}}_{QD}^{ZZ}(s, t, u) &= 2\mathcal{F}_{RD}^{ZZ}(s, t, u).
\end{aligned} \tag{2.136}$$

2.7.6 Box–Born interferences

Any box, described by the amplitude in Eq. (2.98), interfering with γ and Z exchange tree-level amplitudes, gives rise to two contributions to the differential cross-sections, which are useful for internal cross-checks:

$$\begin{aligned}
\sigma_{\text{BOX} \otimes \text{BORN}_\gamma} \propto 8Q_e Q_t \text{Re} \left\{ \left(\left[(s + t_-)^2 + sm_f^2 \right] (\mathcal{F}_{LL} + \mathcal{F}_{RR}) \right. \right. \\
\left. \left. + (sm_f^2 + t_-^2) (\mathcal{F}_{LR} + \mathcal{F}_{RL}) - 2m_f^2 (st + t_-^2) (\mathcal{F}_{LD} + \mathcal{F}_{RD}) \right) \right\},
\end{aligned} \tag{2.137}$$

$$\begin{aligned}
\sigma_{\text{BOX} \otimes \text{BORN}_Z} \propto 8 \text{Re} \left\{ \left(\left[(s + t_-)^2 + sm_f^2 \right] \delta_f (\sigma_e \mathcal{F}_{LL} + \delta_e \mathcal{F}_{RR}) \right. \right. \\
+ 2(s + t_-)^2 a_f \sigma_e \mathcal{F}_{LL} + 2t_-^2 a_f \delta_e \mathcal{F}_{RL} \\
+ (sm_f^2 + t_-^2) \delta_f (\sigma_e \mathcal{F}_{LR} + \delta_e \mathcal{F}_{RL}) + 2sm_f^2 a_f (\sigma_e \mathcal{F}_{LR} + \delta_e \mathcal{F}_{RR}) \\
\left. \left. - 2m_f^2 (st + t_-^2) v_f (\sigma_e \mathcal{F}_{LD} + \delta_e \mathcal{F}_{RD}) \right) \chi_Z^* \right\}.
\end{aligned} \tag{2.138}$$

3 Scalar form factors for electroweak amplitude

Having all the building blocks, it is time to construct *complete* electroweak scalar form factors.

3.1 Vertices scalar form factors

We begin with two vertex contributions:

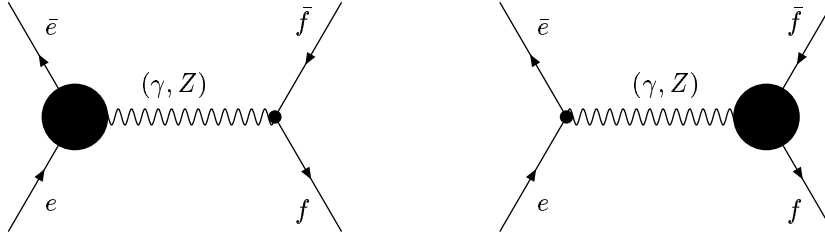


Figure 14: *Electron (a) and final fermion (b) vertices in $e\bar{e} \rightarrow (\gamma, Z) \rightarrow f\bar{f}$.*

In the same way as described in [5], we reduce two vertex contributions to our six form factors:

$$\begin{aligned}
F_{LL}(s) &= F_L^{zee}(s) + F_L^{zff}(s) - 4c_W^2 \Delta(M_W), \\
F_{QL}(s) &= F_Q^{zee}(s) + F_L^{zff}(s) - 2c_W^2 \Delta(M_W) + k [F_L^{\gamma ff}(s) - 2\Delta(M_W)], \\
F_{LQ}(s) &= F_L^{zee}(s) - 2c_W^2 \Delta(M_W) + F_Q^{zff}(s) + k [F_L^{\gamma ee}(s) - 2\Delta(M_W)], \\
F_{QQ}(s) &= F_Q^{zee}(s) + F_Q^{zff}(s) - \frac{k}{s_W^2} [F_Q^{\gamma ee}(s) + F_Q^{\gamma ff}(s)], \\
F_{LD}(s) &= F_D^{zff}(s), \\
F_{QD}(s) &= F_D^{zff}(s) + k F_D^{\gamma ff}(s),
\end{aligned} \tag{3.139}$$

where

$$k = c_W^2 (R_Z - 1). \tag{3.140}$$

With the term containing $\Delta(M_W)$,

$$\Delta(M_W) = \frac{1}{\bar{\varepsilon}} - \ln \frac{M_W^2}{\mu^2}, \tag{3.141}$$

we explicitly show the contribution of the so-called *special* vertices [36]. Note that they accompany every L form factor. The poles $1/\bar{\varepsilon}$ originating from special vertices will be canceled in the sum of all contributions, including self-energies and boxes.

3.2 Bosonic self-energies and bosonic counterterms

The contributions to form factors from bosonic self-energy diagrams and counterterms, originating from bosonic self-energy diagrams, come from four classes of diagrams; their sum is depicted by a black circle in Fig. 15. Their contribution to the four scalar form factors is derived in [11], [5]:

$$F_{LL}^{ct}(s) = \mathcal{D}_Z(s) - s_W^2 \Pi_{\gamma\gamma}(0) + \frac{c_W^2 - s_W^2}{s_W^2} (\Delta\rho + \Delta\bar{\rho}^{\text{bos}}), \tag{3.142}$$

$$F_{QL(LQ)}^{ct}(s) = \mathcal{D}_Z(s) - (\Pi_{Z\gamma}(s) + \bar{\Pi}_{Z\gamma}^{\text{bos}}(s)) - s_W^2 \Pi_{\gamma\gamma}(0) - (\Delta\rho + \Delta\bar{\rho}^{\text{bos}}), \tag{3.143}$$

$$\begin{aligned}
F_{QQ}^{ct,\text{bos}}(s) &= \mathcal{D}_Z^{\text{bos}}(s) - 2 (\Pi_{Z\gamma}^{\text{bos}}(s) + \bar{\Pi}_{Z\gamma}^{\text{bos}}(s)) + k [\Pi_{\gamma\gamma}^{\text{bos}}(s) - \Pi_{\gamma\gamma}^{\text{bos}}(0)] \\
&\quad - s_W^2 \Pi_{\gamma\gamma}^{\text{bos}}(0) - \frac{1}{s_W^2} (\Delta\rho^{\text{bos}} + \Delta\bar{\rho}^{\text{bos}}),
\end{aligned} \tag{3.144}$$

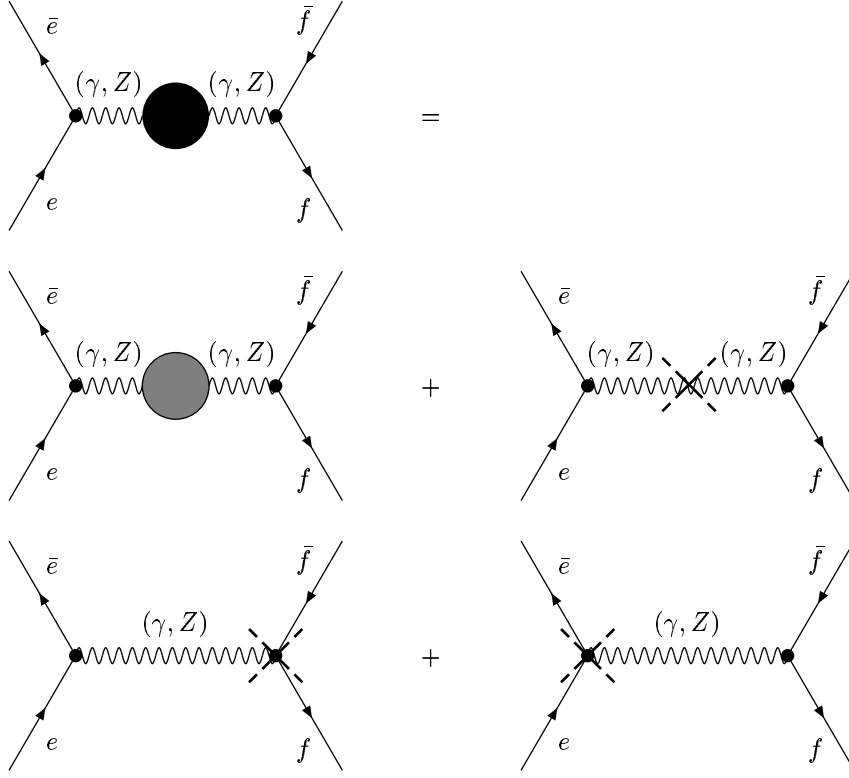


Figure 15: *Bosonic self-energies and counterterms for $e\bar{e} \rightarrow (Z, \gamma) \rightarrow f\bar{f}$.*

$$F_{Q\bar{Q}}^{ct,fer}(s) = \mathcal{D}_Z^{fer}(s) - 2\Pi_{Z\gamma}^{fer}(s) - s_W^2 \Pi_{\gamma\gamma}^{fer}(0) - \frac{1}{s_W^2} \Delta\rho^{fer}. \quad (3.145)$$

We note that the term $k[\Pi_{\gamma\gamma}^{fer}(s) - \Pi_{Z\gamma}^{fer}(s)]$ is conventionally extracted from $F_{Q\bar{Q}}^{ct,fer}(s)$. This contribution is shifted to A_γ^{IBA} , Eq. (1.8).

In Eqs. (3.142)–(3.145) $\Delta\rho^{\text{bos}}$ and $\bar{\Pi}_{Z\gamma}^{\text{bos}}(s)$ stand for shifts of bosonic self-energies. They have the same origin as special vertices and they are equal to:

$$\Delta\rho^{\text{bos}} = 4s_W^2 \Delta(M_W), \quad (3.146)$$

$$\bar{\Pi}_{Z\gamma}^{\text{bos}}(s) = -2R_W \Delta(M_W), \quad (3.147)$$

see Eqs. (6.137) and (6.139) of [11]. These poles also cancel in the sum of all contributions.

3.3 Total scalar form factors of the one-loop amplitude

Adding all contributions together, we observe the cancellation of all poles. The ultraviolet-finite results for six scalar form factors are:

$$\begin{aligned}
F_{LL}(s, t, u) &= \mathcal{F}_L^{zee}(s) + \mathcal{F}_L^{zff}(s) + \mathcal{F}_{LL}^{ct}(s) + 16k\mathcal{F}_{LL}^{\text{BOX}}(s, t, u), \\
F_{QL}(s, t, u) &= \mathcal{F}_Q^{zee}(s) + \mathcal{F}_L^{zff}(s) + k\mathcal{F}_L^{\gamma ff}(s) + \mathcal{F}_{QL}^{ct}(s) + 16k\mathcal{F}_{QL}^{\text{BOX}}(s, t, u), \\
F_{LQ}(s, t, u) &= \mathcal{F}_L^{zee}(s) + \mathcal{F}_Q^{zff}(s) + k\mathcal{F}_L^{\gamma ee}(s) + \mathcal{F}_{LQ}^{ct}(s) + 16k\mathcal{F}_{LQ}^{\text{BOX}}(s, t, u), \\
F_{QQ}(s, t, u) &= \mathcal{F}_Q^{zee}(s) + \mathcal{F}_Q^{zff}(s) - \frac{k}{s_W^2} \left[\mathcal{F}_Q^{\gamma ee}(s) + \mathcal{F}_Q^{\gamma ff}(s) \right] + \mathcal{F}_{QQ}^{ct}(s) \\
&\quad + 16k\mathcal{F}_{QQ}^{\text{BOX}}(s, t, u),
\end{aligned}$$

$$F_{LD}(s, t, u) = \mathcal{F}_D^{zff}(s) + 16k\mathcal{F}_{LD}^{\text{BOX}}(s, t, u),$$

$$F_{QD}(s, t, u) = \mathcal{F}_D^{zff}(s) + k\mathcal{F}_D^{\gamma ff}(s) + 16k\mathcal{F}_{QD}^{\text{BOX}}(s, t, u). \quad (3.148)$$

For $IJ = LQ, QL, QQ, LD, QD$ components of a box contribution we have:

$$\begin{aligned}
\mathcal{F}_{IJ}^{\text{BOX}}(s, t, u) &= k^{AA}\mathcal{F}_{IJ}^{AA}(s, t, u) + k^{ZA}\mathcal{F}_{IJ}^{ZA}(s, t, u) + k^{ZZ}\mathcal{F}_{IJ}^{ZZ}(s, t, u) \\
&\quad + k^{WW}\mathcal{F}_{IJ}^{WW}(s, t, u), \quad (3.149)
\end{aligned}$$

where

$$k^{WW} = \frac{1}{16}. \quad (3.150)$$

Moreover,

$$\mathcal{F}_{L,Q,D}^{\gamma(z)ff}(s) = \sum_{B=A,Z,H,W} \mathcal{F}_{L,Q,D}^{\gamma(z)B}(s), \quad (3.151)$$

except for $\mathcal{F}_L^{\gamma A}(s) = 0$ and $\mathcal{F}_L^{\gamma H}(s) = 0$.

4 Improved Born Approximation cross-section

4.1 Improved Born Approximation cross-section

In this section we give the improved Born approximation (IBA) differential in the scattering angle cross-section. It is derived by simple squaring the $(\gamma + Z)$ exchange IBA amplitude, Eqs. (1.8)–(1.10), and accounting for proper normalization factors. We simply give the result:

$$\frac{d\sigma^{\text{IBA}}}{d\cos\vartheta} = \frac{\pi\alpha^2}{s^3} \beta_t N_c (\sigma_{\gamma\gamma}^{\text{IBA}} + \sigma_{\gamma Z}^{\text{IBA}} + \sigma_{ZZ}^{\text{IBA}}), \quad (4.152)$$

where $\beta_t = \sqrt{1 - 4m_f^2/s}$ and

$$\sigma_{\gamma\gamma}^{IBA} = Q_f^2 (s^2 + 2st + 2t_-^2) |\alpha(s)|^2, \quad (4.153)$$

$$\begin{aligned} \sigma_{\gamma Z}^{IBA} = & 2Q_f \text{Re} \left\{ \chi \left(2 \left[(s + t_-)^2 + sm_f^2 \right] \tilde{F}_{LL}(s, t, u) \right. \right. \\ & + (s^2 + 2st + 2t_-^2) \left[\tilde{F}_{QL}(s, t, u) + \tilde{F}_{LQ}(s, t, u) + \tilde{F}_{QQ}(s, t, u) \right] \\ & \left. \left. - 4m_f^2 (st + t_-^2) \left[\tilde{F}_{LD}(s, t, u) + \tilde{F}_{QD}(s, t, u) \right] \right) \alpha^*(s) \right\}, \quad (4.154) \end{aligned}$$

$$\begin{aligned} \sigma_{ZZ}^{IBA} = & |\chi|^2 \text{Re} \left\{ 8 (s + t_-)^2 \left[\left| \tilde{F}_{LL}(s, t, u) \right|^2 + \tilde{F}_{LL}(s, t, u) \tilde{F}_{QL}^*(s, t, u) \right] \right. \\ & + 2 \left[(s + t_-)^2 + t_-^2 \right] \left| \tilde{F}_{QL}(s, t, u) \right|^2 \\ & + 4 \left[(s + t_-)^2 + sm_f^2 \right] \left[2 \tilde{F}_{LL}(s, t, u) \tilde{F}_{LQ}^*(s, t, u) \right. \\ & + \tilde{F}_{LL}(s, t, u) \tilde{F}_{QQ}^*(s, t, u) + \tilde{F}_{QL}(s, t, u) \tilde{F}_{LQ}^*(s, t, u) \left. \right] \\ & + [s^2 + 2(st + t_-^2)] \left[2 \left| \tilde{F}_{LQ}(s, t, u) \right|^2 + \left| \tilde{F}_{QQ}(s, t, u) \right|^2 \right. \\ & + 2 \left(\tilde{F}_{QL}(s, t, u) + \tilde{F}_{LQ}(s, t, u) \right) \tilde{F}_{QQ}^*(s, t, u) \left. \right] \\ & - 8m_f^2 (st + t_-^2) \left[\left(2 \tilde{F}_{LD}(s, t, u) + \tilde{F}_{QD}(s, t, u) \right) \tilde{F}_{LL}^*(s, t, u) \right. \\ & + \left(\tilde{F}_{LD}(s, t, u) + \tilde{F}_{QD}(s, t, u) \right) \tilde{F}_{QL}^*(s, t, u) \\ & + \left(2 \tilde{F}_{LD}(s, t, u) + \tilde{F}_{QD}(s, t, u) \right) \tilde{F}_{LQ}^*(s, t, u) \\ & + \left(\tilde{F}_{LD}(s, t, u) + \tilde{F}_{QD}(s, t, u) \right) \tilde{F}_{QQ}^*(s, t, u) \left. \right] \\ & - 2m_f^2 (st + t_-^2) \Delta_{3r} \left[2 \left| \tilde{F}_{LD}(s, t, u) \right|^2 \right. \\ & \left. + 2 \tilde{F}_{LD}(s, t, u) \tilde{F}_{QD}^*(s, t, u) + \left| \tilde{F}_{QD}(s, t, u) \right|^2 \right] \left. \right\}. \quad (4.155) \end{aligned}$$

4.2 The $e^+e^- \rightarrow f\bar{f}$ process in the helicity amplitudes

According to the analysis of the EW part and QED parts, we have the **complete** answer for the amplitude of the process $e^+e^- \rightarrow t\bar{t}$.

The aim of this section is to adapt the helicity amplitude techniques for the description of our process. We produced an alternative analytic answer for the same amplitude using the method suggested in Ref. [37].

In general, there are 16 helicity amplitude for any $2f \rightarrow 2f$ process. For the unpolarized case, and when the electron mass is ignored, we are left with only six helicity amplitudes, which depend on kinematical variables and our six scalar form factors:

$$\begin{aligned}
\mathcal{A}_{++++} &= 0, & \mathcal{A}_{+++ -} &= 0, & \mathcal{A}_{++ - +} &= 0, & \mathcal{A}_{+ + - -} &= 0, \\
\mathcal{A}_{+ - + -} &= s(1 - \cos \vartheta) \left(Q_e Q_f F_{GG} + \chi_z \delta_e \left[(1 + \beta_f) I_t^{(3)} F_{QL} + \delta_f F_{QQ} \right] \right), \\
\mathcal{A}_{+ - - +} &= s(1 + \cos \vartheta) \left(Q_e Q_f F_{GG} + \chi_z \delta_e \left[(1 - \beta_f) I_t^{(3)} F_{QL} + \delta_f F_{QQ} \right] \right), \\
\mathcal{A}_{+ - - -} &= \mathcal{A}_{- + - +} = 2\sqrt{s} m_f \sin \vartheta \left(Q_e Q_f F_{GG} \right. \\
&\quad \left. + \chi_z \delta_e \left[I_t^{(3)} F_{QL} + \delta_f F_{QQ} + \frac{1}{2} s \beta_f^2 I_t^{(3)} F_{QD} \right] \right), \\
\mathcal{A}_{- + + +} &= \mathcal{A}_{- + - -} = -2\sqrt{s} m_f \sin \vartheta \left(Q_e Q_f F_{GG} \right. \\
&\quad \left. + \chi_z \left[2I_e^{(3)} I_t^{(3)} F_{LL} + 2I_e^{(3)} \delta_f F_{LQ} + \delta_e I_t^{(3)} F_{QL} + \delta_e \delta_f F_{QQ} \right. \right. \\
&\quad \left. \left. + \frac{1}{2} s \beta_f^2 I_t^{(3)} \left(2I_e^{(3)} F_{LD} + \delta_e F_{QD} \right) \right] \right), \\
\mathcal{A}_{- + + -} &= s(1 + \cos \vartheta) \left(Q_e Q_f F_{GG} + \chi_z \left[(1 + \beta_f) \left(2I_e^{(3)} I_t^{(3)} F_{LL} + \delta_e I_t^{(3)} F_{QL} \right) \right. \right. \\
&\quad \left. \left. + \delta_f \left(2I_e^{(3)} F_{LQ} + \delta_e F_{QQ} \right) \right] \right), \\
\mathcal{A}_{- + - +} &= s(1 - \cos \vartheta) \left(Q_e Q_f F_{GG} + \chi_z \left[(1 - \beta_f) I_t^{(3)} \left(2I_e^{(3)} F_{LL} + \delta_e F_{QL} \right) \right. \right. \\
&\quad \left. \left. + \delta_f \left(2I_e^{(3)} F_{LQ} + \delta_e F_{QQ} \right) \right] \right), \\
\mathcal{A}_{- - + +} &= 0, & \mathcal{A}_{- - + -} &= 0, & \mathcal{A}_{- - - +} &= 0, & \mathcal{A}_{- - - -} &= 0.
\end{aligned} \tag{4.1}$$

Here

$$\cos \vartheta = \left(t - m_f^2 + \frac{s}{2} \right) \frac{2}{s \beta_f}, \tag{4.2}$$

and for the amplitude $\mathcal{A}_{\lambda_i \lambda_j \lambda_k \lambda_l}$, each index $\lambda_{(i,j,k,l)}$ takes two values ($\pm = \pm 1$) meaning 2 times the projection of spins e^+, e^-, t, \bar{t} onto their corresponding momentum. The differential cross-section for the unpolarized case is:

$$\frac{d\sigma}{d\cos\vartheta} = \frac{\pi\alpha^2}{s^3} \beta_f N_c \sum_{\lambda_i \lambda_j \lambda_k \lambda_l} |\mathcal{A}_{\lambda_i \lambda_j \lambda_k \lambda_l}|^2. \quad (4.3)$$

We checked that this expression is analytically identical to Eq. (4.152). Both expressions, Eq. (4.152) and Eq. (4.3), contains, however, spurious contributions of the two-loop order (squares of one-loop terms), which should be suppressed, since we would like to have a complete one-loop result.

This may be achieved with a simple trick. First of all, let us note that if all form factors are: $F_{IJ} = 1$ for $IJ = LL, LQ, QL, QQ$ and $F_{IJ} = 0$ for $IJ = LD, QD$, we have the tree level. At the one-loop level LL, LQ, QL, QQ form factors may be represented as:

$$\mathbf{F}_{IJ} = 1 + \frac{\alpha}{4\pi s_W^2} F_{IJ}, \quad (4.4)$$

and

$$\mathbf{F}_{IJ} = \frac{\alpha}{4\pi s_W^2} F_{IJ}, \quad (4.5)$$

for $IJ = LD, QD$.

Instead of Eq. (4.4) for the four form factors we write

$$\mathbf{F}_{IJ} = Z + \frac{\alpha}{4\pi s_W^2} F_{IJ}, \quad (4.6)$$

and note that the cross section is a function of six form factors.

Then the one-loop result is apparently equal:

$$\frac{d\sigma^{(1)}}{d\cos\vartheta} = \frac{d\sigma}{d\cos\vartheta}[Z = 1] - \frac{d\sigma}{d\cos\vartheta}[Z = 0]. \quad (4.7)$$

5 Annex

5.1 QED vertices and soft-photon contributions

Here we present virtual corrections due to QED vertices, a factorized part due to QED boxes and soft-photon contributions. The expressions in this subsection can be also cast from [11].

The formal structure of factorized virtual and soft contributions is as follows:

$$\delta^{\text{virt+soft}} = \frac{\alpha}{\pi} \left[Q_e^2 \delta_{\text{ISR}}^{\text{virt+soft}} + Q_e Q_f \delta_{\text{IFI}}^{\text{virt+soft}} + Q_f^2 \delta_{\text{FSR}}^{\text{virt+soft}} \right]. \quad (5.1)$$

There are thus three types of contributions: ISR, FSR and IFI.

5.1.1 Initial-state radiation (ISR)

The contributions of the initial-state QED $e^+e^-\gamma$ vertex and ISR soft photon contribution are short, since the electron mass is ignored:

$$\begin{aligned}\delta_{\text{ISR}}^{\text{virt}} &= -\ln \frac{m_e^2}{\lambda^2} (l_e - 1) - \frac{1}{2}l_e^2 + \frac{3}{2}l_e - 2 + 4\text{Li}_2(1), \\ \delta_{\text{ISR}}^{\text{soft}} &= \ln \left(\frac{4\omega^2}{s} \frac{m_e^2}{\lambda^2} \right) (l_e - 1) + \frac{1}{2}l_e^2 - 2\text{Li}_2(1),\end{aligned}\quad (5.2)$$

where

$$l_e = \ln \left(\frac{s}{m_e^2} \right). \quad (5.3)$$

5.1.2 Initial-final state interference (IFI)

This originates from contributions of QED boxes: $\gamma\gamma$, $Z\gamma$ and initial-final state soft photons interference:

$$\delta_{\text{IFI}}^{\text{virt}} = -2 \ln \frac{s}{\lambda^2} \ln \frac{t_-}{u_-}, \quad (5.4)$$

$$\delta_{\text{IFI}}^{\text{soft}} = 2 \ln \frac{4\omega^2}{\lambda^2} \ln \frac{t_-}{u_-} + [F^{\text{soft}}(s, t) - F^{\text{soft}}(s, u)], \quad (5.5)$$

with

$$\begin{aligned}F^{\text{soft}}(s, t) &= -\frac{1}{2}l_e^2 - \frac{1}{2}\ln^2 \eta + 2 \ln \eta \ln \left(1 + \frac{2m_f^2}{\beta_+ t_-} \right) \\ &\quad - \ln^2 \left(1 + \frac{2m_f^2}{\beta_+ t_-} \right) + \ln^2 \left(-\frac{st}{t_-^2} \right) + 2 \ln \left(-\frac{st}{t_-^2} \right) \ln \left(1 + \frac{t_-^2}{st} \right) \\ &\quad + 2\text{Li}_2 \left(1 - \frac{2t}{t_- \beta_+} \right) - 2\text{Li}_2 \left(\frac{-\beta_- t_-}{\beta_+ t_- + 2m_f^2} \right) \\ &\quad - 2\text{Li}_2 \left(-\frac{t_-^2}{st} \right) - 2\text{Li}_2(1),\end{aligned}\quad (5.6)$$

where we introduce the notation:

$$\begin{aligned}\beta \equiv \beta_f &= \sqrt{1 - \frac{4m_f^2}{s}}, \\ \beta_+ &= 1 + \beta, \\ \beta_- &= 1 - \beta, \\ \eta &= \frac{\beta_-}{\beta_+}.\end{aligned}\quad (5.7)$$

5.1.3 Final-state radiation (FSR)

The contributions of one-loop QED $f\bar{f}\gamma$ vertex and final-state soft photon radiation are:

$$\begin{aligned}\delta_{\text{FSR}}^{\text{virt}} &= -\ln \frac{m_f^2}{\lambda^2} \left[-\frac{(1+\beta^2)}{2\beta} \ln \eta - 1 \right] - \frac{3}{2} \beta \ln \eta - 2 \\ &\quad + \frac{(1+\beta^2)}{2\beta} \left[-\frac{1}{2} \ln^2 \eta + 2 \ln \eta \ln(1-\eta) + 2\text{Li}_2(\eta) + 4\text{Li}_2(1) \right], \\ \delta_{\text{FSR}}^{\text{soft}} &= \ln \frac{4\omega^2}{\lambda^2} \left[-\frac{(1+\beta^2)}{2\beta} \ln \eta - 1 \right] - \frac{1}{\beta} \ln \eta \\ &\quad + \frac{(1+\beta^2)}{2\beta} \left[-\frac{1}{2} \ln^2 \eta + 2 \ln \eta \ln(1-\eta) + 2\text{Li}_2(\eta) - 2\text{Li}_2(1) \right].\end{aligned}\quad (5.8)$$

The contribution of the ISR given in Eq. (5.2) may be obtained from these expressions in the limit $m_f = m_e \rightarrow 0$.

5.1.4 Non-factorized final-state vertex ‘anomalous’ contributions

To present this contribution let us introduce the definition

$$L_n = \ln \frac{\beta - 1}{\beta + 1}. \quad (5.9)$$

The ‘anomalous’ part of the QED vertex contribution to the differential cross-section reads:

$$\begin{aligned}\frac{d\sigma^a}{d\cos\vartheta} &= 4\alpha^3 N_c \frac{m_f^2}{s^4} Q_f^2 \left[\left(Q_e^2 Q_f^2 + 2Q_e Q_f v_e v_f \text{Re}(\chi_z) + (v_e^2 + a_e^2) v_t^2 |\chi_z|^2 \right) \right. \\ &\quad \times (st + t_-^2) \text{Re}(L_n) + Q_e Q_f a_e a_f s (s + 2t_-) \text{Re}(L_n \chi_z) \\ &\quad + \left. \left((v_e^2 + a_e^2) a_t^2 \left[s(s - 4m_f^2) + 2(st + t_-^2) \right] \right. \right. \\ &\quad \left. \left. + 2v_e a_e v_f a_f s (s + 2t_-) \right) |\chi_z|^2 \text{Re}(L_n) \right].\end{aligned}\quad (5.10)$$

5.2 An alternative form of the cross-section for QED boxes

Here we present some useful formulae, which are not in the main stream of our approach (described in the previous sections), but were used for internal cross-checks of the calculations of the QED part of the process under consideration.

The QED boxes, Eqs. (2.137) and (2.138), may be greatly simplified purely algebraically if the cross-sections are calculated analytically. For the sum of

AA and ZA boxes one may easily derive the cross-section:

$$\begin{aligned} \frac{d\sigma^{\text{BOX}}}{d\cos\vartheta} = & \frac{2\alpha^3}{s}\beta Q_e Q_f N_c \text{Re} \left\{ Q_e^2 Q_f^2 \mathcal{F}_V \right. \\ & + Q_e Q_f \chi_Z \left[v_e v_f (\mathcal{F}_V^* + \mathcal{H}_V) + a_e a_f (\mathcal{F}_A^* + \mathcal{G}_V) \right] \\ & \left. + |\chi_Z|^2 \left[(v_e^2 + a_e^2) (v_f^2 \mathcal{H}_V + a_f^2 \mathcal{H}_A) + 2a_e v_e a_f v_f (\mathcal{G}_V + \mathcal{G}_A) \right] \right\}, \end{aligned} \quad (5.11)$$

where $\chi_Z(s)$ is defined by Eq. (1.12) and the six *cross-section form factors* are:

$$\begin{aligned} \mathcal{F}_V &= \mathcal{F}_V(t) - \mathcal{F}_V(u), \\ \mathcal{F}_A &= \mathcal{F}_A(t) + \mathcal{F}_A(u), \\ \mathcal{H}_V &= \mathcal{H}_V(t) - \mathcal{H}_V(u), \\ \mathcal{H}_A &= \mathcal{H}_A(t) - \mathcal{H}_A(u), \\ \mathcal{G}_V &= \mathcal{G}_V(t) + \mathcal{G}_V(u), \\ \mathcal{G}_A &= \mathcal{G}_A(t) + \mathcal{G}_A(u), \end{aligned} \quad (5.12)$$

with

$$\begin{aligned} \mathcal{F}_V(t) = & \frac{1}{s} \left\{ \frac{t_-}{4} \left[2m_f^2 + (s + 2t_-) \right] J_{AA}(-s, -t; m_e, m_f) \right. \\ & + \frac{st}{2} C_0(-m_e^2, -m_e^2, -s; 0, m_e, 0) \\ & + t \left(\frac{s - 4m_f^2}{2} + \frac{4m_t^4}{\Delta_{3r}} \right) C_0(-m_f^2, -m_f^2, -s; 0, m_f, 0) \\ & + \frac{2tm_f^2}{\Delta_{3r}} \left[B_0^F(-m_f^2; m_f, 0) - B_0^F(-s; 0, 0) \right] \\ & - \frac{sm_f^2}{t_-} \left[B_0^F(-t; m_e, m_f) - B_0^F(-m_f^2; m_f, 0) \right] \\ & \left. - \frac{(s + t_-)}{2} \left[B_0^F(-t; m_e, m_f) - B_0^F(-s; 0, 0) \right] \right\}, \end{aligned} \quad (5.13)$$

$$\begin{aligned} \mathcal{F}_A(t) = & \frac{1}{s} \left\{ \frac{s + 2t_-}{4} t_- J_{AA}(-s, -t; m_e, m_f) \right. \\ & - m_f^2 \left(\frac{1}{2} s C_0(-m_f^2, -m_f^2, -s; 0, m_f, 0) \right. \\ & \left. + \left(\frac{s}{t_-} + 1 \right) \left[B_0^F(-t; m_e, m_f) - B_0^F(-m_f^2; m_f, 0) \right] \right) \\ & \left. - \frac{(s + t_-)}{2} \left[B_0^F(-t; m_e, m_f) - B_0^F(-s; 0, 0) \right] \right\}, \end{aligned} \quad (5.14)$$

$$\begin{aligned}
\mathcal{H}_0(t) = & \frac{1}{s^2} \left\{ \left(t_-^2 + (s+t_-)^2 \right) \frac{t_-}{2} J_{AA}(-s, -t; m_e, m_f) \right. \\
& + t_- \left[\frac{1}{2} s_- (s_+ + 2t) - \left(t_-^2 + (s+t_-)^2 \right) \right] J_{AZ}(-s, -t; m_e, m_f) \\
& + \left(\frac{ss_- m_f^2}{t_-} M_Z^2 + t_- \left[s_- (s_+ + 2t) - \left(t_-^2 + (s+t_-)^2 \right) \right] \right) \\
& \quad \times C_0(-m_f^2, -m_e^2, -t; m_f, M_Z, m_e) \\
& + s_- \left(st C_0(-m_e^2, -m_e^2, -s; M_Z, m_e, 0) \right. \\
& + st C_0(-m_f^2, -m_f^2, -s; M_Z, m_f, 0) \\
& - \frac{sm_f^2}{t_-} \left[2B_0^F(-t; m_e, m_f) - B_0^F(-m_f^2; m_f, 0) \right. \\
& \quad \left. \left. - B_0^F(-m_f^2; M_Z, m_f) \right] \right) \\
& \left. - (s+t_-) \left[B_0^F(-t; m_e, m_f) - B_0^F(-s; M_Z, 0) \right] \right\}, \tag{5.15}
\end{aligned}$$

$$\begin{aligned}
\mathcal{H}_V(t) = & \mathcal{H}_0(t) - \frac{2t_- m_f^2}{s} \left[J_{AZ}(-s, -t; m_e, m_f) - \frac{1}{2} J_{AA}(-s, -t; m_e, m_f) \right. \\
& \left. + C_0(-m_f^2, -m_e^2, -t; m_f, M_Z, m_e) \right] \\
& - \frac{2m_f^2 s_- t}{s^2} \left(\left(1 - \frac{s_-}{\Delta_{3r}} \right) C_0(-m_f^2, -m_f^2, -s; M_Z, m_f, 0) \right. \\
& - \frac{1}{\Delta_{3r}} \left[2B_0^F(-s; M_Z, 0) - B_0^F(-m_f^2; m_f, 0) \right. \\
& \left. \left. - B_0^F(-m_f^2; M_Z, m_f) \right] \right) \left. \right\}, \tag{5.16}
\end{aligned}$$

$$\begin{aligned}
\mathcal{H}_A(t) = & \mathcal{H}_0(t) + \frac{2m_f^2}{s^2} \left\{ t_- \left[M_Z^2 J_{AZ}(-s, -t; m_e, m_f) \right. \right. \\
& \left. - \frac{1}{2} J_{AA}(-s, -t; m_e, m_f) \right] \\
& + (s_- s_+ + t_- s) C_0(-m_f^2, -m_e^2, -t; m_f, M_Z, m_e) \\
& + s_- \left[-t C_0(-m_f^2, -m_f^2, -s; M_Z, m_f, 0) \right. \\
& \left. \left. - B_0^F(-t; m_e, m_f) + B_0^F(-s; M_Z, 0) \right] \right\}, \tag{5.17}
\end{aligned}$$

$$\begin{aligned}
\mathcal{G}_V(t) = & -\frac{1}{s} \left\{ -\frac{1}{2} (s+2t_-) t_- J_{AA}(-s, -t; m_e, m_f) \right. \\
& + t_- \left[s+2t_- - \frac{s_-}{2s} (s_+ + 2t_-) \right] J_{AZ}(-s, -t; m_e, m_f) \\
& + \left[(s+2t_-) t_- - \frac{s-t_-}{s} (s_+ + 2t_-) - s_- m_f^2 \left(2 + \frac{M_Z^2}{t_-} \right) \right] \\
& \quad \times C_0(-m_f^2, -m_e^2, -t; m_f, M_Z, m_e) \\
& - s_- \left(\frac{1}{2} M_Z^2 \left[C_0(-m_e^2, -m_e^2, -s; M_Z, m_e, 0) \right. \right. \\
& \quad \left. \left. + C_0(-m_f^2, -m_f^2, -s; M_Z, m_f, 0) \right] \right. \\
& + \frac{m_f^2}{t_-} \left[-2B_0^F(-t; m_e, m_f) + B_0^F(-m_f^2; m_f, 0) \right. \\
& \quad \left. + B_0^F(-m_f^2; M_Z, m_f) \right] \\
& \left. - \frac{(s+t_-)}{s} \left[B_0^F(-t; m_e, m_f) - B_0^F(-s; M_Z, 0) \right] \right\}, \quad (5.18)
\end{aligned}$$

$$\begin{aligned}
\mathcal{G}_A(t) = & \mathcal{G}_V(t) - m_f^2 \frac{s_-}{s^2} \left[2s_- C_0(-m_f^2, -m_e^2, -t; m_f, M_Z, m_e) \right. \\
& + s_+ C_0(-m_f^2, -m_f^2, -s; M_Z, m_f, 0) \\
& \left. + 2B_0^F(-t; m_e, m_f) - B_0^F(-m_f^2; M_Z, m_f) - B_0^F(-m_f^2; m_f, 0) \right]. \quad (5.19)
\end{aligned}$$

Note the cancellation of Δ_{4r} , leading to a great simplification of the expressions. Equations (5.11–5.19) were coded as a separate branch of `eeffLib` and, together with the vertex QED contributions described in the previous subsections, were used for an internal cross-check of the QED part of the calculations.

Some factorized part of the AA and ZA boxes contribution is not included in Eq. (5.11). It has the form

$$\frac{d\sigma}{d\cos\vartheta} \frac{\alpha}{\pi} Q_e Q_f \delta_{\text{IFI}}^{\text{virt}}, \quad (5.20)$$

where $\delta_{\text{IFI}}^{\text{virt}}$ is given by Eq. (5.4).

The whole QED contribution can be written as follows

$$\frac{d\sigma^{\text{QED}}}{d\cos\vartheta} = \frac{d\sigma^{\text{BORN}}}{d\cos\vartheta} \delta^{\text{virt+soft}} + \frac{d\sigma^a}{d\cos\vartheta} + \frac{d\sigma^{\text{BOX}}}{d\cos\vartheta}, \quad (5.21)$$

where $\delta^{\text{virt+soft}}$ is defined by Eqs. (5.1)–(5.8).

6 Numerical results and discussion

All the formulae derived in this article are realized in the FORTRAN code with the tentative name `eeffLib`. Numbers presented in this section are produced with the February 2002 version of the code. As compared to the December 2000 version, used to produce numbers for Ref. [23], the current version contains full QED corrections together with the soft-photon contribution to the angular distribution $d\sigma/d\cos\vartheta$. In this section we present several examples of numerical results. In particular, we will show a comparison of the electroweak form factors (EWFF) *including* QED corrections between `eeffLib` and another FORTRAN code, which was automatically generated from form log files with the aid of system `s2n.f` (*symbols to numbers*), producing a FORTRAN source code — a part of our SANC system. This comparison provides a powerful internal cross-check of our numerics that practically excludes the appearance of bugs in numerical results.

We begin with showing several examples of comparison with ZFITTER v6.30 [38]. In the present realization, `eeffLib` does not calculate M_W from μ decay and does not precompute either Sirlin's parameter Δr or the total Z width, which enters the Z boson propagator. For this reason, the three parameters: M_W , Δr , Γ_Z were being taken from ZFITTER and used as INPUT for `eeffLib`. Moreover, present `eeffLib` is a purely one-loop code, while it was not foreseen in ZFITTER, to access just one-loop form factors with the aid of users flags. To accomplish the goals of comparison at the one-loop level, we had to modify the DIZET electroweak library. The most important change was an addition to the SUBROUTINE ROKANC:

```
*
* For eett
*
      FLL=(XROK(1)-1D0+DR)*R1/AL4PI
      FQL=FLL+(XROK(2)-1D0)*R1/AL4PI
      FLQ=FLL+(XROK(3)-1D0)*R1/AL4PI
      FQQ=FLL+(XROK(4)-1D0)*R1/AL4PI
```

with the aid of which we reconstruct four scalar form factors from ZFITTER's effective couplings ρ and κ 's (F_{LD} and F_{QD} do not contribute in the massless approximation).

6.1 Flags of `eeffLib`

Here we give a description of flags (user options) of `eeffLib`. While creating the code, we followed the principle to preserve as often as possible the meaning of flags as described in the ZFITTER description [5]. In the list below, the comment '*as in ZFD*' means that the flag has exactly the same meaning as in [5]. Here we describe the set of flags of the February 2002 version of `eeffLib`.

- ALEM=3 ! as in ZFD
- ALE2=3 ! as in ZFD
- VPOL=0 ! =0 $\alpha(0)$; =1,=2 as in ZFD; =3 is reserved for later use
Note that the flag is extended to VPOL=0 to allow calculations ‘without running of α ’.
- QCDC=0 ! as in ZFD
- ITOP=1 ! as in DIZET (internal flag)
- GAMS=1 ! as in ZFD
- WEAK=1 ! as in ZFD (use WEAK=2 in v6.30 to drop out some higher-order terms)
- IMOMS=1 ! =0 α -scheme; =1 GFermi-scheme
New meaning of an old flag: switches between two renormalization schemes.
- BOXD=6
Together with WEAK=0 is used for an internal comparison of separate boxes and QED contributions:
BOXD ! =1 with AA boxes
! =2 with ZA boxes
! =3 with AA and ZA boxes
! =4 with all QED contributions
Together with WEAK=1 (working option), it has somewhat different meanings:
BOXD ! =0 without any boxes
! =1 with AA boxes
! =2 with ZA boxes
! =3 with AA and ZA boxes
! =4 with WW boxes
! =5 with WW and ZZ boxes
! =6 with all QED and EW boxes

‘Treatment’ options.

- GAMZTR=1 treatment of Γ_Z .
The option is implemented for the sake of comparison with FeynArts:
GAMZTR=0 $\Gamma_Z = 0$
GAMZTR=1 $\Gamma_Z \neq 0$
- EWWFTR=0 treatment of EW form factors.
Switches between form factors and effective ZFITTER couplings ρ and κ ’s. The option is implemented for comparison with ZFITTER:
EWWFTR=0 electroweak form factors
EWWFTR=1 effective couplings ρ and κ ’s
- FERMTR=1 treatment of fermionic masses
Switches between three different sets of ‘effective quark masses’:
FERMTR=1 a ‘standard’ set of fermions masses
FERMTR=2,3 ‘modified’ sets

- **VPOLTR=1** treatment of photonic vacuum polarization
Switches between lowest-order expression $\alpha(s) = \alpha [1 + \Delta\alpha(s)]$ and its ‘resummed’ version, $\alpha(s) = \alpha / [1 - \Delta\alpha(s)]$:
VPOLTR=0 lowest order
VPOLTR=1 resummed
- **EWRCR=2** treatment of electroweak radiative corrections
Switches between three variants for vertex corrections:
EWRCR=0 electroweak form factors contain only QED additions
EWRCR=1 electroweak form factors do not contain QED additions
EWRCR=2 electroweak form factors contain both QED and EW additions
- **EMASTR=0** treatment of terms with $\ln(s/m_e^2)$ in AA and ZA boxes, which are present in various functions but cancel in sum:
EMASTR=0 these terms are suppressed in all functions they enter
EMASTR=1 these terms are retained in all functions, which results in loss of computer precision owing to numerical cancellation; results for EMASTR=0 and EMASTR=1 are equal
- **EWFFV=1** treatment of vertex and box diagrams with virtual W boson, switches between two variants:
EWFFV=0 variant of formulae without b -quark mass
EWFFV=1 variant of formulae with finite b -quark mass

Options affecting QED contributions.

- **IQED=4** variants of inclusion virtual and soft photon QED contributions:
IQED=1 only initial-state radiation (ISR)
IQED=2 only initial-final interference (IFI)
IQED=3 only final-state radiation (FSR)
IQED=4 all QED contributions are included
- **IBOX=4** is active only if IQED=2 or 4 and affects only Eq. (5.11):
IBOX=0 AA boxes interfering with γ exchange BORN
IBOX=1 AA boxes
IBOX=2 ZA boxes
IBOX=3 or 4 $AA+ZA$ boxes

6.2 eeffLib-ZFITTER comparison of scalar form factors

First of all we discuss the results of a computation of the complete EW part of the four scalar form factors (i.e. with WW and ZZ boxes),

$$F_{LL}(s, t), \quad F_{QL}(s, t), \quad F_{LQ}(s, t), \quad F_{QQ}(s, t), \quad (6.1)$$

for three channels: $e^+e^- \rightarrow u\bar{u}$, $d\bar{d}$ and $b\bar{b}$ for light final fermion masses (we set $m_u = m_d = 0.1$ GeV) and for $b\bar{b}$ channel we use the formulae in the limit $m_f = 0$). We remind that ZFITTER is able to deliver only massless results.

In this comparison we use flags as in subsection 6.1 and, moreover,

$$\begin{aligned}
M_W &= 80.4514958 \text{ GeV}, \\
\Delta r &= 0.0284190602, \\
\Gamma_Z &= 2.499776 \text{ GeV}.
\end{aligned}
\tag{6.2}$$

The form factors are shown as complex numbers for the three c.m.s. energies (for $t = m_t^2 - s/2$) and for $\mu = M_W^2$. Table 1 shows very good agreement with ZFITTER results (up to 6 or 7 digits agree). It should be stressed that total agreement with ZFITTER is not expected because in the `eeffLib` for $e^+e^- \rightarrow u\bar{u}$ and $d\bar{d}$ channels we use massive expressions to compute the nearly massless case. Certain numerical cancellations leading to losing some numerical precision are expected. We should conclude that the agreement is very good and demonstrates that our formulae have the correct $m_t \rightarrow 0$ limit. Note, that there is an all digits agreement for $e^+e^- \rightarrow b\bar{b}$ channel since in both cases one uses the formulae in the limit $m_f^2 = 0$.

6.3 `eeffLib`–ZFITTER comparison of IBA cross-section

As the next step of the comparison of `eeffLib` with calculations from the literature, we present a comparison of the IBA cross-section.

In Table 2 we show the differential cross-section Eq. (4.152) in pb for four leptonic channels and in Table 3 for three quarkonic channels ($b\bar{b}$ channel being shown twice for massless and massive b quarks) for three values of $\cos\vartheta = -0.9, 0, +0.9$ with running e.m. coupling $\alpha(s)$. Since the flag setting VPOL=1, which is relevant to this case, affects the ZFITTER numbers, we now use, instead of Eq. (6.2), the new INPUT set:

$$\begin{aligned}
M_W &= 80.4467671 \text{ GeV}, \\
\Delta r &= 0.0284495385, \\
\Gamma_Z &= 2.499538 \text{ GeV}.
\end{aligned}
\tag{6.3}$$

The numbers shown in first two rows of Tabs. 2 and 3 exhibit a very good level of agreement with ZFITTER.

Finally, in Table 4, we give a comparison of the cross-section integrated within the angular interval $|\cos\vartheta| \leq 0.999$. (Flag setting is the same as for Table 4.)

A typical deviation between `eeffLib` and ZFITTER is of the order $\sim 10^{-6}$, i.e. of the order of the required precision of the numerical integration over $\cos\vartheta$. Examples of numbers obtained with `eeffLib`, which were shown in this section, demonstrate that ZFITTER numbers are recovered for light m_t .

²In the preprints [23] and [24] we presented this and the following tables for the three values of scale $\mu = M_W/10, M_W, 10M_W$ and demonstrated the scale independence of `eeffLib` numbers.

Table 1: EWFF for the process $e^+e^- \rightarrow f\bar{f}$. eeffLib-ZFITTER comparison.

\sqrt{s}	100 GeV	200 GeV	300 GeV
FF			
$u\bar{u}$ channel, $m_u = 0.1$ GeV, $m_d = 0$			
F_{LL}	12.89583 - i 1.84786	8.24737 - i 10.64653	8.98371 - i 12.88466
ZF	12.89583 - i 1.84786	8.24736 - i 10.64651	8.98370 - i 12.88466
F_{QL}	29.30446 + i 3.67330	29.38217 + i 2.27613	31.59711 + i 1.59304
ZF	29.30445 + i 3.67330	29.38216 + i 2.27613	31.59710 + i 1.59304
F_{LQ}	29.10831 + i 3.26973	29.48511 + i 0.92311	31.65835 - i 0.89711
ZF	29.10832 + i 3.26973	29.48512 + i 0.92312	31.65835 - i 0.89711
F_{QQ}	44.88228 + i 8.85688	43.31854 + i 9.48286	44.18773 + i 10.25197
ZF	44.88228 + i 8.85688	43.31854 + i 9.48286	44.18773 + i 10.25196
$d\bar{d}$ channel, $m_d = 0.1$ GeV, $m_u = 0$			
F_{LL}	13.70781 - i 1.51002	15.18630 - i 3.93706	8.86000 - i 1.80409
ZF	13.70781 - i 1.51002	15.18629 - i 3.93706	8.86000 - i 1.80409
F_{QL}	29.64340 + i 4.12394	31.96819 + i 6.97877	31.69945 + i 8.03876
ZF	29.64340 + i 4.12394	31.96818 + i 6.97877	31.69944 + i 8.03876
F_{LQ}	29.12112 + i 3.22780	30.28990 + i 1.73736	31.69321 - i 0.07000
ZF	29.12113 + i 3.22780	30.28990 + i 1.73733	31.69323 - i 0.07001
F_{QQ}	44.87608 + i 8.79014	43.94906 + i 9.86523	44.19463 + i 10.38253
ZF	44.87609 + i 8.79014	43.94905 + i 9.86523	44.19462 + i 10.38251
$b\bar{b}$ channel, $m_b = 0$, $m_t = 173.8$ GeV			
F_{LL}	11.16367 - i 0.65244	14.68726 - i 1.85834	11.26568 - i 3.38026
ZF	11.16367 - i 0.65244	14.68726 - i 1.85834	11.26568 - i 3.38026
F_{QL}	26.88634 + i 4.76865	28.08780 + i 5.27877	31.02060 + i 3.91962
ZF	26.88634 + i 4.76865	28.08780 + i 5.27877	31.02060 + i 3.91962
F_{LQ}	29.12113 + i 3.22780	30.28990 + i 1.73733	31.69323 - i 0.07001
ZF	29.12113 + i 3.22780	30.28990 + i 1.73733	31.69323 - i 0.07001
F_{QQ}	44.87609 + i 8.79014	43.94905 + i 9.86523	44.19462 + i 10.38251
ZF	44.87609 + i 8.79014	43.94905 + i 9.86523	44.19462 + i 10.38251

Table 2: Comparison of the differential EW cross-sections, [pb], leptonic channels. First row – ZFITTER, second row – eeffLib.

\sqrt{s}	100 GeV	200 GeV	300 GeV	400 GeV	700 GeV	1000 GeV
$\cos \vartheta$						
$\nu\bar{\nu}$ channel, $m_\nu = 0$						
-0.9	49.100086	0.579630	0.198147	0.101625	0.030297	0.014381
	49.100085	0.579630	0.198147	0.101625	0.030297	0.014381
0	31.834491	0.358941	0.122362	0.062455	0.018431	0.008648
	31.834490	0.358941	0.122362	0.062455	0.018431	0.008648
0.9	66.267213	0.739640	0.234000	0.115572	0.032285	0.014601
	66.267213	0.739640	0.234000	0.115572	0.032285	0.014601
e^-e^+ channel, $m_e = 0$						
-0.9	7.991109	0.533194	0.286463	0.169610	0.058032	0.028672
	7.991110	0.533194	0.286463	0.169609	0.058032	0.028672
0	19.773604	1.121915	0.474004	0.262276	0.084408	0.040933
	19.773604	1.121915	0.474004	0.262276	0.084408	0.040933
0.9	63.501753	3.504349	1.466665	0.811430	0.263378	0.128882
	63.501750	3.504348	1.466665	0.811430	0.263378	0.128882
$\mu^+\mu^-$ channel, $m_\mu = 0.106$ GeV						
-0.9	7.991040	0.533195	0.286463	0.169610	0.058032	0.028672
	7.991028	0.533195	0.286463	0.169610	0.058032	0.028672
0	19.773498	1.121915	0.474004	0.262276	0.084408	0.040933
	19.773506	1.121915	0.474004	0.262276	0.084408	0.040933
0.9	63.501436	3.504346	1.466665	0.811430	0.263378	0.128882
	63.501422	3.504345	1.466664	0.811430	0.263378	0.128882
$\tau^+\tau^-$ channel, $m_\tau = 1.77705$ GeV						
\sqrt{s}	100 GeV	200 GeV	300 GeV	400 GeV	700 GeV	1000 GeV
-0.9	7.971611	0.533509	0.286519	0.169627	0.058034	0.028673
	7.968192	0.533295	0.286477	0.169613	0.058032	0.028672
0	19.743430	1.121827	0.473992	0.262273	0.084407	0.040933
	19.745968	1.121978	0.474021	0.262282	0.084408	0.040933
0.9	63.412131	3.503720	1.466558	0.811398	0.263375	0.128882
	63.408973	3.503524	1.466520	0.811385	0.263373	0.128881

Table 3: Comparison of the differential EW cross-sections, [pb], quarkonic channels. First row – ZFITTER, second row – eeffLib.

\sqrt{s}	100 GeV	200 GeV	300 GeV	400 GeV	700 GeV	1000 GeV
$\cos\vartheta$						
<i>u\bar{u} channel, $m_u = 0.1$ GeV</i>						
-0.9	45.404742	0.386966	0.225923	0.138065	0.048621	0.024156
	45.404602	0.386966	0.225923	0.138065	0.048621	0.024156
0	60.382423	1.882835	0.771939	0.421410	0.133475	0.064245
	60.382566	1.882837	0.771939	0.421410	0.133475	0.064245
0.9	173.467517	6.450000	2.510881	1.346620	0.417295	0.198842
	173.467551	6.450000	2.510881	1.346620	0.417295	0.198842
<i>dd channel, $m_d = 0.1$ GeV</i>						
-0.9	86.554414	0.430807	0.136720	0.069644	0.020899	0.009978
	86.554110	0.430807	0.136720	0.069644	0.020899	0.009978
0	72.820806	1.180211	0.419410	0.219070	0.066312	0.031351
	72.820908	1.180212	0.419411	0.219070	0.066312	0.031351
0.9	176.717336	3.770861	1.469194	0.796291	0.255118	0.124714
	176.717376	3.770861	1.469194	0.796291	0.255118	0.124714
<i>dd channel, $m_b = 0.1$ GeV</i>						
-0.9	84.970331	0.416155	0.136467	0.071144	0.020786	0.009868
	84.970030	0.416155	0.136467	0.071144	0.020786	0.009868
0	71.762397	1.185284	0.426009	0.219777	0.067063	0.031698
	71.762496	1.185285	0.426009	0.219777	0.067063	0.031698
0.9	174.716111	3.819650	1.442852	0.764945	0.249501	0.123086
	174.716145	3.819651	1.442852	0.764945	0.249501	0.123086
<i>dd channel, $m_b = 4.7$ GeV</i>						
-0.9	84.350009	0.416665	0.136590	0.071186	0.020792	0.009870
	84.084519	0.415686	0.136435	0.071137	0.020786	0.009868
0	71.232935	1.183490	0.425748	0.219707	0.067058	0.031697
	71.248102	1.184186	0.425882	0.219745	0.067061	0.031697
0.9	173.420486	3.812786	1.441766	0.764642	0.249478	0.123084
	173.041374	3.811860	1.441592	0.764577	0.249464	0.123077

Table 4: Comparison of the total EW cross-sections, [pb]. First row – ZFITTER, second row – eeffLib.

100 GeV		200 GeV		300 GeV	
σ_{tot}	σ_{FB}	σ_{tot}	σ_{FB}	σ_{tot}	σ_{FB}
$\nu\bar{\nu}$ channel, $m_\nu = 0$					
84.81710	9.509864	0.963362	0.089665	0.320985	0.021592
84.81710	9.509865	0.963362	0.089665	0.320985	0.021592
e^-e^+ channel, $m_e = 0$					
52.61662	30.78899	2.980668	1.654673	1.276008	0.648414
52.61662	30.78899	2.980667	1.654673	1.276008	0.648414
$\mu^+\mu^-$ channel, $m_\mu = 0.106$ GeV					
52.61634	30.78885	2.980667	1.654671	1.276008	0.648414
52.61634	30.78885	2.980667	1.654671	1.276008	0.648414
$\tau^+\tau^-$ channel, $m_\tau = 1.77705$ GeV					
52.53632	30.75010	2.980435	1.654149	1.275972	0.648324
52.53661	30.75024	2.980443	1.654156	1.275974	0.648326
$u\bar{u}$ channel, $m_u = 0.1$ GeV					
160.8980	70.98406	5.021808	3.360848	2.031754	1.269556
160.8981	70.98416	5.021810	3.360848	2.031754	1.269556
$d\bar{d}$ channel, $m_d = 0.1$ GeV					
193.7658	50.03208	3.120724	1.867871	1.149479	0.725581
193.7658	50.03227	3.120725	1.867871	1.149479	0.725581
$b\bar{b}$ channel, $m_b = 0.1$ GeV					
191.0416	49.76543	3.134547	1.892628	1.149243	0.720476
191.0416	49.76562	3.134547	1.892629	1.149243	0.720476
$b\bar{b}$ channel, $m_b = 4.7$ GeV					
189.6321	49.39098	3.129824	1.888530	1.148541	0.719805
189.3855	49.32791	3.129858	1.888542	1.148565	0.719802

We conclude this subsection with a comment about the technical precision of our calculations. We do not use the `looptools` package [39]. For all PV functions but one, namely the D_0 function, we use our own coding, where we can control precision internally and, typically, we can guarantee 11 digits precision. For the D_0 function we use, instead, `REAL*16 TOPAZO` coding [8] and the only way that is accessible to us to control the precision is to compare our results with those computed with the `looptools` package. This was done for typical D_0 functions entering the ZZ box contributions. We obtained an agreement within 14 or 15 digits between these two versions for all $\sqrt{s} = 400$ – 10000 GeV and $\cos\vartheta = 0.99, 0, -0.99$.

6.4 Comparison with a code generated by s2n.f

Here we present a numerical comparison of the complete scalar form factors of Eq. (3.148), extracted from two independently created codes: the ‘manually written’ `eeffLib` and a code ‘automatically generated’ by the `s2n.f` software. We use a special input parameter set here: all lepton masses α and a conversion factor from GeV^{-1} to pb are taken from the 2000 Particle Data Tables while for quark and photon and gauge boson masses we use:

$$\begin{aligned} m_{u,d,c,s,t,b} &= 0.062, 0.083, 1.50, 0.215, 173.8, 4.70 \text{ GeV}, \\ \lambda &= 1 \text{ GeV}, M_Z = 91.1867 \text{ GeV}, M_W = 80.4514958 \text{ GeV}. \end{aligned} \quad (6.4)$$

As seen from Table 5, the numbers agree within 11–13 digits, i.e. `REAL*8` computational precision is saturated. The form factors $F_{LD,QD}$ are multiplied by 10^4 to make more digits visible.

Table 5: EWFF for the process $e^+e^- \rightarrow t\bar{t}$. First row – `eeffLib`, second row – `s2n.f`.

\sqrt{s}		400 GeV		700 GeV	
$\cos \vartheta$	FF				
-0.9	F_{LL}	68.36399900074 - i1.24743850729	68.36399900068 - i1.24743850728	79.63957322115 - i20.53758995637	79.63957322113 - i20.53758995637
	F_{QL}	75.12465846647 + i34.81991916400	75.12465846641 + i34.81991916400	76.19283172015 + i28.44336684106	76.19283172013 + i28.44336684106
	F_{LQ}	81.01546270426 + i19.81343626967	81.01546270420 + i19.81343626968	82.67283873006 + i13.79952080171	82.67283873004 + i13.79952080171
	F_{QQ}	225.63977621858 + i154.37838168488	225.63977621832 + i154.37838168491	207.09189805263 + i133.45188150116	207.09189805254 + i133.45188150117
	F_{LD}	-0.57522852857 + i0.34010611241	-0.57522852857 + i0.34010611241	-0.33030593699 + i0.14897150833	-0.33030593699 + i0.14897150833
	F_{QD}	0.16677424366 - i0.34326069364	0.16677424366 - i0.34326069364	0.29925308488 - i0.14107543098	0.29925308488 - i0.14107543098
0.0	F_{LL}	48.42950001713 + i8.26103890366	48.42950001707 + i8.26103890367	28.23570422021 + i2.43705570966	28.23570422019 + i2.43705570966
	F_{QL}	68.02678564355 + i37.08805801477	68.02678564349 + i37.08805801477	58.00469565609 + i33.82433896562	58.00469565607 + i33.82433896562
	F_{LQ}	73.37133716227 + i22.69397728402	73.37133716220 + i22.69397728403	62.40775508619 + i20.75544388763	62.40775508616 + i20.75544388764
	F_{QQ}	196.60425612149 + i162.74818773960	196.60425612123 + i162.74818773963	132.63279537966 + i152.68259938740	132.63279537957 + i152.68259938741
	F_{LD}	-0.56319765502 + i0.33645326768	-0.56319765502 + i0.33645326768	-0.29067043403 + i0.13992893252	-0.29067043403 + i0.13992893252
	F_{QD}	0.15893936555 - i0.37254018572	0.15893936555 - i0.37254018572	0.26429138671 - i0.15437851127	0.26429138671 - i0.15437851127
0.9	F_{LL}	35.17736865724 + i14.84038724783	35.17736865718 + i14.84038724784	0.21531292996 + i13.66645015866	0.21531292994 + i13.66645015866
	F_{QL}	61.03099608324 + i39.09196533610	61.03099608324 + i39.09196533611	40.77942026097 + i37.94118444135	40.77942026095 + i37.94118444136
	F_{LQ}	66.08215572929 + i25.04151178685	66.08215572929 + i25.04151178685	44.50915974057 + i25.51875704261	44.50915974055 + i25.51875704261
	F_{QQ}	167.63393504130 + i170.36384103672	167.63393504130 + i170.36384103675	59.87568281297 + i168.13599380718	59.87568281288 + i168.13599380719
	F_{LD}	-0.56772633347 + i0.34299744419	-0.56772633347 + i0.34299744419	-0.32035310873 + i0.14419510235	-0.32035310873 + i0.14419510235
	F_{QD}	0.18031346246 - i0.40091423652	0.18031346246 - i0.40091423652	0.34968026058 - i0.16945266925	0.34968026058 - i0.16945266925

The next Table 6 shows a comparison of `eeffLib-s2n.f` for the complete one-loop differential cross-sections $d\sigma^{(1)}/d\cos\vartheta$, for the standard input parameter set Eq. (6.4). As seen, numbers agree within 12 or 13 digits.

Table 6: $\frac{d\sigma^{(1)}}{d\cos\vartheta}$ for the process $e^+e^- \rightarrow t\bar{t}$. `eeffLib-s2n.f` comparison.

\sqrt{s}	400 GeV	700 GeV	1000 GeV
$\cos\vartheta$			
-0.9	0.22357662754774 0.22357662754769	0.06610825350063	0.02926006442715 0.02926006442715
0.0	0.34494634728716 0.34494634728707	0.14342802645636 0.14342802645634	0.06752160108814 0.06752160108813
0.9	0.54806778978208 0.54806778978194	0.33837133344667 0.33837133344664	0.16973989931024 0.16973989931023

6.5 About a comparison with the other codes

As is well known, the one-loop differential cross-section of $e^+e^- \rightarrow t\bar{t}$ may be generated with the aid of the FeynArts system [22]. Previous attempts to compare with FeynArts are described in [23]. In December 2001, we were provided with the numbers computed with the FeynArts system [41] for $d\sigma/d\cos\vartheta$, with and without QED contributions, at $\sqrt{s} = 700$ GeV and three values of $\cos\vartheta = 0.9, 0, -0.9$. With the current versions of `eeffLib` and `s2n.f` we have 11 digits agreement for both the tree-level and one-loop-corrected cross-sections.

Table 7: $\frac{d\sigma^{(1)}}{d\cos\vartheta}$ for the process $e^+e^- \rightarrow t\bar{t}$ with soft photons, $E_\gamma^{\max} = \sqrt{s}/10$.

\sqrt{s}	400 GeV	700 GeV	1000 GeV
$\cos\vartheta$			
-0.9	0.17613018248935	0.05199100267864	0.02310170508071
-0.5	0.21014509428358	0.06560630503586	0.02882301902010
0.0	0.27268108572063	0.11496514450150	0.05495088904853
0.5	0.35592722356682	0.19615154401629	0.09941700898317
0.9	0.43637377538440	0.27915043976042	0.14426233253975

Recently, the Bielefeld-Zeuthen team [33] performed an alternative calculation using the DIANA system [40]. Working in close contact with this team, we managed to perform several high-precision comparisons, reaching for separate contributions an agreement up to 10 digits.

The results of a comparison between FeynArts and the Bielefeld-Zeuthen team are presented in detail in [34].

As another example we present in Table 7 the same cross-section $[\frac{d\sigma}{d\cos\vartheta}]_{\text{SM}}$ as given in the tables of [34]. For the complete cross-section, including soft

photons, we agree with the Bielefeld–Zeuthen calculations within 8 digits. (See also [35].)

Two more graphical examples of the differential and the total EWRC for the process $e^+e^- \rightarrow t\bar{t}$ are shown in the figures 16 and 17, correspondingly.

Acknowledgements

We are indebted to G. Passarino for valuable discussions. We would like to thank W. Hollik and C. Schappacher for a discussion of issues of the comparison with FeynArts. We acknowledge a common work on numerical comparison with J. Fleischer, A. Leike, T. Riemann, and A. Werthenbach, which helped us to debug our ‘manually written’ code `eeffLib`. We also wish to thank G. Altarelli for extending to us the hospitality of the CERN TH Division at various stages of this work.

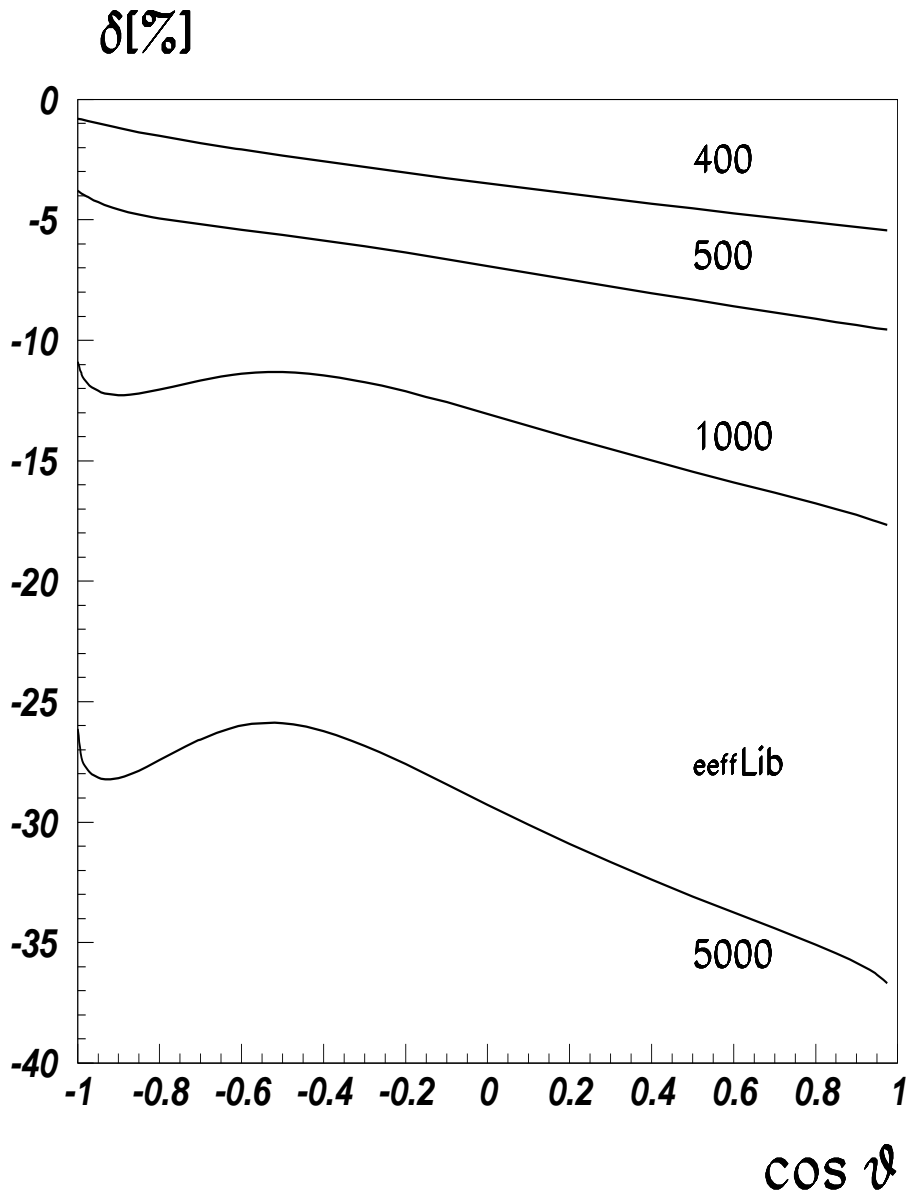


Figure 16: Relative EWRC $\delta(\sqrt{s}, \cos \vartheta) = \frac{d\sigma^{(1)}(s, t)/dt}{d\sigma^{(0)}(s)/dt} - 1$ to the $e^+e^- \rightarrow t\bar{t}$ differential cross-section. Numbers near the curves show \sqrt{s} in GeV.

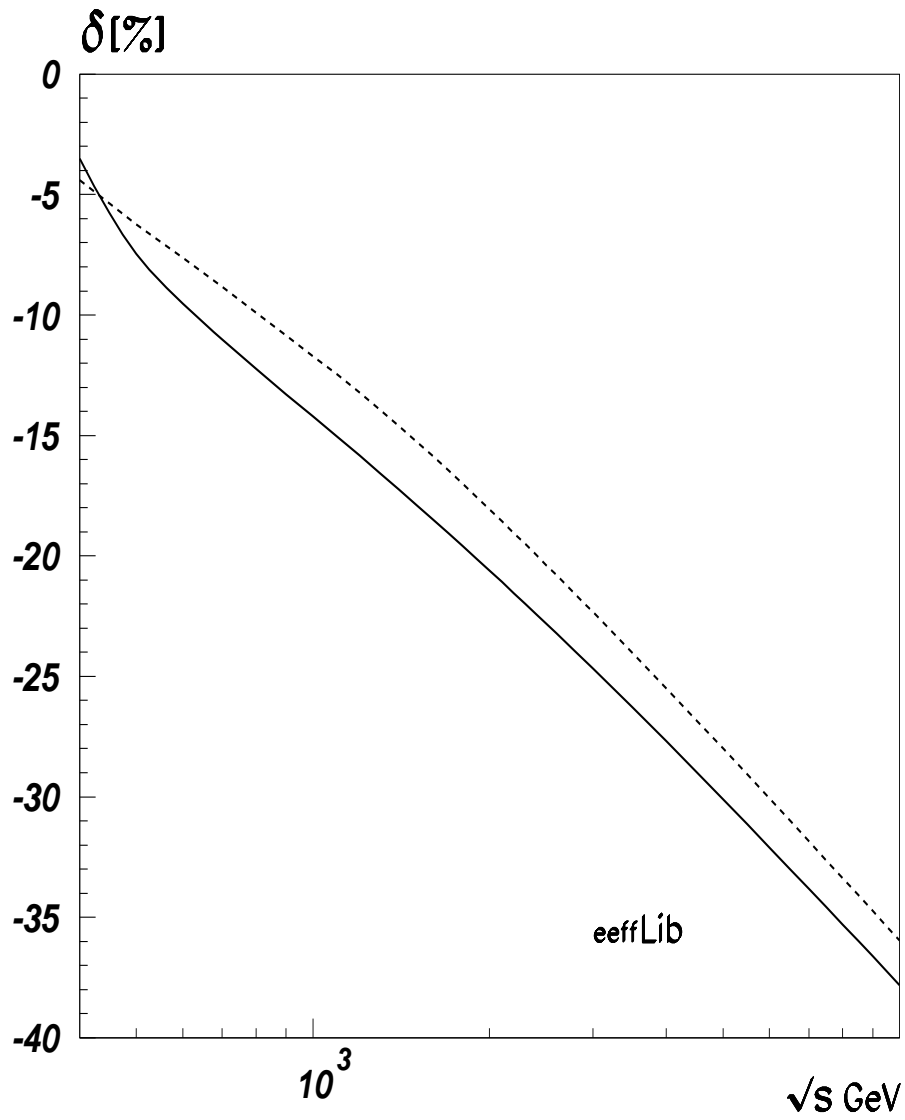


Figure 17: Relative EWRC to $e^+e^- \rightarrow t\bar{t}$ for $M_H = 100$ GeV (solid line) and $M_H = 1000$ GeV (dashed line).

References

- [1] G. Passarino and M. Veltman, *Nucl. Phys.* **B160** (1979) 151.
- [2] D. Bardin, P. Christova and O.M. Fedorenko, *Nucl. Phys.* **B175** (1980) 235; *Nucl. Phys.* **B197** (1982) 1.
- [3] F.A. Berends, G. Burgers and W.L. Neerven, *Nucl. Phys.* **B297** (1988) 429; *E Nucl. Phys.* **B304** (1989) 543.
- [4] W. Hollik, *Fortschritte Phys.* **38** (1990) 3.
- [5] D. Bardin, M. Bilenky, P. Christova, M. Jack, L. Kalinovskaya, A. Olchevski, S. Riemann, and T. Riemann, ‘ZFITTER v.6.21: A semi-analytical program for fermion pair production in e^+e^- annihilation’, DESY–Zeuthen preprint 99-070 (1999), hep-ph/9908433, *Comput. Phys. Commun.*, **133** (2001) 229–395.
- [6] G. Burgers, W. Hollik and M. Martinez (1990), program BHM;
- [7] W. Beenakker, F.A. Berends and S.C. van der Mark, *Nucl. Phys.* **B349** (1991) 323.
- [8] G. Montagna, O. Nicosini, F. Piccinini and G. Passarino, *Comput. Phys. Commun.* **117** (1999) 278.
- [9] M. Grünewald, *Experimental Tests of the Electroweak Standard Model at High Energies*, Phys. Rep. **322** (1999) 125.
- [10] The LEP Collaborations ALEPH, DELPHI, L3, OPAL, the LEP Electroweak Working Group and the SLD Heavy Flavour and Electroweak Groups, *A combination of Preliminary Electroweak Measurements and Constraints on the Standard Model*, CERN–EP–2000–016, January 21, 2000.
- [11] D. Bardin and G. Passarino, ‘The standard model in the making: Precision study of the electroweak interactions’, Oxford, UK: Clarendon, 1999.
- [12] J. Fujimoto and Y. Shimizu, *Mod. Phys. Lett.* **3A** (1988) 581.
- [13] W. Beenakker, S. C. van der Marck, and W. Hollik, *Nucl. Phys.* **B365** (1991) 24–78.
- [14] W. Beenakker and W. Hollik, *Phys. Lett.* **B269** (1991) 425–431.
- [15] ECFA/DESY LC Pphysics Working Group (J. Aguilar-Saavedra et.al.), ‘TESLA Technical Design Report Part III: Physics at an e^+e^- Linear Collider’, preprint DESY 2001-011 (2001), hep-ph/0106315.

- [16] M. Beneke *et al.*, ‘Top quark physics’, in *Proc. of the Workshop on Standard Model Physics (and More) at the LHC*, CERN 2000–004, G. Altarelli and M. Mangano, eds., CERN, Geneva, 2000, 419–529.
- [17] W. Beenakker, A. Denner, and A. Kraft, *Nucl. Phys.* **B410** (1993) 219–244.
- [18] V. Driesen, W. Hollik, and A. Kraft, ‘Top pair production in e^+e^- collisions with virtual and real electroweak radiative corrections’, Karlsruhe University preprint (1996), hep-ph/9603398.
- [19] F. Piccinini, *Nucl. Phys. Proc. Suppl.* **89** (2000) 31.
- [20] A. Denner, S. Dittmaier, M. Roth, and D. Wackerroth, *Nucl. Phys.* **B587** (2000) 67–117.
- [21] M. L. Nekrasov, *Eur. Phys. J.* **C19** (2001) 441–454.
- [22] J. Küblbeck, M. Böhm, A. Denner, *Comput. Phys. Commun.* **60** (1990) 165; T. Hahn, M. Perez-Victoria, *Comput. Phys. Commun.* **118** (1999) 153; T. Hahn, *Nucl. Phys. Proc. Suppl.* **89** (2000) 231; T. Hahn, *Comput. Phys. Commun.* **140** (2001) 418; T. Hahn, C. Schappacher, hep-ph/0105349.
- [23] D.Yu. Bardin, L.V. Kalinovskaya and G. Nanava, ‘An electroweak library for the calculation of EWRC to $e^+e^- \rightarrow f\bar{f}$ within the CalcPHEP project.’, JINR-E2-2000-292, hep-ph/0012080, Revised version, 2001, CERN-TH/2001-308.
- [24] A. Andonov, D. Bardin, S. Bondarenko, P. Christova, L. Kalinovskaya, and G. Nanava, ‘Further study of the $e^+e^- \rightarrow t\bar{t}$ process with the aid of CalcPHEP system’, hep-ph/0202112, CERN-TH/2002-068.
- [25] D. Bardin, G. Passarino, L. Kalinovskaya, P. Christova, A. Andonov, S. Bondarenko and G. Nanava, ‘Project CalcPHEP: Calculus for Precision High Energy Physics’, hep-ph/0202004, in *Proc. of the International Workshop ‘Computer Algebra and its Application to Physics’, CAAP-2001*, V.P. Gerdt ed., Dubna 2001, pp. 12–26; ‘SANC press release’, to appear in ACAT2002 Proceedings; ‘Project SANC (former CalcPHEP): Support of Analytic and Numeric calculations for experiments at Colliders’, CERN-TH/2002-245, hep-ph/0209297, to appear in ICHEP2002 Proceedings.
- [26] J. Vermaseren, ‘New features of FORM’, preprint NIKHEF-00-032 (2000), math-ph/0010025.
- [27] J. Fleischer and F. Jegerlehner, *Phys. Rev.* **D23** (1981) 2001–2026.

- [28] F. Jegerlehner, Talk presented at Topical Conf. on Radiative Corrections in $SU(2)_L \otimes U(1)$, Trieste, Italy, 1983.
- [29] F. Jegerlehner and J. Fleischer, *Phys. Lett.* **B151** (1985) 65–68.
- [30] F. Jegerlehner and J. Fleischer, *Acta Phys. Polon.* **B17** (1986) 709.
- [31] J. Fleischer, F. Jegerlehner, and M. Zralek, Presented at 11th Int. School of Theoretical Physics, Testing the Standard Model, Szczyrk, Poland, 1987.
- [32] L. Kalinovskaya, ‘About implementation of $e^+e^- \rightarrow f\bar{f}$ processes into the framework of SANC system’, to appear in ACAT2002 Proceedings; D. Bardin, P. Christova, L. Kalinovskaya, ‘SANC Status Report’, to appear in RADCOR2002 Proceedings.
- [33] J. Fleischer, T. Riemann and A. Werthenbach, the FORTRAN code `topfit`, February 2002.
- [34] J. Fleischer, T. Hahn, W. Hollik, T. Riemann, C. Schappacher and A. Werthenbach, ‘Complete electroweak one-loop radiative corrections to top-pair production at **TESLA** – a comparison’, LC-TH-2002-002, hep-ph/0202109.
- [35] J. Fleischer, J. Fujimoto, T. Ishikawa, A. Leike, T. Riemann, Y. Shimizu and A. Werthenbach, ‘One-loop corrections to the process $e^+e^- \rightarrow t\bar{t}$ including hard bremsstrahlung’, hep-ph/0203220.
- [36] G. Passarino, *Nucl. Phys.* **B361** (1991) 351–391.
- [37] R. Vega and J. Wudka, *Phys. Rev.* **D53** (1996) 5286.
- [38] D. Bardin, M. Bilenky, P. Christova, M. Jack, L. Kalinovskaya, A. Olchevski, S. Riemann and T. Riemann, ZFITTER v.6.30, obtainable from <http://www.ifh.de/~riemann/> and also from [/afs.cern.ch/user/b/bardindy/public](http://afs.cern.ch/user/b/bardindy/public).
- [39] T. Hahn, M. Perez-Victoria, *Comput. Phys. Commun.* **118** (1999) 153.
- [40] J. Fleischer and M. Tentyukov, ‘A Feynman diagram analyser DIANA’ – Graphic facilities, hep-ph/0012189, contribution to the *Proc. of 7th International Workshop on Advanced Computing and Analysis Techniques in Physics Research* (ACAT 2000), Batavia, Illinois, (2000).
- [41] The numbers for the comparison were provided by C. Schappacher.